# LUMINESCENCE STUDIES IN CADMIUM SULPHIDE

by

JAN CONRADI

B.Sc., Queen's University, 1962
D.I.C., Imperial College, 1963
M.Sc., University of Birmingham, 1964

A DISSERTATION SUBMITTED IN PARTIAL FULFILLMENT
OF THE REQUIREMENTS FOR THE DEGREE OF
DOCTOR OF PHILOSOPHY

In the Department
of
Physics


SIMON FRASER UNIVERSITY
December 1968

EXAMINING COMMITTEE APPROVAL

R. R. Haering
Senior Supervisor

J. C. Irwin
Examining Committee

K. Colbow
Examining Committee

PARTIAL COPYRIGHT LICENSE

I hereby grant to Simon Fraser University the right to lend my thesis or dissertation (the title of which is shown below) to users of the Simon Fraser University Library, and to make partial or single copies only for such users or in response to a request from the library of any other university, or other educational institution, on its own behalf or for one of its users. I further agree that permission for multiple copying of this thesis for scholarly purposes may be granted by me or the Dean of Graduate Studies. It is understood that copying or publication of this thesis for financial gain shall not be allowed without my written permission.

Title of Thesis/Dissertation:

_____

_____

_____

_____

Author: _____

(signature)

_____

(name)

_____

(date)

## ABSTRACT

This thesis describes some properties of the luminescence from single crystals and evaporated thin films of CdS under optical and electron beam excitation.

A comparison of optical and electron beam excitation mechanisms, as applied to the study of luminescence from solids, is made. It is concluded that the variable penetration depth of high energy electrons with accelerating voltage can be readily used to distinguish between surface and bulk effects, and that electron beam excitation can be used to advantage when the efficiency of a radiative process is low and high excitation intensity is required. The main advantage of optical excitation is in the vertical excitation of electrons from lower to higher energy levels which arises from the negligible momentum of the incident photons.

Optical excitation spectra of various bound exciton emission lines in single crystals of Cds are presented. It is shown that the complex responsible for the so-called $I_1$ emission, due to the annihilation of an exciton bound to a neutral acceptor, is created by the direct formation of bound excitons on the impurity site and by the formation of free or intrinsic excitons which are subsequently trapped on the impurity.

The complexes responsible for the so-called $I_2$ and $I_5$ emission are also created by the formation of intrinsic excitons but more

importantly they are created by direct phonon assisted formation of excitons bound to neutral and ionized impurities. It is concluded that the impurity involved is a donor.

Electron beam excited luminescence from evaporated thin films of CdS is obtained. The transitions giving rise to this luminescence are identified as resulting from the recombination of free electrons with bound holes (free-bound emission) and from the recombination of bound electrons with bound holes (bound-bound emission) with the simultaneous emission of n LO phonons (n = 0, 1, 2, ...).

It is shown that if the films are coated with a 2000A thick layer of $SiO_x$, causing the CdS energy bands to be bent down at the $SiO_x$ - CdS interface, the peak position of the free-bound emission is shifted toward higher energies when the incident electrons have a small penetration depth (low energy). This is shown to result from an accumulation layer of electrons at the $SiO_x$ - CdS interface.

TABLE OF CONTENTS

# LIST OF TABLES

## LIST OF ILLUSTRATIONS

ACKNOWLEDGEMENTS

The author owes a considerable debt of gratitude to Dr. R. R. Haering for the many long (and short) fruitful discussions which have contributed so much in the course of this work -- this is meant in the literal, not platitudinous, sense. It is also a pleasure to thank Drs. J. C. Irwin and K. Colbow for critically reading the draft version of this thesis and for their useful comments and to thank Dr. D. E. Brodie for his comments on and critical reading of a later version of the manuscript.

It is also a pleasure to acknowledge the many useful (and sometimes friendly, sic!) discussions with and manual assistance of my colleagues in the lab, most notable among which are John (O'Twit) O'Hanlon, Gordon McCallum, Pete Barnes and Ken Lyall (in approximate chronological order of their crossing my path). The evaporated films used in some of the experiments were kindly made by John O'Hanlon and/or Mr. Joël Mercier, whose assistance on various other technical matters and skill in making some of the drawings herein is also gratefully acknowledged. Thanks also go to Mrs. Sharon Ginetz for her accurate typing of the thesis and accurate interpretation of my own typing.

I would also like to express many thanks to Messrs. F. Wick, A. Stevens and D. Shay of the Machine Shop for their skill and advice in producing the electron gun and other mechanical things and to Messrs. A. Stuart, D. Robinson and A. M. Cutteridge of the

Glassblowing Shop for making the glass helium dewars.

Many thanks also to Mr. R. R. Hill of Lawrence Radiation Laboratories for providing the drawings for the electron gun.

I would also like to thank my wife Lois for her encouragement (and financial support!).

The work described in this thesis was supported by the National Research Council of Canada.

# 1. INTRODUCTION

## 1.1 Single Crystals of CdS

The optical properties of single crystals of CdS have been under investigation for some time and much detailed understanding of the absorption, reflection and luminescence spectra of this material has now been gained, particularly as a result of the work of Thomas and Hopfield.[1-8] These properties have been the subject of a two part review article.[9, 10]

The spectra of CdS fall into two basic categories:

(a) broad band luminescence spectra which have been shown to result from the recombination of an electron, either free or bound to a donor, with a hole bound to an acceptor with the simultaneous emission of one or more (k = 0) LO phonons[1, 10-13] and

(b) narrow band spectra which result from the absorption (emission) of a photon and the simultaneous creation (annihilation) of an exciton which is free or is bound to a neutral or ionized impurity.[3, 7-10] Since the absorption, reflection and luminescence peaks corresponding to the creation and recombination of the free excitons are an intrinsic property of the material they are often referred to as intrinsic excitons. The excitons bound to impurities are observed at energies lower than the

intrinsic excitons, and are often referred to as extrinsic excitons.

Each of the three above mentioned techniques (absorption, reflection and luminescence spectra) is very useful in documenting the optical properties of a material but of these, only luminescence studies have revealed interactions between elementary excitations (phonons in this instance) and the complex responsible for the luminescence. One still does not know exactly what happens to an exciton for instance once it is created. In this regard two further experimental techniques are useful: (a) photoconductivity spectra and (b) excitation spectra of particular emission lines. Photoconductivity spectra allow one to observe how free electrons (or holes) are created as a result of the absorption of photons of a particular energy. For example, the photoconductivity of some CdS crystals shows a maximum when the energy of the incident photons is equal to the free exciton energy and a minimum when the energy of the incident photons is greater than the intrinsic exciton by an integral multiple of the LO phonon energy.[14, 15] Haering and Batra[16] have proposed that this is the result of the absorption coefficient due to exciton formation having a maximum whenever the energy of the incident photon is equal to the exciton energy plus n LO phonons (n = 0, 1, 2, ...). Physically this corresponds to saying that the free exciton is created directly by the

absorption of one photon and the simultaneous emission of one or more LO phonons. Excitation spectra on the other hand, where one monitors the luminescent intensity of a particular emission line as a function of the energy of the incident light, allow one to observe how a particular luminescent complex is created.

## 1.2 Evaporated Films of CdS

The optical properties of evaporated thin films of CdS have been hardly studied at all.[17-22] The only known studies of the luminescence and reflection spectra of evaporated CdS films are those of Shalimova and co-workers[19-21] whose films exhibit spectra more characteristic of single crystal material, although this was not the interpretation they gave to their results.

Two likely reasons exist for the lack of work on the optical properties of evaporated CdS:

(1) good quality single crystals have been available for some time where considerable structure is seen and is or was in need of interpretation, and

(2) the luminescence in evaporated films of CdS is very inefficient and requires high intensity sources such as electron beams for excitation.

## 1.3 Scope of this Work

This thesis describes a study of some properties of several complexes responsible for luminescence in single crystal and evaporated films of CdS.

The advantages and disadvantages of optical and electron beam excitation are discussed and each technique is used in those circumstances where it is of maximum effectiveness.

Optical excitation spectra of extrinsic exciton emission in single crystal CdS are obtained which show how the exciton-impurity complexes responsible for the emission are created. A preliminary report of this part of the work has been published.[23]

Electron beam excited luminescence from evaporated films of polycrystalline CdS is obtained and the transitions giving rise to the luminescence are identified. Advantage is taken of the variation in penetration depth of the incident electrons with beam voltage to distinguish surface from bulk effects. The effect of surface treatment on the luminescence is shown to correlate, at least qualitatively, with the effect of surface treatment on electrical conductivity.[24]

# 2. REVIEW OF THE OPTICAL PROPERTIES OF CdS

## 2.1 Introduction

This chapter reviews some of the optical properties of CdS. Emphasis is given to those properties which affect the luminescence seen in CdS at low temperatures. The optical properties of single crystal and polycrystalline evaporated CdS are discussed and compared.

## 2.2 Single Crystals

The emission spectrum of single crystal CdS at low temperatures usually consists of two overlapping series of broad emission bands in the wavelength interval 5100-5600A and, at higher excitation levels, a number of narrow emission lines in the wavelength interval 4850-5000A (Figures 2.1 and 2.2). In addition a number of sharp and often strong absorption and reflection peaks occur in the wavelength interval 4700-4900A.[3,6-8]

### 2.2.1 Broad Band Emission

The broad emission bands in CdS were first observed by Kröger[25] in crystals subjected to ultraviolet radiation at 93°K. Since this first observation, detailed studies have been made on these emission bands at temperatures down to 4.2°K.[26-30] At the higher temperatures an emission line at 5130A is observed

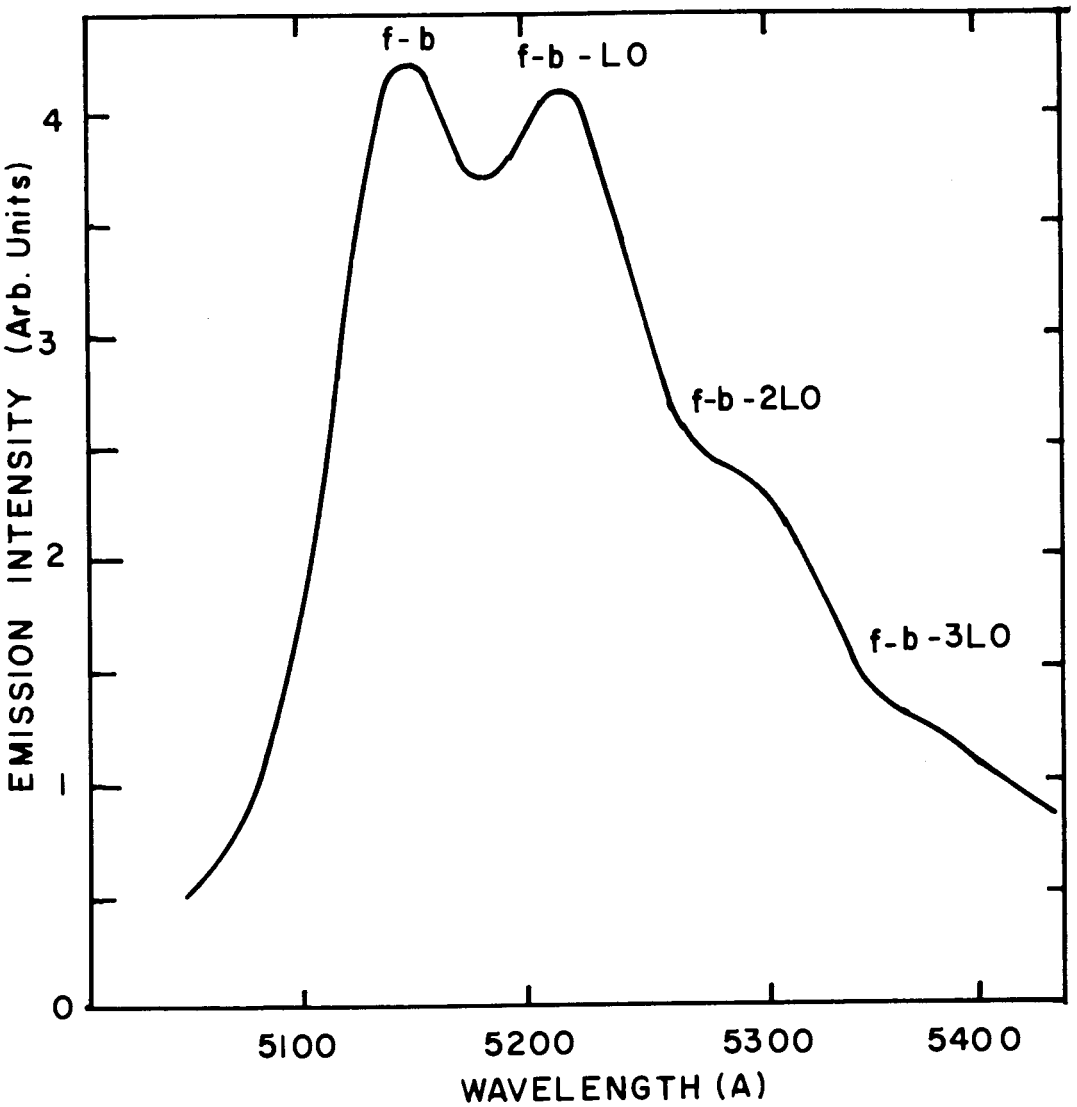


Figure 2.1 Typical CdS emission spectrum at 77°K.

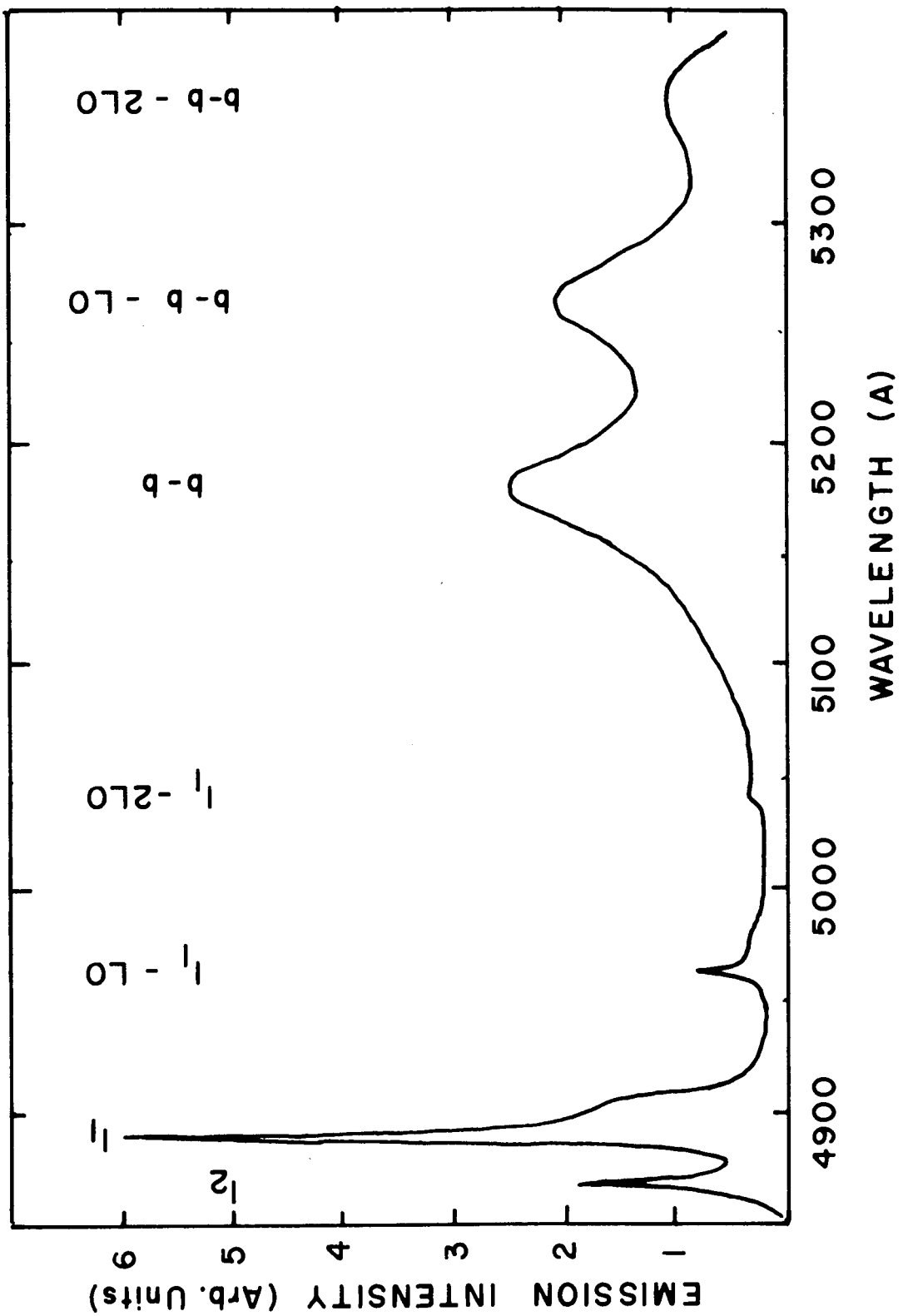


Figure 2.2 Typical CdS emission spectrum at helium temperature (taken under electron-beam excitation).

which is repeated at equal energy intervals on the low energy side of the main peak, the energy spacing being equal to the LO phonon energy. If the temperature is lowered to 4°K there is an apparent shift in the peaks to lower energy, the main peak now appearing at 5175A. Pedrotti and Reynolds[29] studied the spectral position and intensity of the emission as the temperature is changed from 4°K to 77°K and find that the peak at 5130A which is dominant at 77°K gradually diminishes in intensity as the temperature is lowered while the peak at 5175A gradually grows (Figure 2.3). These observations tend to confirm an explanation offered by Thomas and Hopfield[3] in which it is assumed that a bound state of an electron exists from which recombination with a bound hole can take place. At 77°K the recombination causing the emission takes place between an unbound or free electron and a bound hole while at 4°K both the electron and hole are bound. An energy model for this recombination is shown in Figure 2.4. At 4°K the donor is sufficiently populated so that the dominant recombination is between bound electrons and bound holes (bound-to-bound emission). As the temperature of the sample is increased the donor becomes thermally depopulated and recombination takes place between an electron in the conduction band and a bound hole (free-to-bound emission).

Further support to this model has been given by the theoretical analysis by Thomas et al[1] of the spectral line

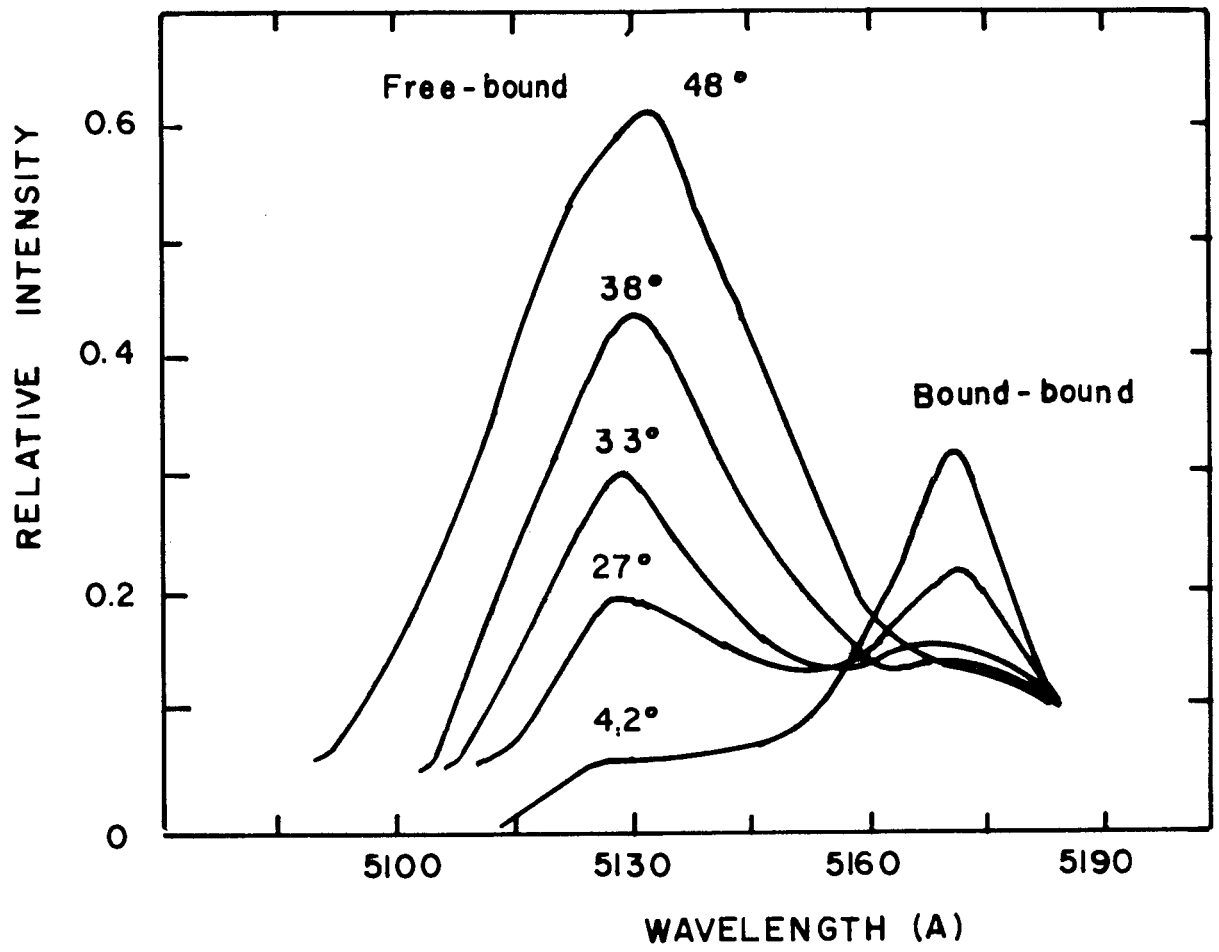


Figure 2.3 Luminescence spectrum of CdS as a function of temperature. Zero phonon peaks only are shown. (After Pedrotti and Reynolds[30]).

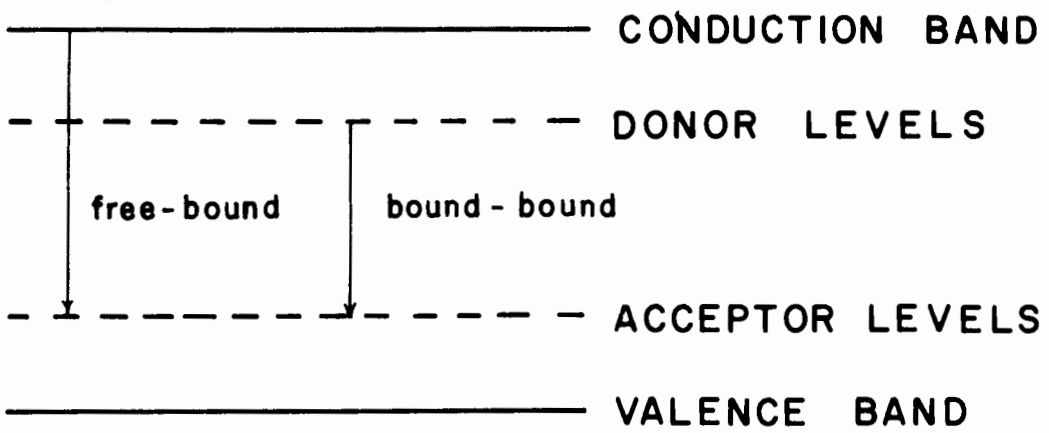


Figure 2.4 Energy band model for free-bound and bound-bound emission.

shape and intensity of the bound-bound emission as a function of time after flash excitation and the experimental confirmation of the theory by Thomas et al[11] and Colbow.[13]

2.2.1 Narrow Line Spectra - Excitons

At low temperatures a number of sharp and often strong lines appear in the absorption, reflection and emission spectra of CdS at energies just below the fundamental absorption edge.[3, 4, 6-8, 31] A summary of these lines is given in Table 2.1.

In the absorption and reflection spectra at 4°K the observed lines at wavelengths less than 4860A are strong and are an intrinsic property of the crystals. They are therefore attributed to exciton states, and are referred to as intrinsic excitons. At 77°K similarly shaped but less well resolved absorption and reflection spectra appear, but shifted slightly to lower energies, corresponding to a dilation of the energy gap. The reflection spectrum of CdS at 4°K showing the peaks due to intrinsic excitons is shown in Figure 2.5. The peaks labelled A, B and C correspond to direct allowed excitons. The evidence for the direct nature of these transitions comes from absorption spectra at energies below the reflection peaks where good agreement between experimental and theoretical determination of the absorption coefficient is obtained if a process is postulated in which excitons are

| Line | Position (A) | Position (ev) | Active For | Ground State |
|---|---|---|---|---|
| **Intrinsic Excitons** | | | | |
| A(n=1) | 4854.5 | 2.5537 | $E \perp c$ | |
| A(n=2) | 4812.9 | 2.5758 | $E \perp c$ | |
| B(n=1) | 4826.1 | 2.5686 | $E \perp c$ and $E \parallel c$ | |
| B(n=2) | 4784.9 | 2.5908 | $E \perp c$ and $E \parallel c$ | |
| C | | 2.616 | $E \perp c$ and $E \parallel c$ | |
| **Bound Excitons** | | | | |
| $I_1$ | 4888.5 | 2.5359 | $E \perp c$ | Neutral Acceptor |
| $I_{1B}$ | 4863.7 | 2.5489 | $E \perp c$ and $E \parallel c$ | Neutral Acceptor (Trapped exciton from band B) |
| $I_{1B'}$ | 4860.8 | 2.5504 | | |
| $I_2$ (Many lines) | eg 4867.15 | 2.5471 | $E \perp c$ | Neutral Donor |
| $I_{2B}$ | 4837.7 | 2.5626 | $E \perp c$ and $E \parallel c$ | Neutral Donor (Trapped exciton from band B) |
| $I_3$ | 4861.7 | 2.5499 | $E \perp c$ | Ionized Donor |
| $I_5$ | 4869.14 | 2.5459 | $E \perp c$ | ? |

Table 2.1 A summary of the exciton lines in CdS.

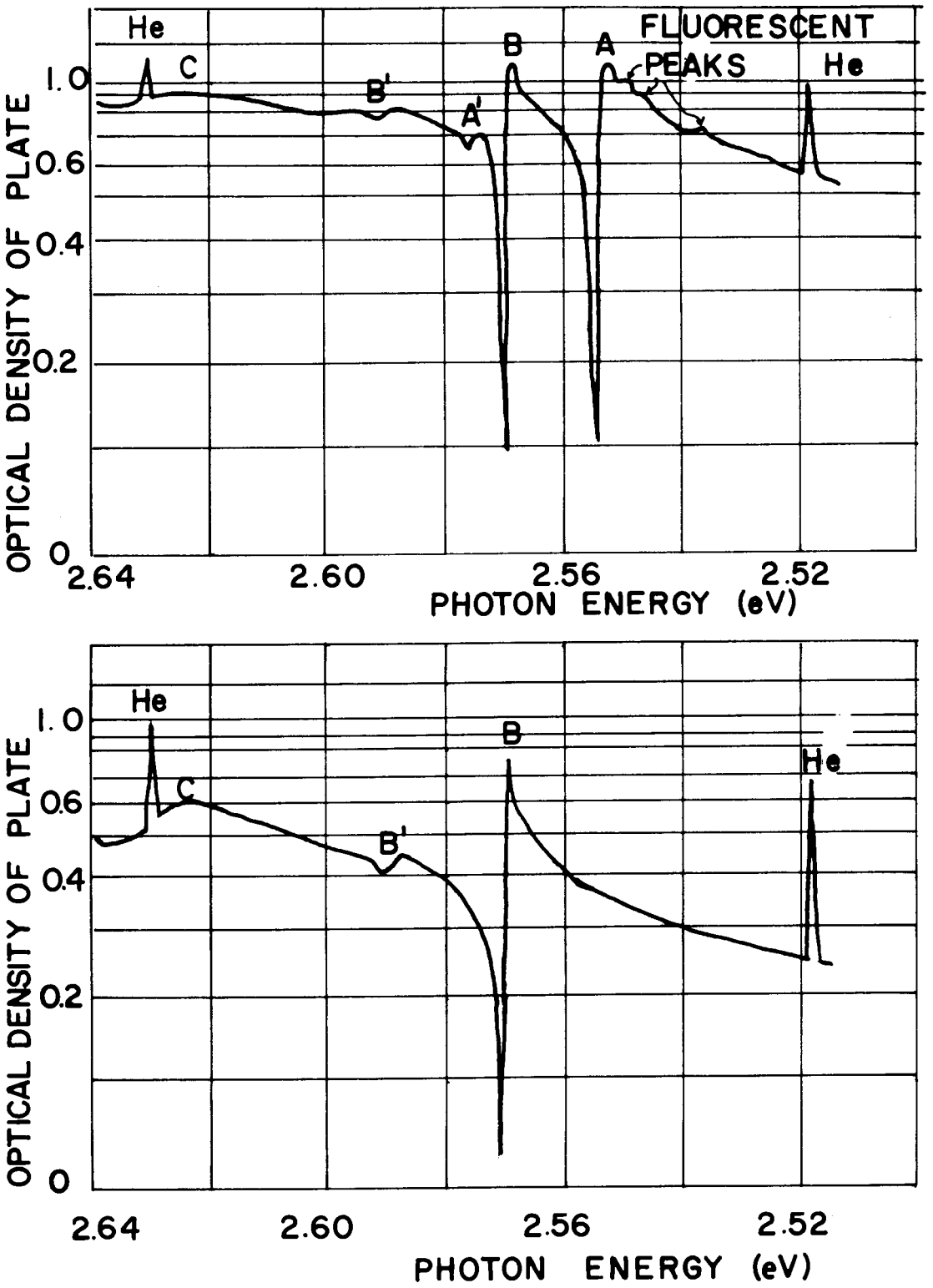


Figure 2.5 Reflection spectrum of CdS at 4.2°K for light polarized with (a) E⊥c and (b) E∥c. (After Thomas and Hopfield[3].)

formed with the simultaneous absorption of an LO phonon, both particles having a small wave vector.[4] The existence of three peaks is due to the crystal field and spin orbit splitting of the valence band, which is a consequence of the hexagonal crystal structure of CdS. The polarization dependence of the peaks corresponds to the symmetry assignments of the valence bands[2, 6] (Figure 2.6). The labelling of the intrinsic excitons as A, B and C excitons indicates the valence band from which the dominant part of the hole wavefunction is derived. The peaks labelled A' and B' correspond to the n = 2 excited states of excitons A and B.

If a hydrogenic model for these excitons is assumed, the ionization energy of the excitons and hence the energy gaps for the two upper most valence bands can be accurately deduced from the difference in energy between the n = 1 ground state and n = 2 excited state of the A and B excitons. Although no excited states of the C excitons have been seen, an estimate of the depth of the C valence band below the other bands can still be made on the basis of the separation between the reflectivity peaks.

In addition to these intrinsic excitons a variety of sharp lines are seen in absorption and fluorescence, but at energies slightly lower than the intrinsic excitons.[8, 31] Many of these lines are due to transitions involving bound excitons in

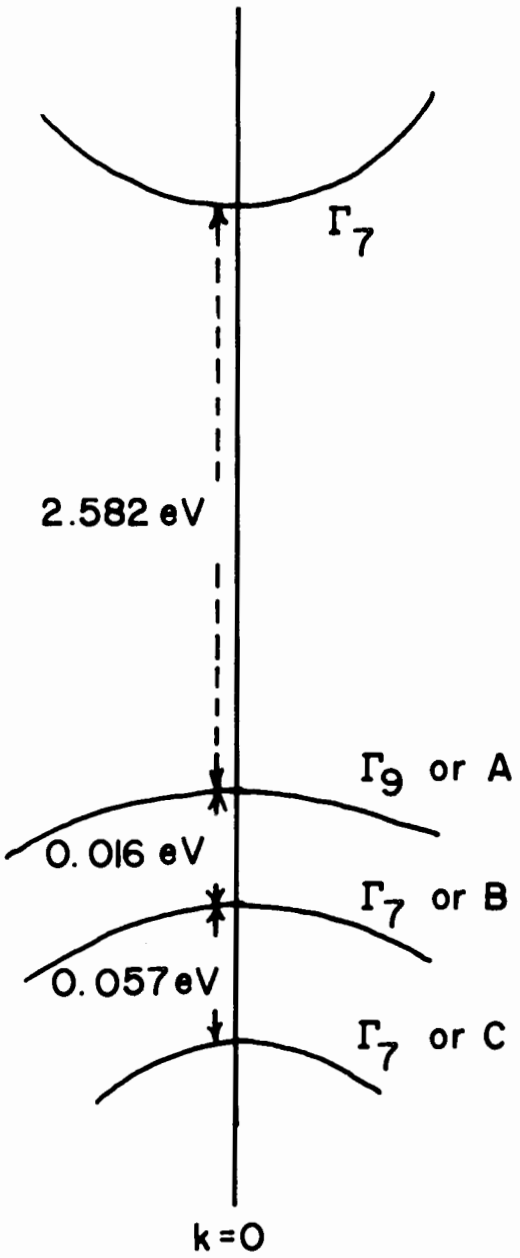


Figure 2.6 Sketch of the band extrema in CdS. The $\Gamma_9$ valence band is strongly active only for light with E⊥c; the $\Gamma_7$ valence bands interact strongly with both modes of polarizations.

which an exciton bound to a neutral or ionized donor or acceptor is created or destroyed.

Nearly all crystals show a line at 4888.5A at 4°K which has been labelled $I_1$[8] (Figure 2.2). In emission this line is replicated at lower energies with the spacing between lines equal to the LO phonon energy. Nearer the intrinsic A exciton is a group of very closely spaced lines labelled $I_2$ which are seen in absorption and fluorescence at 4867-4870A[8] (Figure 2.2). Both $I_1$ and $I_2$ are strongly active only for the electric vector of the light normal to the crystal c-axis ($E \perp c$) and the hole associated with these excitons must therefore be from the A valence band.

If $I_1$ and $I_2$ are studied in absorption and emission under the influence of a strong magnetic field[7, 8, 31] it is found that each line splits into a quartet, the splitting being a linear function of magnetic field. Since the splitting is linear the ground and excited states of $I_1$ and $I_2$ have only one unpaired spin and the centers therefore arise from excitons associated with neutral donors or acceptors (the two electrons on a neutral donor and the two holes on a neutral acceptor will have their spins antiparallel). Since the electron g value is isotropic and the hole g value has the form[7] $g = g_{\parallel} \text{Cos } \theta$ where $\theta$ is the angle between the magnetic field and the crystal c-axis, one can identify the impurity from the intensity of the different split components when seen in absorption. It is concluded that $I_1$ is

associated with a neutral acceptor and $I_2$ with a neutral donor.[7, 8]

In addition to $I_1$ and $I_2$, which are active for $E \perp c$ there are two broader absorption lines, active in both polarization modes ($E \perp c$ and $E \| c$) which are spaced from exciton B by nearly the same energy as $I_1$ and $I_2$ are spaced from exciton A. It is therefore concluded that these lines arise from the same impurities as $I_1$ and $I_2$ but from exciton B rather than exciton A. Consequently these broad lines are called $I_{1B'}$ and $I_{2B}$. Thomas and Hopfield[8] suggest that the width of the $I_{1B'}$ and $I_{2B}$ lines is due to lifetime broadening resulting from the short lifetime of the B hole which is converted to an A hole with the simultaneous emission of a phonon. This hole conversion mechanism will be invoked in Chapter 4 as a possible explanation of some of the polarization effects reported there. Another narrow absorption line active for both polarization modes is seen at an energy only slightly different from $I_{1B'}$ (1.5 meV below) which is labelled $I_{1B}$. This line too is the $I_1$ exciton with the hole from the B valence band and differs from $I_{1B'}$ in that the two holes in the $I_{1B'}$ complex have their angular momenta parallel, and parallel to the crystal c-axis, while in the $I_{1B}$ complex their angular momenta are anti-parallel.[8]

Finally, a line $I_3$ is observed only in absorption in "crystals of suitable thickness and quality".[8] This line can

be seen conveniently when a minimum of band-gap radiation is used and it can be enhanced by illuminating the crystal with infra-red radiation. The magnetic field behaviour of $I_3$ suggests that it arises from an ionized center. This conclusion is hardened by the fact that absorption due to $I_3$ can be enhanced while $I_1$ and $I_2$ are diminished, if the crystal is simultaneously irradiated by infra-red light. The infra-red radiation serves to ionize neutral impurity sites. Since the binding energy of the $I_3$ exciton is only 3.8 meV (3.8 meV below the intrinsic A exciton) it is concluded that $I_3$ is bound to an ionized donor.[8] If $I_3$ were an exciton bound to an ionized acceptor it is to be expected that the binding energy would be larger since the acceptor binding energy is 170 meV while the donor binding energy is 30 meV, as in II-VI compounds the binding energy of an exciton to a donor (acceptor) is proportional to the donor (acceptor) binding energy.[61] The exciton binding energy is 0.1-0.2 times the impurity ionization energy.

The most commonly seen exciton fluorescence lines are the $I_1$ and $I_2$ lines. Reynolds[31] has seen another strong emission and absorption line $I_5$ at 4869.14Å which, on the basis of the intensity of the split components in a magnetic field, is attributed to an exciton bound to a neutral acceptor, even though the splitting as a function of the angle between the magnetic field and crystalline c-axis is the same as for $I_2$. Some variation in the relative intensities of the magnetic field split

components of $I_5$ was however observed from crystal to crystal and the assignment of $I_5$ must be regarded as tentative.

## 2.3 CdS Evaporated Films

In stark contrast to single crystals of CdS very little work has been performed on the luminescence from thin CdS films. Nearly all the work on CdS films has been concentrated on producing films suitable for photo-voltaic[32] or photo-conductive devices[33] or for field-effect transistors,[34] although some reports exist of luminescence in sintered CdS phosphors.[35] The phosphors have usually had some impurity added in order to produce luminescence at energies considerably below the band gap energy. Most work on phosphors has, however, been concentrated on ZnS whose band gap is considerably larger than that of CdS and where efficient visible luminescence can be obtained at room temperature. The light seen from room temperature CdS phosphors is usually in the red region.

The meager information available on evaporated or sublimed films of CdS suggests[19-21] that if the substrate temperature during evaporation is less than 300°C only a simple and weak luminescence spectrum of the form shown in Figure 2.7 can be obtained at 77°K. As the temperature of the substrate is raised toward 500°C the luminescence spectrum at 77°K assumes the form shown in Figure 2.8. The peaks have all been attributed to electronic transitions from different excited states to the ground

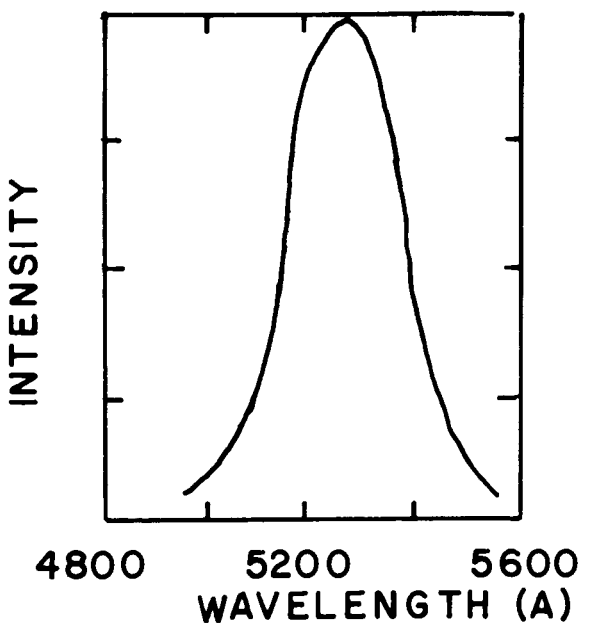


Figure 7.7 Emission spectrum at 77°K of a CdS film deposited on a cool substrate (After Shalimova et. al.(19).)

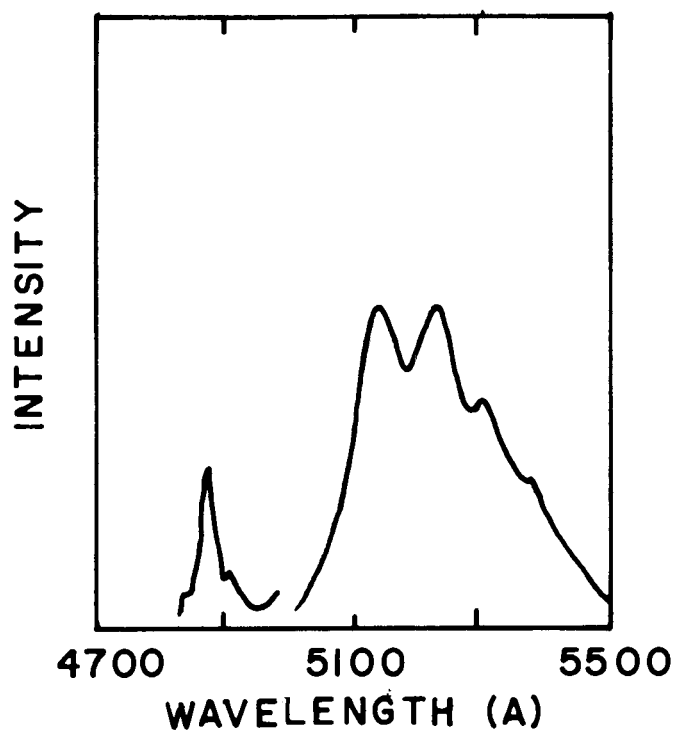


Figure 2.8 Emission spectrum at 77°K of a CdS film deposited in vacuum at 500°C. (After Shalimova et. al.(19).)

state of excess cadmium atoms. Atomic cadmium has two valence electrons in the 5s state. Thus the ground state of cadmium is a singlet state with inner quantum number J = 0, or in spectroscopic notation we have a $^1S_0$ state. The excited states which are said to be operative are the triplet P states $^3P_2$, $^3P_1$ and $^3P_0$. The blue emission is supposed to result from a $^3P_2$ - $^1S_0$ transition and the green emission from $^3P_1$ - $^1S_0$ and $^3P_0$ - $^1S_0$ transitions. Spectroscopic selection rules however prohibit all of these. It is conceivable however that the selection rules would be relaxed somewhat under the influence of crystalline fields. However, according to the energy diagram of the cadmium atom all the above atomic transitions would, assuming they can take place, emit in the wavelength interval 3100-3300A, whereas the actual lines occur in the interval 4800-5500A. Furthermore, when impurities are introduced into a semiconductor their energy states can often be treated as hydrogen-like states within the framework of the effective mass approximation.[36] Finally the green luminescence that is seen coincides with the free-bound emission and the blue luminescence occurs in the region where free and bound excitons are seen in single crystal CdS.[9, 10] Since it is known that heat treatments cause recrystallization of evaporated CdS,[37] it would appear as if the spectra observed are characteristic of bulk CdS and not of atomic Cd.

## 2.4 Conclusions

The emission, absorption and reflection spectra of single crystal CdS have been well documented and can be understood in terms of transitions involving free and bound electrons with bound holes (broad band luminescence) and in terms of intrinsic and bound excitons (narrow line spectra). The spectra of evaporated or sublimed films of CdS are poorly documented and studied, and have in one instance been badly misinterpreted.

# 3. COMPARISON OF OPTICAL AND ELECTRON BEAM EXCITATION METHODS IN THE STUDY OF OPTICAL PROPERTIES OF SEMICONDUCTORS

## 3.1 Introduction

This chapter will review some theoretical aspects of optical absorption and electron beam stopping in solid semiconductors and discuss the advantages and disadvantages of each method in the study of the luminescence and other optical properties of semiconductors.

## 3.2 Optical Excitation[38, 39]

The interaction of a system of N charged particles with electromagnetic radiation can be described by the Hamiltonian

$$H = V_o + \sum_{i=1}^{N} \left\{ q_i \varphi + (\vec{p}_i - q_i \vec{A}/c)^2/2m_i \right\} \qquad (3.2.1)$$

where $\varphi$ and $\vec{A}$ are the scalar and vector potentials of the applied field, $m_i$ and $q_i$ are the mass and charge of the ith particle and $(\vec{p}_i - q_i \vec{A}/c)$ is its conjugale momentum. $V_o$ is the potential energy of the system in the absence of external fields.

Choosing the gauge $\varphi = 0$ and assuming the external field is sufficiently small that the problem may be treated in perturbation theory, we have

$$H = H_o + H_I \tag{3.2.2}$$

$$H_o = V_o + \sum_{i=1}^{N} p_i^2/2m_i \tag{3.2.3}$$

$$H_I = - \sum_{i=1}^{N} \frac{q_i}{2cm_i} (\vec{A}\cdot\vec{p}_i + \vec{p}_i\cdot\vec{A}) \tag{3.2.4}$$

Let the external field be transverse and of the form

$$\vec{A} = \vec{A}_o \exp (i\vec{k}\cdot\vec{r} - i\omega t) \tag{3.2.5}$$

and since for our gauge $\vec{A}\cdot\vec{p}_i = \vec{p}_i\cdot\vec{A}$ then

$$I = - \sum_{i=1}^{N} \frac{q_i}{cm_i} \vec{A}\cdot\vec{p}_i \tag{3.2.6}$$

If the wave function $\psi$ on which H acts is expanded in stationary eigenfunctions $u_k(r)$ of the unperturbed Hamiltonian $H_o$ with time dependent coefficients, then if the system were initially in state $|j\rangle$ the probability of finding it at some later time t in a higher state $|m\rangle$ is

$$w_{mj} = 4|\langle m| \frac{e}{mc} \exp (i\vec{k}\cdot\vec{r}) \vec{A}_o\cdot \sum_{i=1}^{N} \vec{p}_i |j\rangle|^2 \frac{\sin^2 \frac{1}{2} (\omega_{mj} - \omega)t}{[\hbar(\omega_{mj} - \omega)]^2} \tag{3.2.7}$$

where $\hbar\omega_{mj} = E_m - E_j$ is the energy difference between the upper and lower states and we have let $q_i/m_i = -e/m$.

If $\rho(E)dE$ is the number of states for which $E_m - E_j$ lies between $\hbar\omega$ and $\hbar\omega + dE$ then an integration of (3.2.7) over these states gives a transition rate for upward transitions

$$r_o = \frac{2\pi e^2}{m^2 c^2 \hbar^2} |\vec{A}_o|^2 \; |\langle m|\vec{a}_o \exp(i\vec{k}\cdot\vec{r})\cdot \sum_{i=1}^{N} \vec{p}_i |j\rangle|^2 \; \rho(E) \qquad (3.2.8)$$

where $\vec{a}_o$ is a polarization vector.

Since the transition probability $w_{mj} = w_{jm}$, the net rate of induced transitions from state $|j\rangle$ to state $|m\rangle$ is

$$r_{ind.} = r_o \left\{ f(E_j) - f(E_m) \right\} \qquad (3.2.9)$$

where $f(E_i)$ is the probability of the state $|i\rangle$ being occupied.

The absorption coefficient $\alpha$ is the power absorbed per unit volume divided by the incident flux. The magnitude of the incident flux is

$$|\vec{S}| = \frac{n\omega^2}{2\pi c\mu} |\vec{A}_o|^2 \qquad (3.2.10)$$

n is the index of refraction and $\mu$ the relative permeability of the medium. The absorption coefficient then becomes

$$\alpha(\omega) = \frac{\hbar\omega\, r_{ind.}}{|\vec{S}|}$$

$$= \frac{\mu e^2}{m^2 n\omega} \left| \langle m | \vec{a}_o \exp(i\vec{k}\cdot\vec{r}) \cdot \sum_{i=1}^{N} \vec{p}_i | j \rangle \right|^2 \rho(E) \left\{ f(E_j) - f(E_m) \right\} \tag{3.2.11}$$

$$= \frac{\mu e^2}{m^2 n\omega} |M|^2 \rho(E) \left\{ f(E_j) - f(E_m) \right\}$$

If we can use a one electron approximation we can describe the transition as a change in the state of a single electron, and if the total wavefunction can be taken as a determinant of one electron wavefunctions then

$$M = \langle m | \vec{a}_o \exp(i\vec{k}\cdot\vec{r}) \cdot p | j \rangle \tag{3.2.12}$$

where $|m\rangle$ and $|j\rangle$ are now one electron states, and since we are interested in what happens in a solid the one electron states in our case will have the Bloch form

$$|j\rangle = u_j(r) \exp(i\vec{k}_j \cdot \vec{r}) \tag{3.2.13}$$

M vanishes unless $k_m = k_j + k$ and since for optical radiation $k << k_i$ and $k_m$ we will have only direct vertical transitions on an E - k diagram.

The intensity of the radiation as a function of distance into the material will be

$$I = I_o \, e^{-\alpha x} \tag{3.2.14}$$

and the differential energy loss for light is of the form

$$- \frac{dI}{dx} = \alpha I_o \, e^{-\alpha x} \tag{3.2.15}$$

Thus the distinguishing features of optical excitation are the vertical transitions in k-space and the exponential form of the differential energy loss. The absorption coefficient is a function of the energy of the incident photons, with the actual functional dependence on the energy requiring detailed knowledge of the band structure of the material. However, in general the absorption coefficient is small ($< 10^3$ $cm^{-1}$) at energies somewhat below the energy of the band gap and large ($> 10^5$ $cm^{-1}$) for energies above the band gap.

## 3.3 Electron Beam Excitation

### 3.3.1 Calculation of dE/ds, the Energy Loss Per Unit Distance along the Electron Trajectory

Consider an electron which has been scattered off a potential V(r). The unnormalized wavefunction of the electron at a large distance from the scattering center is of the form

$$\psi(r) = e^{ik\vec{n}_o\cdot\vec{r}} + f(\theta, \varphi)\frac{e^{i\vec{k}\cdot\vec{r}}}{r} \qquad (3.3.1)$$

where the scattering amplitude $f(\theta, \varphi)$ is

$$f(\theta, \varphi) = -\frac{2m}{4\pi\hbar^2}\int e^{-i\vec{k}\cdot\vec{r}'} V(r')\psi(r')d\vec{r}' \qquad (3.3.2)$$

and $\vec{n}_o$ is a unit vector in the direction of the incoming electron.

This is the exact asymptotic form for $f(\theta, \varphi)$. Let us now use the first Born approximation and let $\psi = e^{ik\vec{n}_o\cdot\vec{r}'} = e^{i\vec{k}_o\cdot\vec{r}'}$ in the right hand side of equation (3.3.2). $f(\theta, \varphi)$ then becomes

$$f(\theta, \varphi) = -\frac{2m}{4\pi\hbar^2}\int e^{i(\vec{k}_o-\vec{k})\cdot r'} V(r')\, d\vec{r}' \qquad (3.3.3)$$

Consider first the case where the incoming electron scatters off free atoms, leaving the atom behind in an excited state n. If

we consider that the electron scatters off the Z atomic electrons then

$$V(r') = \int \sum_{s=1}^{Z} \frac{e^2}{|\vec{r}' - \vec{r}_s|} \varphi_o \varphi_n^* \, d\tau_1 \ldots\ldots d\tau_Z \qquad (3.3.4)$$

$$= V_{on}(r')$$

where $\varphi_o$ and $\varphi_n$ are wavefunctions of the atom in the ground state o and an excited state n.

Therefore

$$f(\theta, \varphi) = -\frac{2m}{4\pi\hbar^2} \int V_{on}(r') \, e^{i\vec{\kappa n}\cdot\vec{r}'} \, dr' \qquad (3.3.5)$$

where $\vec{\kappa n} = \vec{k n_o} - k_n \vec{n}_1$, $k_n \vec{n}_1 = \vec{k}$, $k_n$ is the magnitude of the wave-vector of the electron after exciting the atom to state n, and $\vec{n}_1$ is a unit vector in the direction of the scattered electron.

Now since

$$\int \frac{e^{i\vec{\kappa n}\cdot\vec{r}'}}{|\vec{r}' - \vec{r}_s|} \, d\tau' = \frac{4\pi}{\kappa^2} e^{i\vec{\kappa n}\cdot\vec{r}_s} \qquad (3.3.6)$$

the scattering amplitude $f(\theta, \varphi)$ becomes

$$f(\theta, \varphi) = - \frac{2me^2}{\hbar^2 \kappa^2} \int \varphi_o \, \varphi_n^* \sum_{s=1}^{Z} e^{i\vec{\kappa n}\cdot\vec{r_s}} \, d\tau_1 \ldots\ldots d\tau_Z$$

$$= - \frac{2me^2}{\hbar^2 \kappa^2} \sum_{s=1}^{Z} \langle n | \, e^{i\vec{\kappa n}\cdot\vec{r_s}} | 0 \rangle \qquad (3.3.7)$$

$$= - \frac{2me^2}{\hbar^2 \kappa^2} F_n \, (\kappa)$$

where

$$F_n(\kappa) = \sum_{s=1}^{Z} \langle n | \, e^{i\vec{\kappa n}\cdot\vec{r_s}} | 0 \rangle \qquad (3.3.8)$$

Now, if $Q = \frac{\hbar^2 \kappa^2}{2m}$ is the energy transferred to the atom, then with the restriction $\frac{\kappa}{k}, \frac{k - k_n}{k}, \frac{v - v'}{v} << 1$ where v and v' are the velocities of the electron before and after collision respectively, we find (see Figure 3.1)

$$\kappa^2 = k^2 + k_n^2 - 2kk_n \, \text{Cos} \, \theta$$

$$\simeq 4 \, k^2 \, \text{Sin}^2 \, \theta/2 \qquad (3.3.9)$$

Thus $f_n(\theta, \phi)$ falls off very rapidly as $\theta$ increases, so that the major contribution to $f_n(\theta, \varphi)$ comes from the first non-vanishing

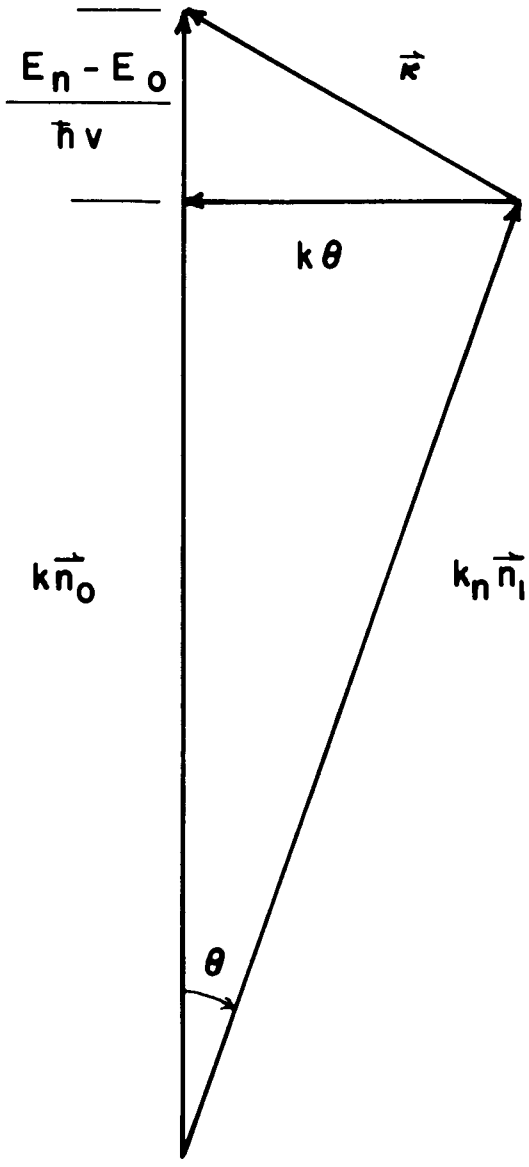


Figure 3.1 Momentum transfer diagram for an inelastic collision.

terms in a power series expansion of $e^{i\vec{\kappa n}\cdot\vec{r}_s}$ and we can write

$$|F_n(\kappa)|^2 \simeq \kappa^2 \left|\langle n| \sum_{s=1}^{Z} r_s |0\rangle\right|^2 = \frac{Q\ Z\ f_n}{E_n - E_o} \tag{3.3.10}$$

where $f_n$ is the oscillator strength for the dipole transition and the $f_n$ are subject to the sum rule

$$\sum_n f_n = 1 \tag{3.3.11}$$

The differential scattering cross-section for scattering into the solid angle $d\Omega = d\ (\mathrm{Cos}\ \theta)\ d\varphi$ is

$$\begin{aligned} \sigma(\theta,\ \varphi) &= \frac{k_n}{k} |f_n(\theta,\ \varphi)|^2 \\ &\simeq |f_n(\theta,\ \varphi)|^2 \\ &\simeq \left(\frac{2me^2}{\hbar^2 \kappa^2}\right)^2 \frac{Q\ Z\ f_n}{E_n - E_o} \\ &= \frac{e^2 Z}{Q} \frac{f_n}{E_n - E_o} \end{aligned} \tag{3.3.12}$$

and the energy loss rate can then be written as

$$-\frac{dE}{ds} = \sum_n N_n \int (E_n - E_o)\ \sigma\ (\theta,\ \varphi)\ d\ (\mathrm{Cos}\ \theta)\ d\varphi \qquad (3.3.13)$$

The sum is over the number of atoms $N_n$ capable of a transition to the state n. Since $\sigma\ (\theta,\ \varphi)$ is peaked for small $\theta$ we may write $d\ (\mathrm{Cos}\ \theta) \simeq \frac{dQ}{E}$ where $E = \frac{\hbar^2 k^2}{2m}$ is the energy of the incoming electron. Therefore

$$-\frac{dE}{ds} \simeq \sum_n N_n \frac{2\pi\ e^4\ Z\ f_n}{E} \int \frac{dQ}{Q} \qquad (3.3.14)$$

and the integral over Q is subject to limits determined by the minimum and maximum energy transfer to the atom. From the momentum transfer diagram we see $\kappa^2 \simeq \frac{(E_n - E_o)^2}{\hbar^2\ v^2} + k^2\ \theta^2$ and $Q_{min.}$ occurs for $\theta = 0$ and $Q_{min.} = (E_n - E_o)^2/4E$. The maximum value of Q is simply $E_n - E_o$ if we neglect transitions to the continuum. Therefore, writing $E_n$ for $E_n - E_o$,

$$-\frac{dE}{ds} = \sum_n \frac{2\pi\ e^4\ Z\ N_n\ f_n}{E}\ \ell n\ \left(\frac{4E}{E_n}\right) \qquad (3.3.15)$$

$$= \frac{2\pi\ e^4\ N\ Z}{E}\ \ell n\ \left(\frac{4E}{I}\right)$$

where

$$\ell n\ I = \sum_n f_n\ \ell n\ E_n \qquad (3.3.16)$$

Equation (3.3.15) is usually referred to as the Bethe Law, and in its above form is strictly valid only for non-relativistic particles, which poses no problem in our case, as we shall always be performing experiments with non-relativistic electrons. Furthermore, in deriving equation (3.3.15) it was assumed that the energy levels involved were those of isolated atoms. In solids the displacement of an electron from its equilibrium position sets up a polarization of the surrounding medium which tends to oppose the initial displacement.[40] This tends to change the effective frequency of the electron oscillations about equilibrium due to atomic binding forces from $\omega_n$ to $\omega_n'$ where $\omega_n'^2 = \omega_n^2 + \omega_p^2$ and $\omega_p = \sqrt{4\pi ne^2/m}$ is the plasma frequency. For nearly free electrons in a solid $\omega_n$ is very small, $\omega_n' \approx \omega_p$, and we have a loss mechanism which is characteristic of the solid, but which may be treated with a formalism established for free atoms. In fact in some solids, notably the metals, energy loss via plasmon formation can be the dominant loss mechanism i.e. it has the largest oscillator strength.[42] This is evident from experiments on the transmission of kilovolt electrons through thin foils in which it is found that the emerging electron has lost energy in amounts corresponding to the plasma energy. In addition to the plasmon losses there appear losses which arise from interband transitions of the electrons in the solid.[42, 43] These two loss mechanisms provide a solid state modification to the value of I, a mean excitation potential, in equation (3.3.15). Little theory is available for finding I and it is usually

determined from experiments on electron stopping powers, where the energy of a fast particle is determined after it has passed through successive thicknesses of material. In general, at least for large Z materials, $I/Z \approx 10\text{-}15$ e.v., with the lower value for high Z;[44] however, dE/ds is not particularly sensitive to the value of I.

The validity of the Bethe Law, equation (3.3.15) has been shown in experiments on the range of fast electrons in solids.[45-47] The Bethe range is defined by

$$R_B = \int_0^{E_o} \frac{dE}{dE/ds} \qquad (3.3.17)$$

This is the total distance an electron travels inside the material in coming to rest. What is measured in most experiments is the energy of an incoming fast electron which is just sufficient to penetrate a given thickness of the material, and this thickness is then called the range of the electron. Different definitions of range exist. In Figure 3.2 is shown an absorption curve for aluminum in which the current transmitted through the material into a $2\pi$ geometry collecting system is measured for a given thickness of material as a function of the energy of the incident electron. The energy marked $E_c$ is often called the "critical energy", and is defined by extrapolating the linear portion of the absorption curve. The critical energy corresponds to the so-called "practical range". The energy $E_{th}$ is called the "threshold

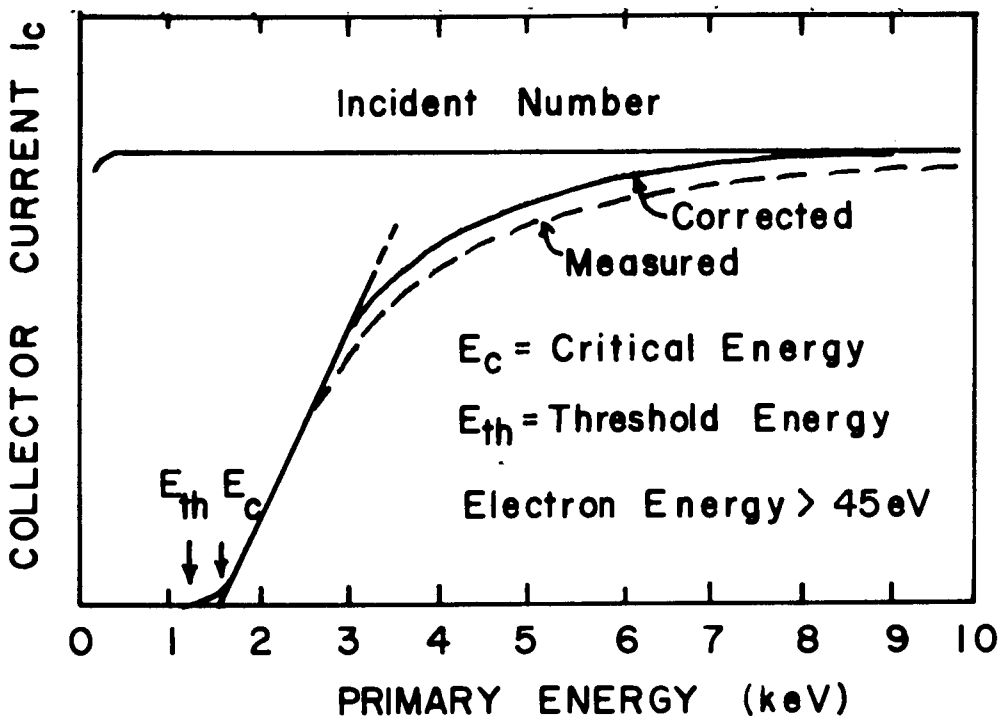


Figure 3.2 Typical electron absorption curve for an aluminum film of 17$\mu g/cm^2$ thickness (after Kanter and Sternglass(46).)

$E_c$ = Critical energy; $E_{th}$ = Threshold energy

The corrected curve includes corrections for the effect of secondary electrons emitted from the collector.

energy" and corresponds more closely to the maximum range, or Bethe range, of the electrons in the material, but is not as uniquely determined experimentally as the critical energy.

If experiments are performed at very high energies such that the path the incident particle follows is nearly straight, except for some straggling at the very end, then one can be reasonably assured that the range one measures is close to the integrated path length, or Bethe range. This has been done for a variety of materials and the Bethe Law verified, in that for each material, good agreement with experiment was obtained for a particular value of I, the mean excitation potential.[48] Ehrenberg and King[47] have shown that the calculated integrated path length, or Bethe range, scales with the measured range in a variety of materials in the energy range 10-80 keV, so that the Bethe Law appears to be valid down to these low energies. In fact Young[49] has shown that in $Al_2O_3$ agreement is obtained down to 0.6 keV. Also it has been shown that for materials with $Z \lesssim 25$ there exists a nearly constant relation between the two energies $E_c$ and $E_{th}$, such that $E_c = 1.4\ E_{th}$.[46]

So far we have found how the energy of the electron varies along the path it follows; the observable quantity in an experiment and the quantity of interest is the energy loss of the electron per unit distance into the material, i.e. we have found $dE/ds$ but we want $dE/dx$, where x is normal to the surface of a crystal and is also the direction of incidence of our fast electrons.

### 3.3.2 Spencer's Theory of Electron Penetration[44]

The theory which appears to rest on soundest theoretical foundation is that of Spencer[44] who has developed a method for finding the moments of the spatial energy distribution.

Spencer's model is the following: consider a monoenergetic electron source located at the plane $x = 0$ of an infinite medium. The source emits electrons in a direction normal to the $x = 0$ plane. A transport equation for the electron flux can then be written which takes into account both elastic and inelastic scattering. This transport equation can be transformed into a linked system of equations in the various spatial moments of the electron distribution, which can then be solved numerically. It should be mentioned that the moment equations involve a set of derived parameters which depend on the electron stopping power, electron range, and elastic scattering cross section. The stopping power, i.e. $dE/ds$, and the electron range ($R_B = \int \frac{dE}{dE/ds}$) are calculated from the Bethe formula, while the elastic scattering cross sections are the nuclear scattering cross sections modified to take screening by the atomic electrons into account.

Spencer has performed these calculations for some materials with initial energies down to 25 kv, and the results are given in tabular form in Reference 50 where methods for interpolating between different atomic numbers of the materials and between

different initial energies are given. The agreement with experiment is quite good where experimental data exists (see Figure 3.3). The data shown in Figure 3.3 is taken with a geometry, approaching as nearly as possible the infinite geometry assumed in the theory. The portion of the curve for $x < 0$ is the backscattered fraction of the incident energy which is smaller in Spencer's infinite geometry than in the conventional semi-infinite geometry of our experiments. In the conventional geometry those electrons which are backscattered leave the material while in Spencer's geometry they may be scattered again but into the positive half of the infinite medium where they can lose energy. This tends to raise the total area under the dE/dx vs x curve for $x > 0$.

### 3.3.3 Klein's Model of Electron Penetration[51]

Klein's approach is to bypass the electron transport equation and its mathematical complexity and seek an approximate phenomenological model that yields satisfactory agreement with experimental evidence.

The experimental evidence on which the model is based is the data of Ehrenberg and King[47] on the penetration of electrons into luminescent material. From a study of the glow-profile it is found that the glows show approximately spherical shapes or segments which move deeper into the material as the energy of the incident electrons increases and that along any radius vector from

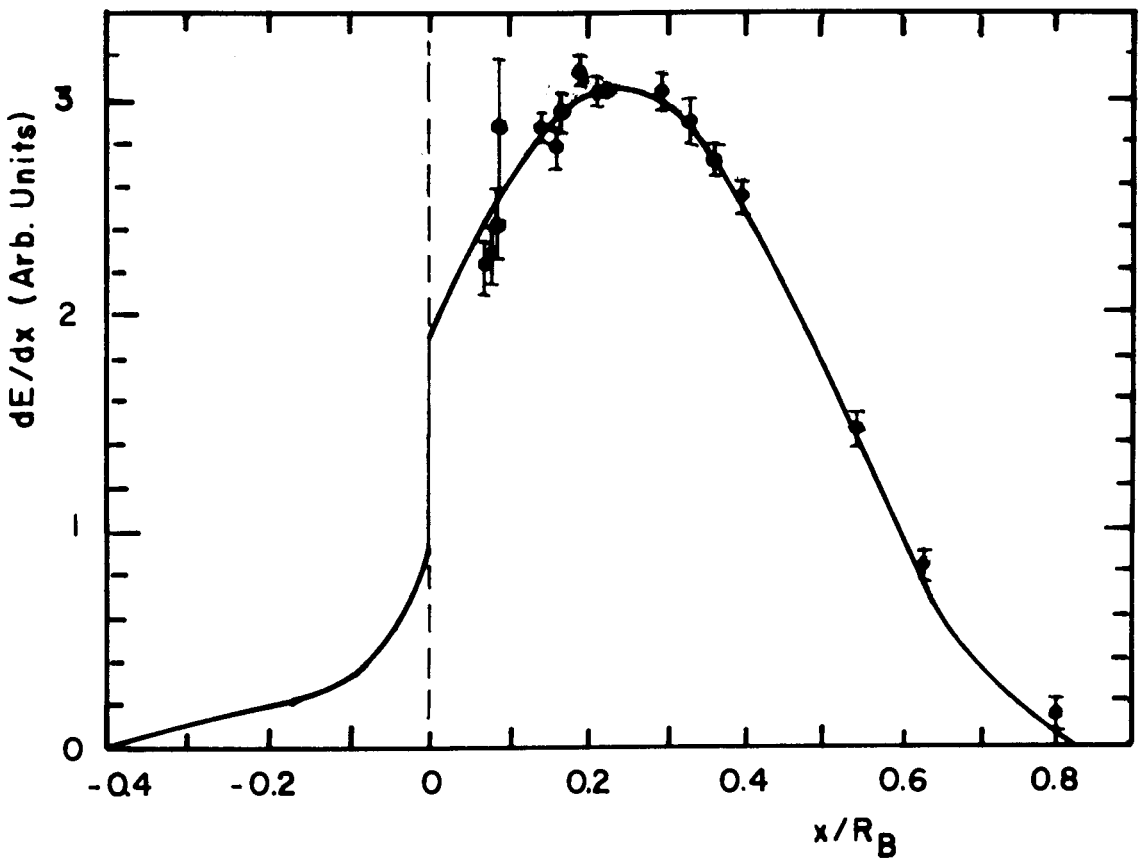


Figure 3.3 Comparison of experimental data in aluminum with energy dissipation data from Spencer(50). Experimental points 104 keV, curve theory 100 keV. $R_B$ is the Bethe range of the incident electrons.

the center of the glow the intensity varies very nearly in an exponential fashion.

The model then is to assume that the electrons travel straight into the material down to a certain distance $X_D$, without loss of energy, the "depth of complete diffusion", from which they move evenly in all directions to cover an overall path equal to the Bethe range $R_B$, see Figure 3.4. The model gives a representation of the observed isotropic spreading of electrons and automatically makes allowance for backscattering because some of the diffusing electrons recross the surface and cease participating in the excitation process.

If the energy dissipation density is C exp $(-\mu r)$, then the initial energy $E_o$ of the electron is

$$E_o = 4\pi C \int_o^{R_B - X_D} r^2 \exp(-\mu r)\, dr$$

$$\simeq 4\pi C \int_o^{\infty} r^2 \exp(-\mu r)\, dr \qquad (3.3.20)$$

$$= \frac{4\pi C}{\mu^3}$$

Therefore

$$C = \frac{\mu^3 E_o}{8\pi} \qquad (3.3.21)$$

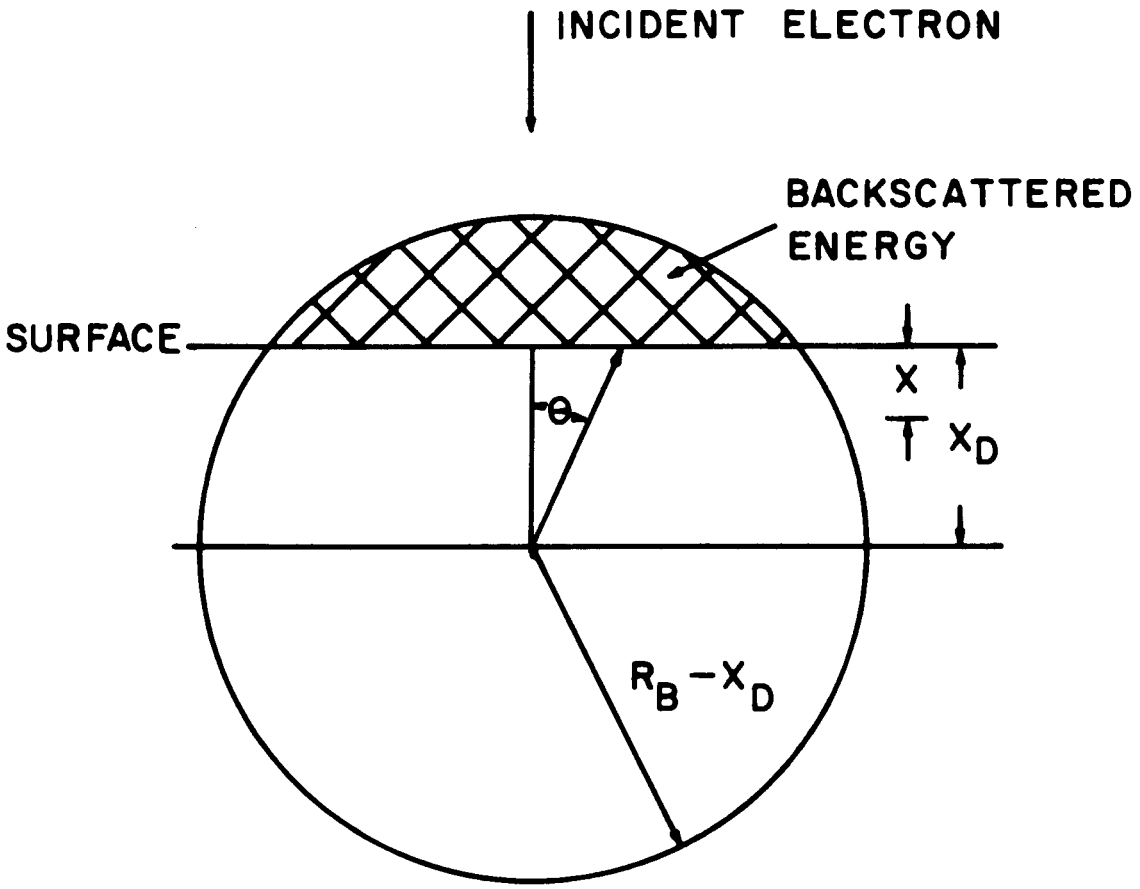


Figure 3.4 Illustrating energy backscattered.

We shall justify taking the upper limit as $\infty$ presently.

The energy backscattered into an annulus of radius r is then

$$dE = - \frac{E_o \mu^3}{8\pi} \exp(-\mu r)\, 2\pi r^2\, d(\cos\theta)\, dr \qquad (3.3.22)$$

and the total energy backscattered is, again taking the upper limit on the r integration as $\infty$,

$$\Delta E = - \frac{E_o \mu^3}{8\pi} \int_{r=X_D}^{\infty} dr \int_{\cos\theta=1}^{X_D/r} d(\cos\theta)\, 2\pi r^2 \exp(-\mu r) \qquad (3.3.23)$$

$$= \frac{E_o}{2}\left(1 + \frac{\mu X_D}{2}\right) \exp(-\mu X_D)$$

The energy E absorbed up to a distance X from the surface is $E = E' - \Delta E$ where $E'$ is the total energy lost by absorption and backscattering

$$E' = - \frac{E_o \mu^3}{8\pi} \int_{|X_D - X|}^{\infty} dr \int_{1}^{|X_D - X|/r} d(\cos\theta)\, 2\pi r^2 \exp(-\mu r) \qquad (3.3.24)$$

$$= \frac{E_o}{4}\left\{\mu|X_D - X| + 2\right\} \exp\left\{-\mu|X_D - X|\right\}$$

$$\frac{dE}{dX} = \frac{dE'}{dX}$$

$$= \frac{E_o \mu}{4} (1 - \mu|X_D - X|) \exp(-\mu|X_D - X|) \tag{3.3.25}$$

Since dE/dX peaks at $X = X_D$, a measure of the depth of complete diffusion can be obtained from Spencer's tabulations.[50] This gives, for $Z \geq 10$

$$x_D = X_D/R_B \simeq 3.1/Z \tag{3.3.26}$$

over the whole range of nonrelativistic energies.

In terms of $x = X/R_B$ the fraction of backscattered energy becomes

$$\frac{\Delta E}{E_o} = \frac{1}{2} \left[1 + \mu R_B \frac{x_D}{2}\right] \exp(-\mu R_B x_D) \tag{3.3.27}$$

while the differential energy loss is

$$\frac{dE}{dX} = \frac{E_o}{R_B} ① \tag{3.3.28}$$

$$① = \frac{\mu R_B}{4} (1 + \mu R_B |x - x_D|) \exp(-\mu R_B |x - x_D|) \tag{3.3.29}$$

Klein has plotted the backscattered energy fraction for different values of $\mu R_B$ against atomic number and compared his

results with experiment, and gets reasonable agreement with $\mu R_B \approx 11$. We see now that we are justified in letting $(R_B - X_D)$ become infinite in our integrations, in that $X_D << R_B$ and $\exp - \mu (R_B - X_D) \approx 0$. A comparison of Klein's and Spencer's theories is shown in Figure 3.5.

The function $\Phi$ depends on $\mu R_B$ and $x_D$, the reduced depth of complete diffusion, and determines the shape of the energy dissipation along the direction of penetration of primary electrons. The problem of determining the actual energy dissipation in a real crystal reduces to a determination of the Bethe range, which is done for the materials used in these experiments in Section 3.3.4.

In many respects it is really remarkable that such a simple theory, with one adjustable parameter gives such good agreement with experiment.

The physical origins of the peaking of the differential energy loss at some distance into the material are twofold - in the Bethe Law itself and in the change in direction of the incident electron as it moves into the material. From the Bethe Law (Equation 3.3.17) it is easy to show that there is a maximum in the differential energy loss at an energy $E = eI/4$, where e is the base of naperian logarithms. Since this energy is much smaller than the energy of the incident particle, the primary electron will have to travel some distance into the material

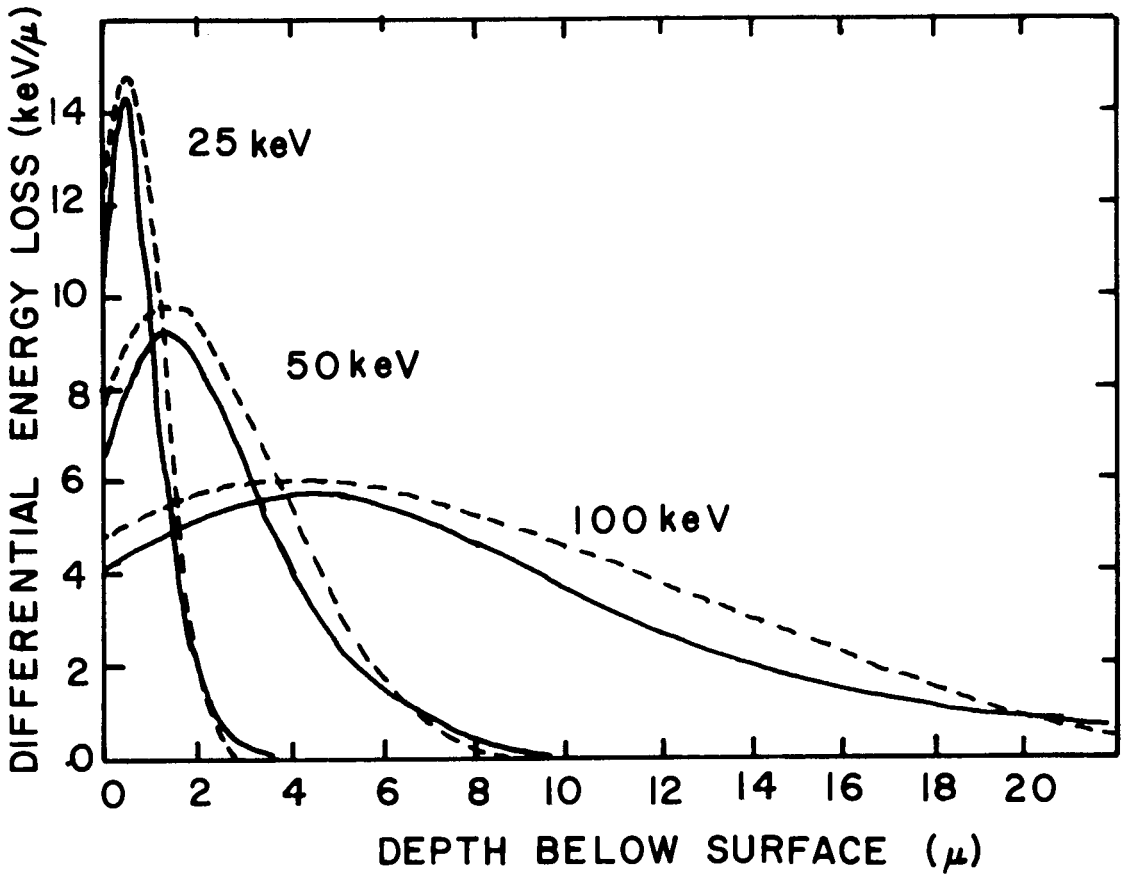


Figure 3.5 Energy dissipation pattern of 25, 50 and 100 kilo-volt electrons in GaAs (after Klein(51).) —— Klein, ---- Anderson(52) after Spencer(50). Spencer.

before the distance at which dE/ds peaks is attained. As an aside, it should also be mentioned that dE/ds at the surface of the material is smaller for larger energies - the origin of this is also in the Bethe Law. The other reason for the peak is in the change in direction the incident particle undergoes, upon suffering a collision. This has the effect of decreasing the component of the mean free path between collisions normal to the surface and increasing dE/dz. This occurs primarily near the end of the particle path when the total angular deviation of the particle path from the surface normal is greatest.

So far we have seen how the energy of the high energy electron is spatially deposited in the solid. This energy goes into the production of plasmons, the ionization of deeper lying atomic levels and the direct production of electron-hole pairs as well as phonons. Eventually the plasmons will decay producing electrons, holes and phonons, similarly for the higher energy excitations. The electrons and holes can and will be produced almost anywhere in k-space as the momentum of the incoming electron must be taken up somewhere. Unfortunately little can be said about the actual energy distribution of the electrons and holes produced by the incoming electron except that initially they can have any energy consistent with the band structure of the material and that the electrons and holes then decay separately via phonon emission to states at conduction band minima and valence band maxima respectively. This and the

spatial distribution of the energy are the two features of electron beam excitation which distinguish it from optical excitation.

### 3.3.4 Determination of dE/dx for CdS, $SiO_x$ and $CaF_2$

As mentioned in Section 3.3.3, Klein's theory for determining the differential energy loss can be used once the Bethe range of the high voltage electrons is known. There are two methods by which we may determine the Bethe range: (a) Spencer's tabulations[50] using appropriate interpolations between the materials for which range-energy data is tabulated, and (b) using Ehrenberg's data[47] on the luminescence profile in a variety of materials. We prefer to use Ehrenberg's data because his electron range is determined over a range of energies which is much closer to that used in our experiments and over a range of atomic numbers which brackets those used in our experiments much more closely. Also, Spencer's geometry is somewhat different from that of our experiments in that the zero plane is inside an infinite material while in the experiments, both ours and Ehrenberg's, the zero plane is the crystal surface bounded by vacuum. This causes Spencer's backscattered energy to be lower than found experimentally, since some energy is regained by the medium, and hence the area under Spencer's curves is too large (see Figure 3.5), and the range correspondingly smaller.

The Bethe range $R_B$ is found from

$$R_B = \int_0^{E_o} \frac{dE}{dE/ds} \qquad (3.3.30)$$

If we write dE/ds in a slightly different form from Equation (3.3.15)

$$\frac{dE}{ds} = 2\pi e^4 \, NZ \, \frac{\ell n \, (4E/I)}{E}$$
$$= 2\pi e^4 \, \left(\frac{Z}{A}\right) \, \rho \, \frac{\ell n \, (4E/I)}{E} \qquad (3.3.31)$$

where $\rho$ = density of the material. We see that

$$\rho \, R_B = \frac{1}{2\pi e^4 \, (Z/A)} \int_o^{E_o} \frac{E dE}{\ell n \, (4E/I)} \qquad (3.3.32)$$
$$\simeq B(Z) \, E_o^n$$

This integral can in fact be taken exactly in terms of a power series, but the series is very slowly convergent and the exponent n is best found from experiment for the energy range of interest. Over the energy range 10-80 keV, Ehrenberg's data gives an exponent n = 1.65. The problem now has been reduced to finding the constant B = B(Z). It was found that a good fit to a straight line could be obtained from Ehrenberg's data by plotting $B(Z) \cdot (Z/A)_{eff.}$ vs. Z, where for a complex molecule (formula $U_pY_q$) the effective value of Z/A is[45]

$$(Z/A)_{eff.} = \frac{p \, Z_u + q \, Z_y}{p \, A_u + q \, A_y} \qquad (3.3.33)$$

If a least squares fit to a straight line is performed we find

$$B\cdot(Z/A)_{eff.} = (4.486 + 0.02419Z)\cdot 10^{-3} \qquad (3.3.34)$$

if $\rho$ is in $gm/cm^3$, $R_B$ in cm and E in kev., which is shown in Figure 3.6.

A summary of the various parameters involved in electron penetration calculations in those materials used in our experiments is given in Table 3.1, and dE/dx for these materials is plotted in Figures 3.7 - 3.9 for a number of representative electron energies. For $CaF_2$ and $SiO_x$ we have used the value of B and the energy dependence of $R_B(n = 1.73)$ for Aluminum and scaled B for density only as our interpolation procedures become inaccurate for low Z. This procedure should not introduce appreciable error into our calculations as for these materials we are interested only in that small fraction of the total energy which is lost in the thin coating of $CaF_2$ or $SiO_x$ on top of the material of interest.

Also shown in Figure 3.7 is the absorption of 3000A photons whose absorption coefficient is $\sim 5 \times 10^4$ $cm^{-1}$.(22)

### 3.3.5 Use of the Curves of dE/dx when Crystal Coated with a Layer of $CaF_2$ or $SiO_x$

To find the energy loss inside the material of interest when it is coated with a layer of $CaF_2$ or $SiO_x$ we need to account

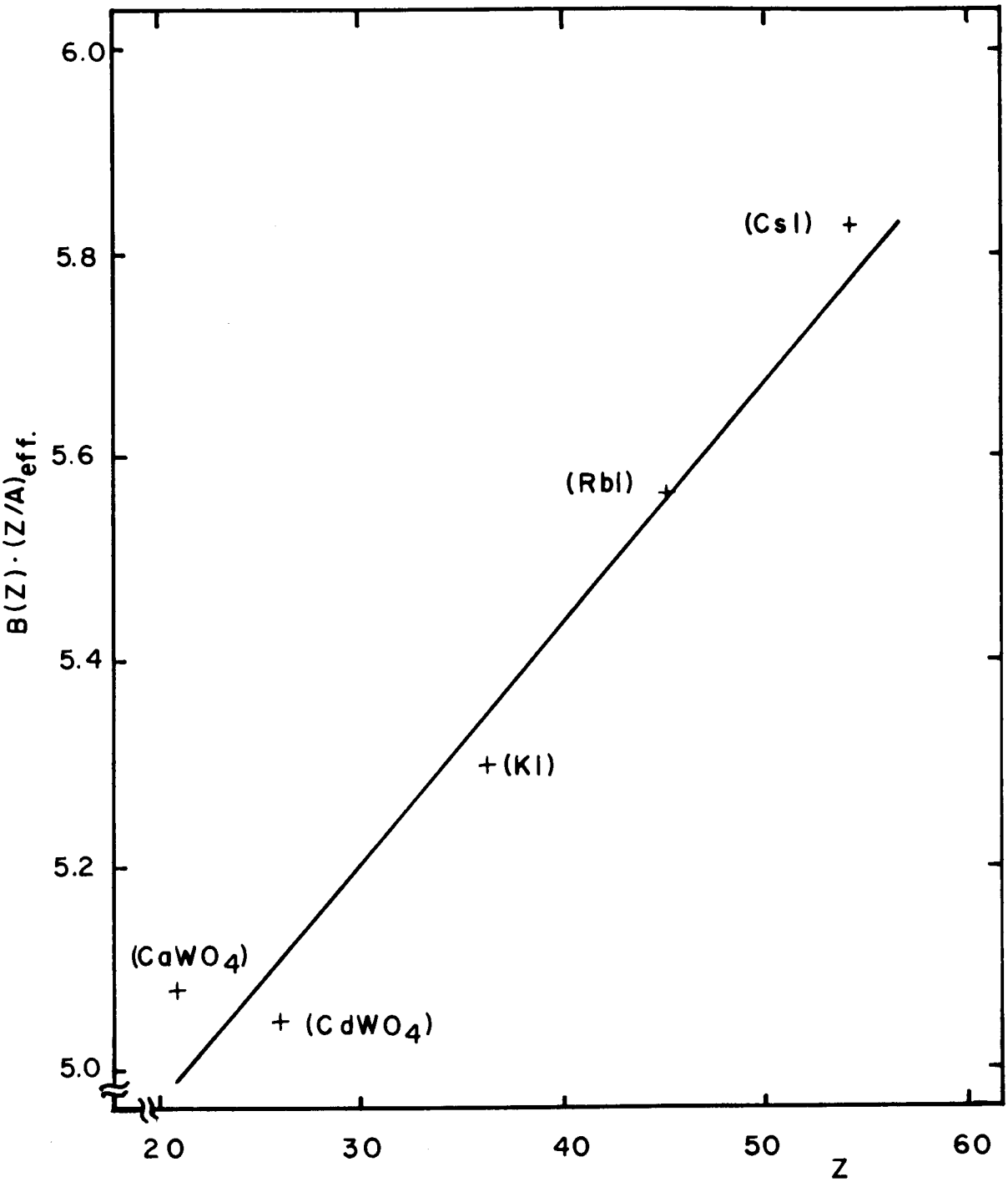


Figure 3.6 $B(Z)\ (Z/A)_{eff.}$ vs. Z. X Experimental, —— least squares fit.

| Material | $Z_{eff.}$ | $(Z/A)_{eff.}$ | Density $gm/cm^3$ | B x $10^3$ for $R_B$ in $gm/cm^2$ | $x_D$ | B for $R_B$ in Microns |
|---|---|---|---|---|---|---|
| CdS | 32 | 0.443 | 4.82 | 11.87 | 0.097 | 0.0246 |
| ZnTe | 41 | 0.425 | 6.34 | 12.9 | 0.0756 | 0.0204 |
| $CaF_2$ | 12.7 | 0.487 | 1.68 | 9.84 | 0.246 | 0.0585 |
| $SiO_x$ | 10.5 | 0.5 | 2.0-2.3 | 9.48 | 0.246 | 4.40* |
| Al | 13 | | 2.7 | 6.48 | 0.246 | 0.024 |

* Using Density 2.15 $gm/cm^3$.

Table 3.1 Parameters used in calculations of electron stopping.

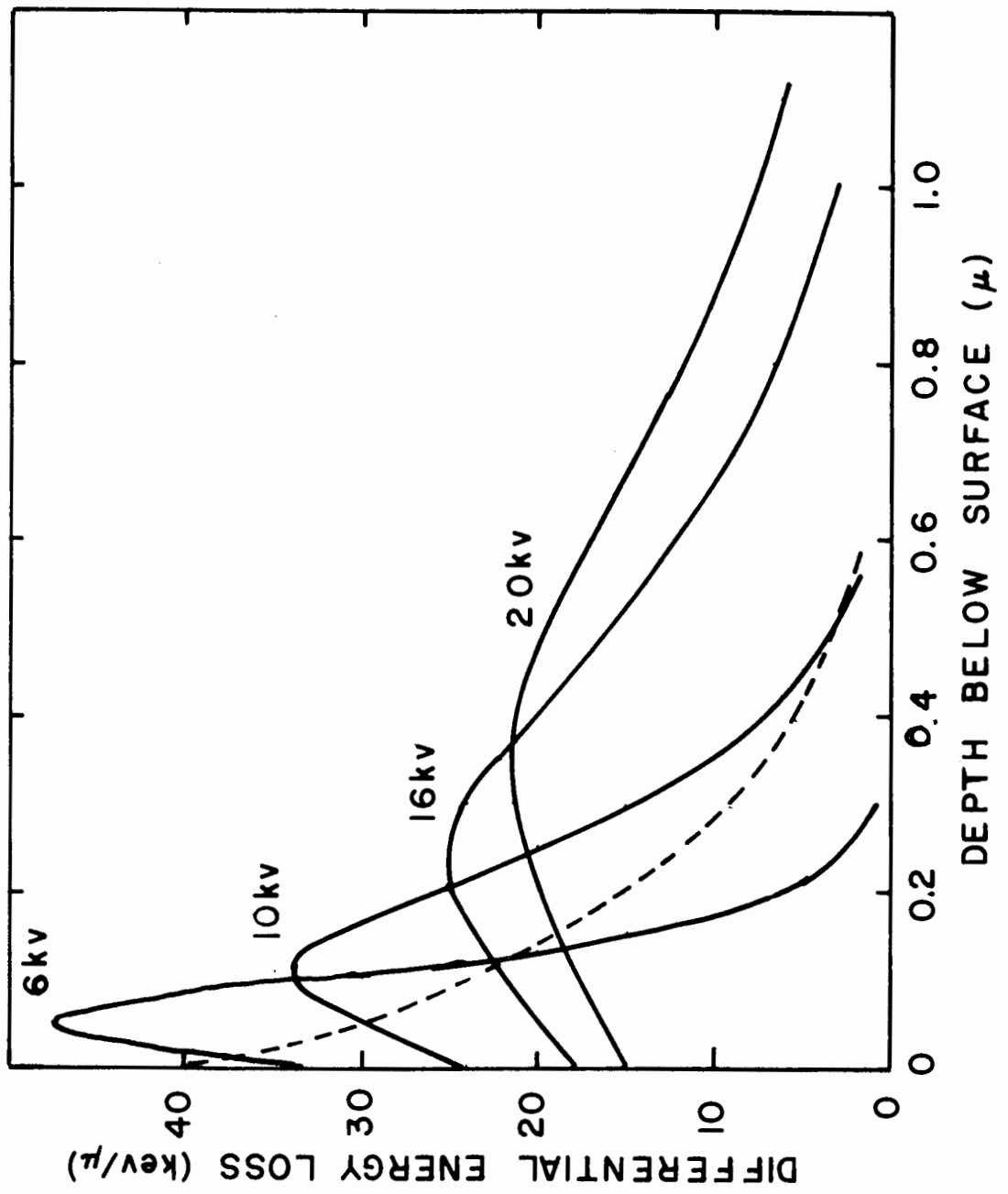


Figure 3.7 Energy dissipation pattern of 6, 10, 16 and 20 kV electrons in CdS. Dashed line - absorption of light whose absorption coefficient is $5 \times 10^4$ $cm^{-1}$.

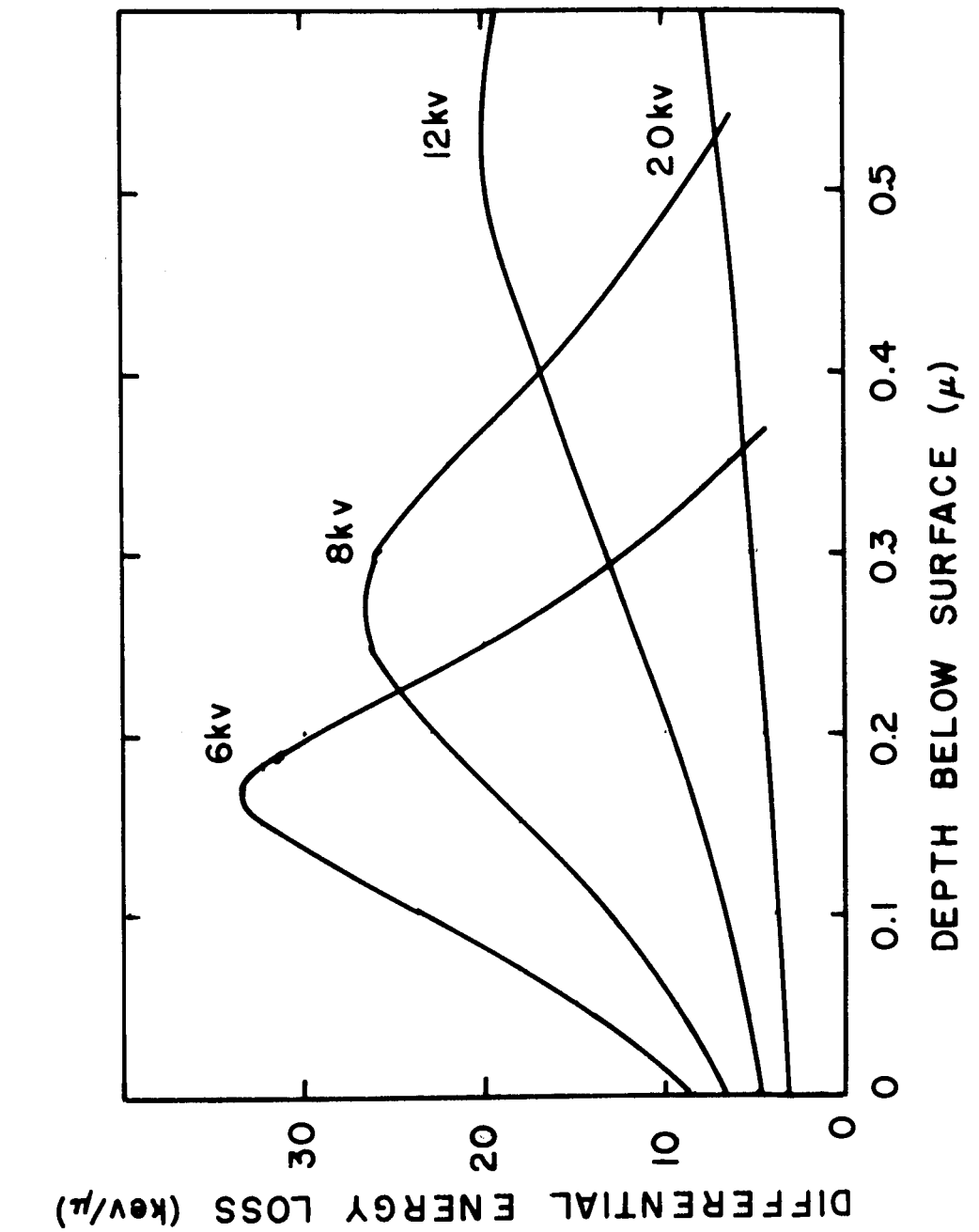


Figure 3.8 Energy dissipation pattern of 6, 8, 12 and 20 kv electrons in $SiO_x$.

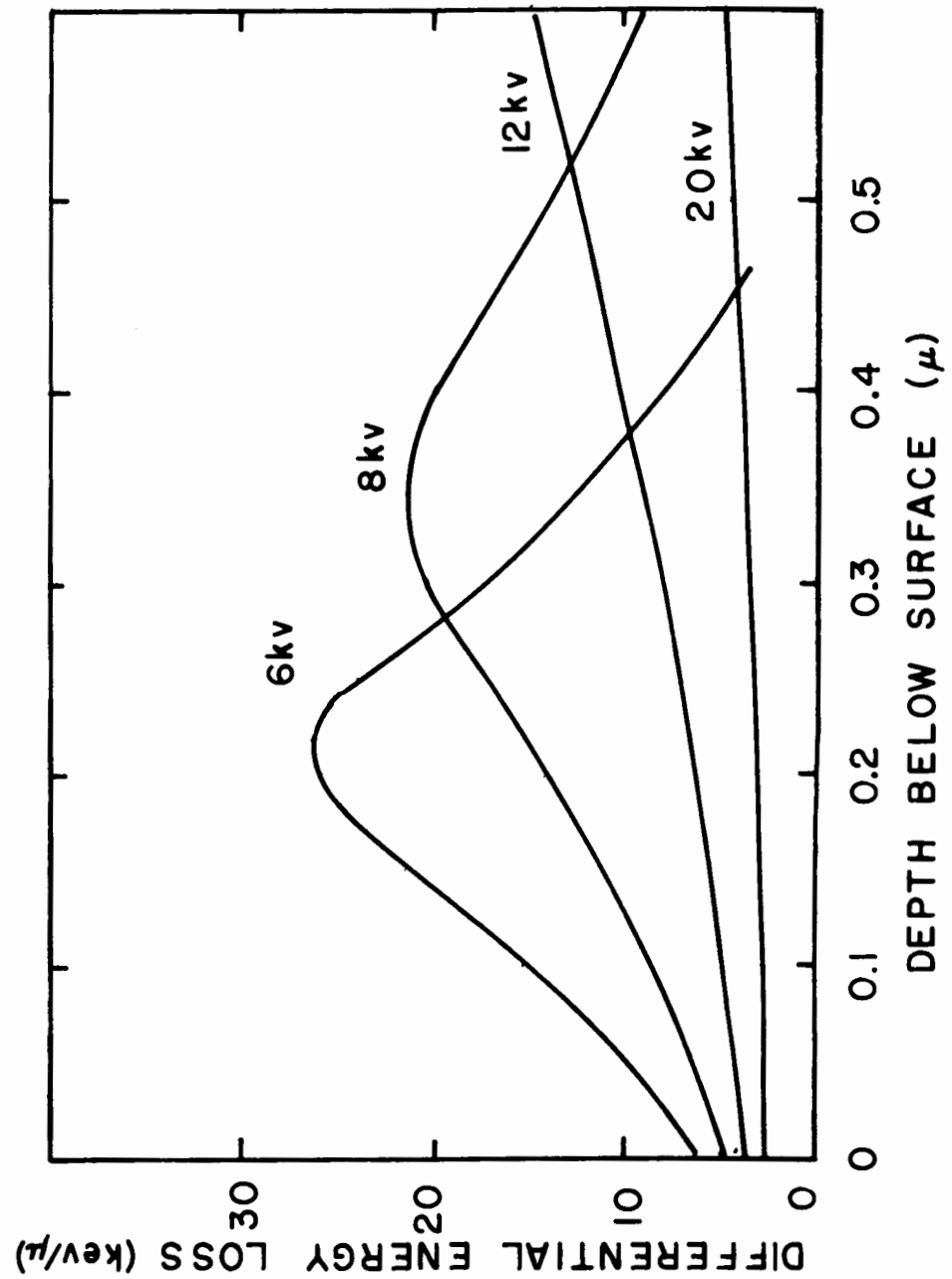


Figure 3.9 Energy dissipation pattern of 6, 8, 12 and 20 kv electrons in $CaF_2$.

for the energy lost in the coating. This can be done in one of two ways: (a) find the energy lost in the coating, subtract this from the beam energy and regard the electrons as entering the material with a new energy lowered by the amount lost in the coating or (b) find the energy lost in the coating and relocate the surface of the material of interest $\Delta_x$ further away from the zero plane of the dE/dx curves in such a fashion that the energy lost in the distance $\Delta_x$ is the same as the energy lost in the coating. The latter method is likely the more physical, but since the energy lost in the coatings is a fairly small fraction of the total beam energy, either method would be satisfactory as shown in Figure 3.10.

## 3.4 Comparison of Optical and Electron Beam Excitation

From Equation (3.2.15) we see that if we want to penetrate deeply into a solid using optical excitation we must use light of small absorption coefficient, which means light of energy less than the band gap energy and it may not be possible to excite higher energy states deep inside the crystal. Thus, if deep penetration is desired, as in cases where it is necessary to distinguish between surface and bulk effects, and it is desired to populate states at energies near or above the conduction band edge it may be necessary to use an electron beam as the exciting source. Another instance where electron beam excitation is preferable over optical excitation occurs when the efficiency

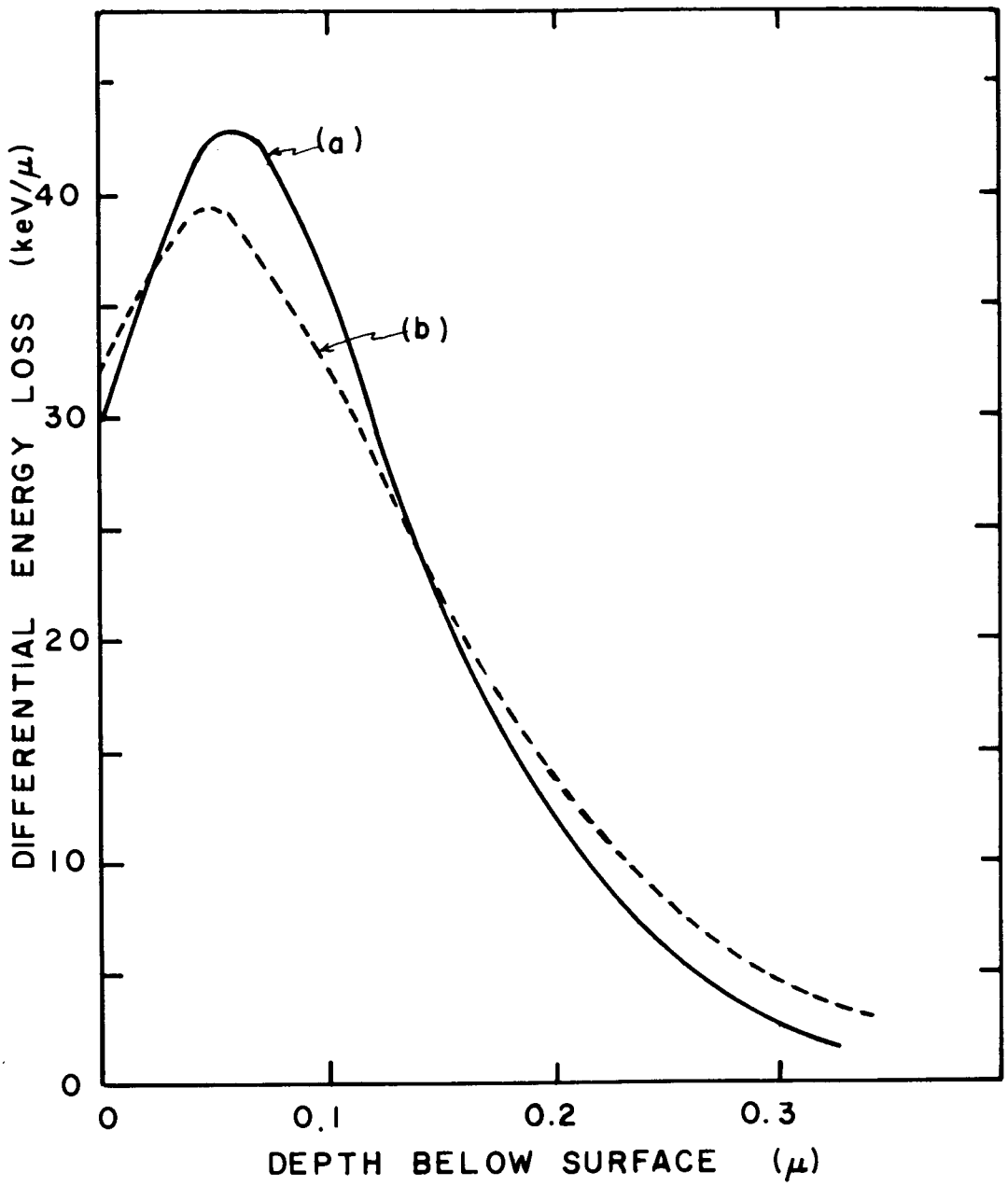


Figure 3.10 Energy dissipation pattern of 8 kv electrons in CdS. (a) Initial energy recalculated, (b) zero plane relocated.

of a radiative process of interest is very low and existing light sources are not sufficiently intense to provide sufficient stimulation. An example of this is the electron beam excited semiconductor laser where conventional light sources provide insufficient radiation at energies that are not absorbed in a very narrow region near the surface; electron beams can provide ample power to depths of tens of microns where the extent of the radiating region is sufficiently large that diffraction losses are small. For example, electron guns can readily supply 100 m.a. at 25 kv, or 2500 watts, either pulsed or continuously, while the total useable power from the best available conventional light sources will rarely exceed one watt. Another example of the advantage of the electron beam is in the work reported in Chapter 5, where an inefficient luminescent process is studied and the effect of surface treatments is probed by varying the penetration depth of the incident electrons.

The main advantage of optical excitation is in the vertical excitation of electrons from lower to higher energy levels which arises from the negligible momentum of the incident photons. This kind of selective excitation is certainly not possible with electron beams. An example of the advantage of optical excitation is the study of optical excitation spectra of different luminescent centers or complexes which allow one to deduce creation mechanisms for these centers. This kind of study is reported in Chapter 4.

# 4. OPTICAL EXCITATION SPECTRA

## 4.1 Introduction

This chapter deals with the design criteria of equipment needed for the study of optical excitation spectra. Results are presented on the excitation spectra of several exciton emission lines in CdS.

## 4.2 Experimental Techniques and Apparatus

In studies of photo luminescent properties of materials it is usual to use a broad band monochromator or narrow pass filter to select above-band-gap radiation which is incident on the sample. A high resolution spectrometer is then desirable for use as the detecting instrument in order to determine accurately the wavelength and lineshape of the emitted radiation. When studying the excitation spectrum of the emitted radiation the detecting spectrometer need have only sufficient resolution to discriminate between the different emission lines but it should have a large acceptance angle so that as much emitted light as possible may be detected. The requirements for the monochromator now are that it accept as much light as possible from the light source and have high resolution as well.

In our case the lamps used, either a high pressure xenon or mercury lamp, could be focussed to give a spot about 1-2 mm in diameter with a beam angle of approximately 10°. This beam angle

corresponds almost exactly to the acceptance angle of the Spex Industries Model 1700 spectrometer whose dispersion in second order with the grating used is 5A/mm. Thus a slit width of 1 mm allows nearly all the light from the lamp to be accepted by the spectrometer while a monochromatic beam of light whose spectral full width at half maximum intensity (FWHM) is about 5A is obtained. This is adequate for most of the experiments performed, although in some cases the FWHM used was less than 2A. In CdS the emission lines are at least 20A apart, so that a resolution of 5A in the detecting spectrometer is quite adequate.

The apparatus used for studying the optical excitation spectra of CdS is shown schematically in Figure 4.1. An innovation included in the arrangement is the use of an electronic dividing network to normalize the intensity of the emitted light with respect to the intensity of the light incident on the crystal. This is achieved by removing a small fraction (about 4%) of the incident light with a beam splitter, (in reality a glass slide) detecting this light with a photomultiplier and electrometer and feeding the signal from this photomultiplier into the denominator of the divider while the signal from the detecting photomultiplier goes into the numerator. In this way fluctuations in the intensity of the lamp and variations in the lamp spectrum are electronically taken care of, eliminating the need for tedious hand normalization of data. This technique is

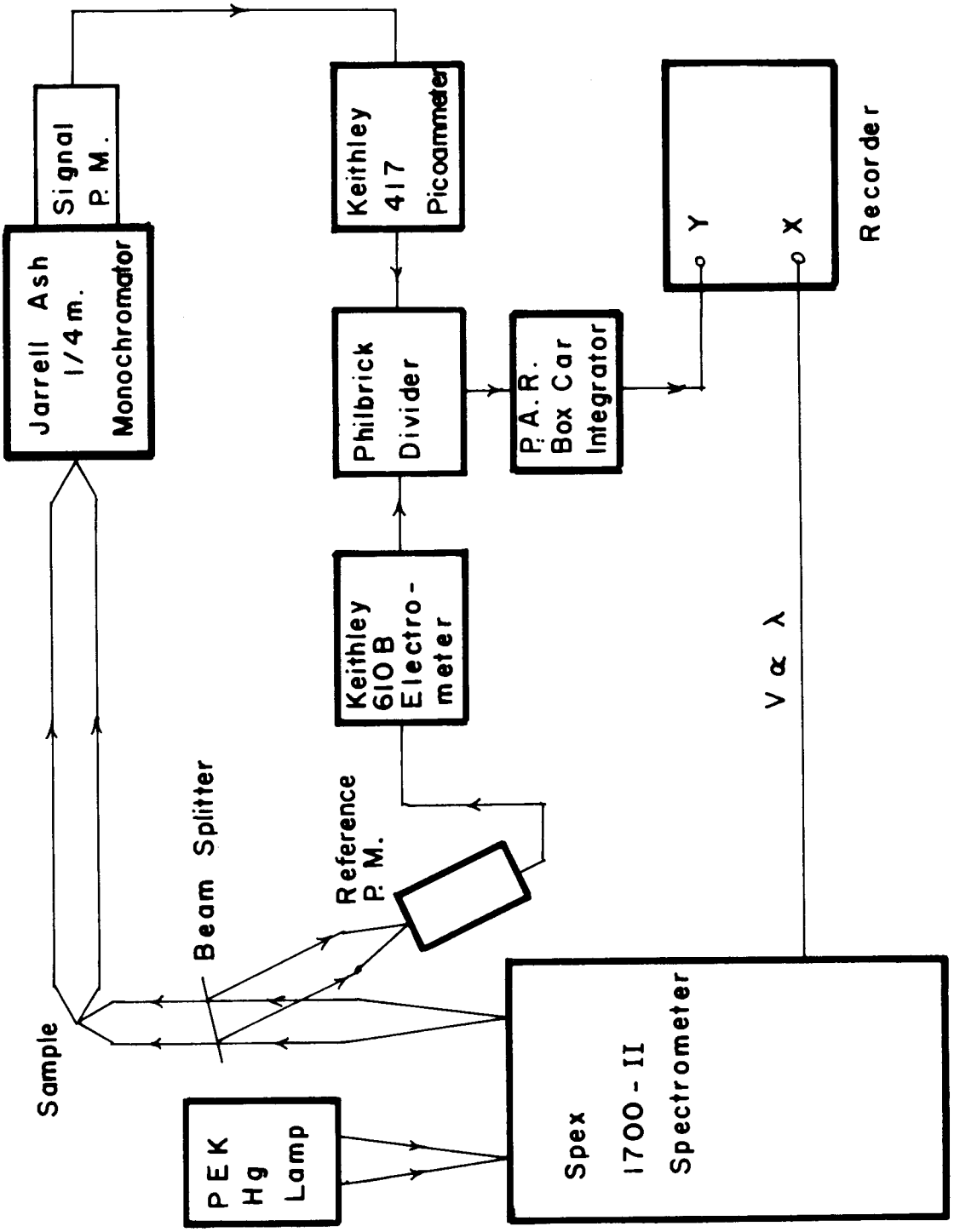


Figure 4.1 Schematic of apparatus used to obtain optical excitation spectra.

valid provided the emission from the crystal bears a linear relationship to the intensity of the incident radiation.

When using polarized incident light the polarizer must be placed between the monochromator and the beam splitter in order that the emission intensity be normalized with respect to the intensity of the light incident on the sample, not to the intensity of the light from the monochromator which is itself strongly polarized.

## 4.3 Sample Preparation and Mounting

In nearly all cases the samples used had been freshly cleaved and mounted with rubber cement or silicon vacuum grease. In some cases, where material was scarce, the samples were etched at room temperature with concentrated sulphuric acid in which enough $KMnO_4$ had been dissolved to turn the acid light green. This etch allowed the structure in the excitation spectra to be as sharp and well defined as for cleaved surfaces, but in some cases the relative intensities of some peaks changed, presumably due to changed surface recombination velocities.

The samples were either immersed in liquid helium or liquid nitrogen or mounted in high vacuum on the helium finger of a dewar the end of which was made of high conductivity copper so that the sample was in contact with a surface whose temperature differed only slightly from that of the refrigerant.

All exciton excitation spectra were taken at liquid helium temperatures.

Care had to be taken in aligning the crystal to ensure that as little incident light as possible was reflected into the collecting optics. The reasons for this are two-fold; (a) the weaker the reflected or scattered light the closer to the emission lines could one look for structure in the excitation spectrum and (b) all grating spectrometers have grating ghosts, which can be reflected into the detecting system and misinterpreted as structure in the excitation spectrum. This is of importance when the intensity of the emitted light is comparable to or weaker than the intensity of the grating ghosts which is the case in some of our experiments.

## 4.4 Excitation Spectra of CdS

### 4.4.1 Emission Lines Studied

The apparatus described for taking excitation spectra has been used to study the exciton excitation spectra of three different CdS samples in detail. These samples, labelled 1, 2 and A, each show two exciton emission lines. All samples have one emission line $I_1$ at 4888.5 Å in common. This line has been identified by Hopfield and Thomas[8] as resulting from the recombination of an exciton bound to a neutral acceptor. The hole of the exciton is a hole from the A or uppermost valence band, which is active for $E \perp c$; therefore $I_1$ is emitted with the

light strongly polarized with the E vector normal to the crystal c-axis. Weaker satellite lines are also seen at energies corresponding to $I_1 - n\hbar\Omega$ (n = 1, 2), where $\hbar\Omega$ is the LO phonon energy.

Crystals 1 and 2 have their second emission line at 4869.5 Å while crystal A emits at 4868.3 Å. Reynolds and Litton[31] have observed an emission line $I_5$ in some CdS crystals at 4869.14 Å which they identify as the recombination of an exciton bound to a neutral acceptor, although their data is such as to make this identification somewhat tentative. Thomas and Hopfield[8] on the other hand conclude that emission lines near 4867.14 Å result from the recombination of an exciton bound to a neutral donor. Thomas, Dingle and Cuthbert[53] have shown that crystals grown under different but controlled atmospheres have a sharp emission line in the range 4867-4870 Å which is taken as evidence that the exciton responsible for this emission is bound to a neutral donor, the nature of the donor depending on the atmosphere in which the crystal was grown. The similarity of the excitation spectra for the 4868.3 and 4869.5 Å lines supports Thomas'[53] hypothesis.

This second emission line is also polarized strongly with the E vector normal to the crystal c-axis indicating that the recombination involves a hole from the A valence band.

### 4.4.2 Excitation Spectrum of $I_1$

Shown in Figure 4.2 is the excitation spectrum of the $I_1$ line in crystal 1. Except for some differences in the relative intensities of the different lines the spectrum is the same for crystal 2 and, under certain conditions to be discussed, also for crystal A. The wavelengths and energies of all the peaks are summarized in Table 4.1.

From this data it is concluded that the complex responsible for the $I_1$ emission is formed preferentially either directly by the production of a bound A, B or C exciton on a neutral acceptor, resulting in the peaks labelled $I_1$ (seen in the phonon replica emission), $I_{1B}$ and $I_{1C}$ or by the formation of free A, B or C excitons which diffuse through the crystal and are subsequently trapped on a neutral acceptor.

The exciton-impurity complex so formed consists of one electron, a hole from the A, B or C valence band and the hole which neutralized the acceptor. This latter hole is most likely a hole from the A valence band. Since the emitted light is strongly polarized with $E \perp c$ this suggests that the hole taking part in the emission is the hole neutralizing the acceptor, if the other hole is not from the A valence band. Care must be taken in talking of the hole of an exciton being associated with a particular valence band, particularly one of the lower valence bands, in that the wavefunction for such a hole is bound to be

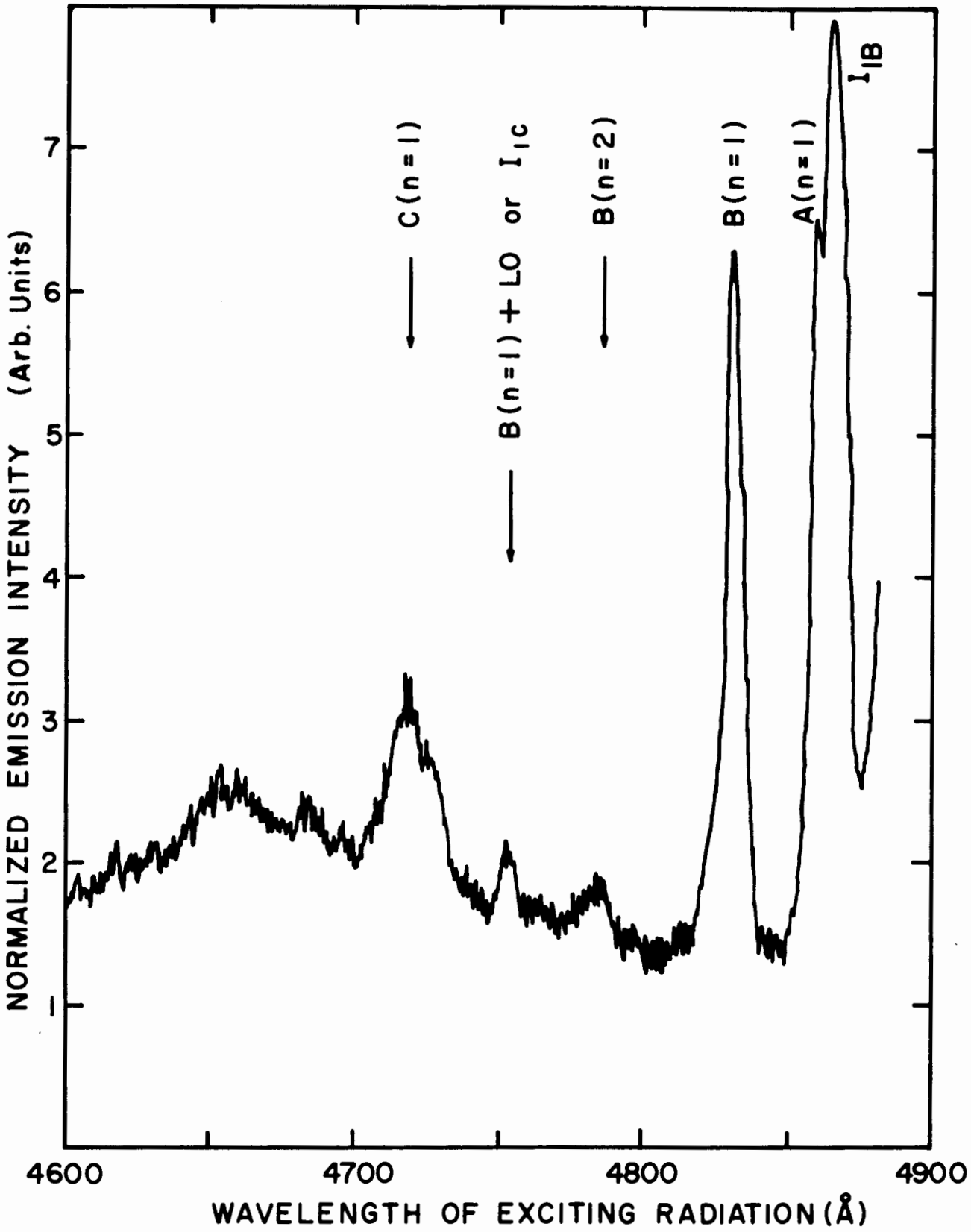


Figure 4.2 Excitation spectrum of the $I_1$ emission line.

| Crystal | Emission Line | Peak Position in Excitation Spectrum | | Polarization Active in Formation of Exciton Complex | | Assignment | Remarks |
|---|---|---|---|---|---|---|---|
| | | Wavelength (Å) | Energy (e.v.) | E⊥c | E∥c | | |
| 1 | $I_1$ | 4862.5 ± 2 | 2.5494 | | Yes | $I_{1B}$ (2.5488 e.v.) | Strong |
| | | 4856.0 ± 2 | 2.5528 | Yes | | A (n = 1)(E = 2.5537 e.v.) | Strong |
| | | 4827.5 ± 2 | 2.5679 | Yes | Yes | B (n = 1)(E = 2.5686 e.v.) | Strong |
| | | 4781.5 ± 5 | 2.5926 | Yes | Yes | B (n = 2)(E = 2.5908 e.v.) | Weak |
| | | 4751.0 ± 5 | 2.6092 | Yes | Yes | B (n = 1) + LO (E = 2.606 e.v.) or $I_{1c}$ (E ~ 2.606 e.v.) | Weak |
| | | 4715.0 ± 5 | 2.6291 | Yes | Yes | C (n = 1)(E = 2.632 e.v.) | Weak |
| | $I_1$ - LO | 4828.5 ± 2 | 2.5673 | Yes | Yes | B (n = 1)(E = 2.5686 e.v.) | |
| | | 4857.5 ± 2 | 2.5520 | Yes | | A (n = 1)(E = 2.5537 e.v.) | |
| | | 4865.0 ± 2 | 2.5481 | | Yes | $I_{1B}$ (E = 2.5488 e.v.) | |
| | | 4890.0 ± 2 | 25351 | Yes | | $I_1$ (E = 2.5359 e.v.) | |
| 2 | $I_1$ | 4860 ± 2 | 2.5510 | | Yes | $I_{1B}$ | |
| | | 4851 | 2.5555 | Yes | | A (n = 1) | |
| | | 4827.5 | 2.5682 | | Yes | B (n = 1) | |
| | | 4826 | 2.5690 | Yes | | B (n = 1) | |
| A | $I_1$ | 4862 ± 2 | 2.5500 | | Yes | $I_{1B}$ | Cooled under u.v. illumination |
| | | 4855 | 2.5537 | Yes | | A (n = 1) | |
| | | 4826 | 2.5693 | Yes | Yes | B (n = 1) | |
| | $I_1$ | 4860 ± 2 | 2.5510 | | Yes | $I_{1B}$ | Cooled in dark |
| | | 4862 ± 2 | 2.5495 | Yes | | $I_{1B}$ | |
| | | 4827 | 2.5685 | | Yes | B (n = 1) | |
| | | 4826.5 | 2.5687 | Yes | | B (n = 1) | |

Table 4.1

Position of Peaks in the Excitation Spectrum of $I_1$ and $I_1$ - LO.

an admixture of states from all bands. It is then possible for a "B hole" to change its character and become an "A hole" before the exciton recombines. If this occurs then the emission will be polarized with the E vector normal to the c-axis irrespective of the nature of the exciton which was created on the impurity site.

All lines in the excitation spectrum have the polarization dependence corresponding to the valence band from which the hole of the exciton originates, although it is not understood why the $I_{1B}$ peak is active only for $E \| c$ and not for $E \perp c$.

The above described excitation spectrum for the $I_1$ emission line is found in crystals 1 and 2 and in crystal A if it is cooled from room temperature with above-band-gap radiation incident on the crystal. If crystal A is cooled in the dark the peak corresponding to the formation of free A excitons disappears and $I_{1B}$ is now active in both polarization modes. This suggests that there is some competition between $I_{1B}$ and the free A exciton, the relative strength of the two lines depending on the initial conditions of the experiment.

It should be mentioned that all crystals used, but crystal A in particular, showed thermo-luminescence as the crystal was heated from 77°K after exposure to ultraviolet radiation, so the crystal has some long-lived or metastable states at low temperatures which may be responsible for the absence of some peaks in the $I_1$ excitation spectrum.

### 4.4.3 Excitation Spectra of $I_5$ and $I_2$

While the complex responsible for the $I_1$ emission is created preferentially by the production of free A, B and C excitons and the creation of A, B or C excitons directly on the acceptor site, the complex responsible for the $I_2$ or $I_5$ emission is created predominantly by phonon assisted formation, although each of the three crystals has a somewhat different excitation spectrum.

The excitation spectrum of the 4869.5 A line in crystal 1 is shown in Figure 4.3. Peaks in the emission intensity are observed whenever the energy of the exciting light differs from $I_5$ by an integral multiple of $\hbar\Omega$, the (k = 0) LO phonon energy. The fact that the spacing of the peaks corresponds to $\hbar\Omega$ rather than to $\hbar\Omega\ (1 + m_c/m_v)$ where $m_c$ and $m_v$ are the conduction and valence band electron effective masses, means that the bound exciton complex is formed directly with the emission of one or more LO phonons. If we were dealing with the formation of electrons and holes with the electron decaying via LO phonon relaxation, the hole, if it is to have the same momentum as the electron, must lose energy $\hbar\Omega m_c/m_v$, and the total energy difference between peaks would be $\hbar\Omega\ (1 + m_c/m_v)$. This type of behaviour is seen in the photoconductivity spectrum of InSb.[54]

A peak in the $I_5$ emission is also seen when the energy of the incident light corresponds to that of the free B exciton.

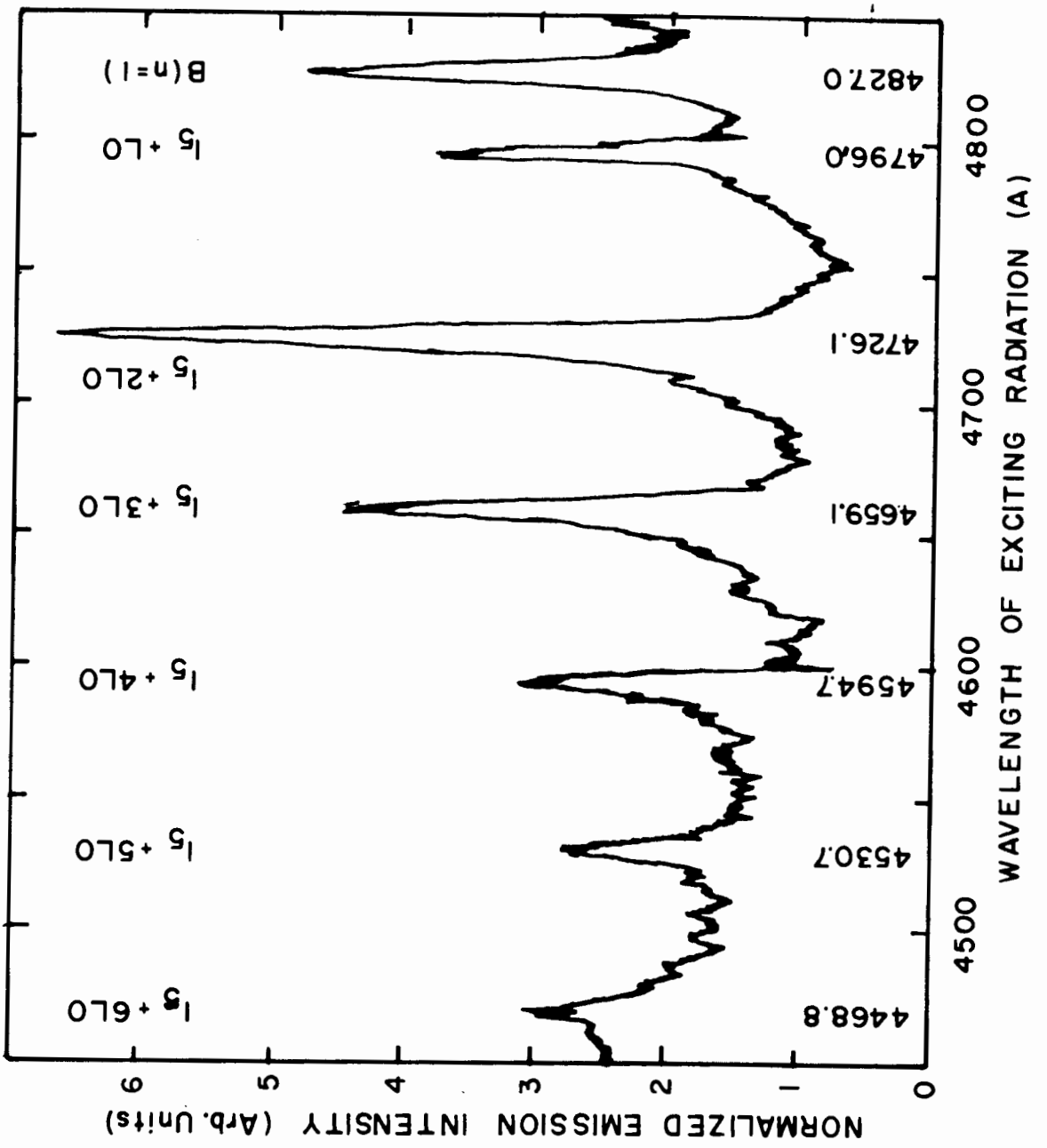


Figure 4.3 Excitation spectrum of the $I_5$ emission line. in crystal #1.

These excitons diffuse through the crystal and are captured by the impurity and recombine emitting light corresponding to $I_5$. This formation mechanism is the same as for the $I_1$ emission except that the impurity is different. Again, since the emission is strongly polarized with $E \perp c$ it would appear that recombination of an electron with an "A-hole" takes place. If the $I_5$ emission results from the recombination of an exciton bound to a neutral donor the hole must have changed its character prior to recombination, which was postulated as a possible mechanism in the $I_1$ emission. Other evidence for this hole conversion exists in the absorption spectrum of $I_2$, an exciton bound to a neutral donor.[8] As mentioned in Chapter 2 a broad absorption line $I_{2B}$ exists which is identified as the direct formation of a B exciton on the neutral donor site. The large width of this line is attributed to the short lifetime of the B-hole which converts very quickly to an A-hole. A similar conversion would appear to be operative here.

The excitation spectrum for the $I_5$ emission line in crystal 2 is shown in Figure 4.4. This spectrum is the same, within experimental error, as the $I_5$ excitation spectrum in crystal 1, except for the addition of a weak peak at 4838.5A and a second series of peaks which are separated from the $I_5 + m\hbar\Omega$ peaks by a fixed energy $\Delta E = 3.9 \pm 0.8$ mev. This spacing is, within experimental error, equal to the spacing of the $I_2$ and $I_3$ absorption lines seen by Thomas and Hopfield[6, 8] which they have

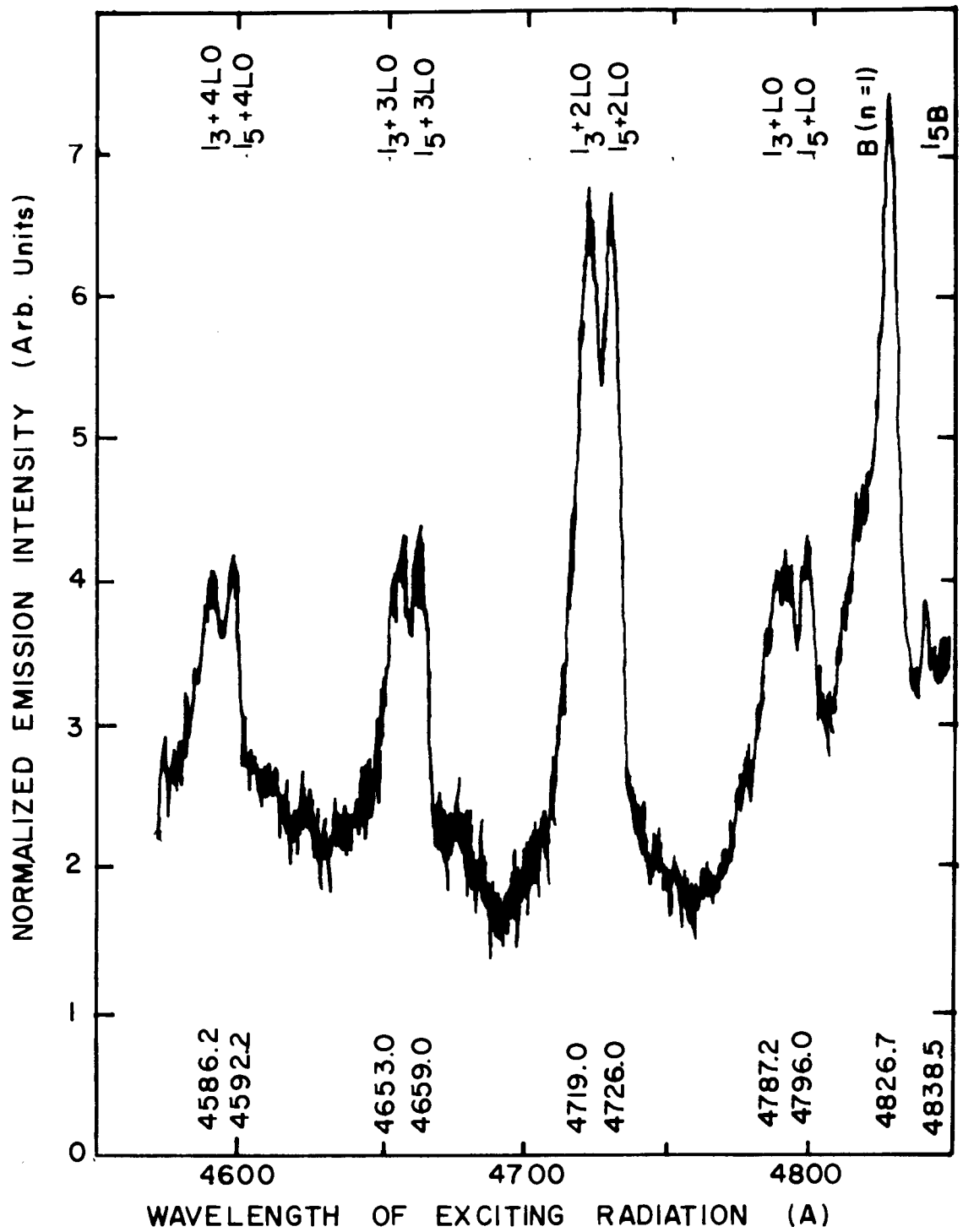


Figure 4.4 Excitation spectrum of the $I_5$ emission line in crystal #

attributed to excitons bound to neutral and ionized donors. The peak at 4838.5A corresponds, by comparison with $I_2$, to the direct formation of a B exciton on the impurity site and is labelled $I_{5B}$.

Both crystals 1 and 2 are high resistivity n-type crystals, the room temperature resistivity being in excess of $10^7$ ohm-cm.(55) The crystals must therefore either be of extremely high purity or, more likely, be compensated with the result that the donors are nearly all ionized. Thus there is a large density of ionized donors on which excitons may be formed. The two series of peaks result from the direct phonon-assisted formation of excitons on neutral and ionized donors. In the case of the series based on $I_5$, the exciton bound to a neutral donor, the donor must be neutral before the exciton can be created directly on the impurity. The donor is neutral either by virtue of the material being n-type, i.e. the density of donors exceeds the density of acceptors, or if the material contains a substantial density of ionized donors the ionized donor first captures an electron, the electron having been excited into the conduction band by the external light source, and the exciton is then created on the neutral donor where it recombines giving off light corresponding to $I_5$. In the case of the series based on $I_3$, the exciton bound to an ionized donor, the exciton is first formed directly on the ionized donor, this complex then captures an electron which has been excited into the conduction band and emission at the energy corresponding to $I_5$ can now take place.

The two series of peaks thus result from essentially the same two physical processes - direct phonon assisted creation of an exciton bound to an impurity and electron capture - only the order in which the processes occur is reversed.

All the peaks in the $I_5$ excitation spectrum occur in both polarizations ($E \perp c$ and $E \parallel c$) of the incident light with about equal efficiency except that the one phonon peak is very weak for $E \parallel c$ indicating that the valence band states involved in this one case are predominantly from the A valence band.

In view of the two physical processes involved in creating the exciton-neutral donor complexes it is perhaps intuitively reasonable that the two series of peaks should have nearly the same intensity. However, as will be shown below, the relative intensity of the two peaks is affected by parameters of the crystal about which little is known, and the relative intensities may in fact be quite different.

Let us assume for simplicity we are dealing with a perfectly compensated crystal in which all donors are ionized, and let the optical absorption coefficient be the sum of three separate contributions from (1) interband absorption $\alpha_n$ (2) direct phonon assisted exciton formation on neutral donors $\alpha_2$ and (3) direct phonon assisted exciton formation on ionized donors $\alpha_3$. At this stage any rigorous distinction between $I_2$ and $I_5$ will be dropped as both are excitons bound to neutral donors. For convenience

only the emission line at 4869.5A in crystals #1 and #2 will be referred to as $I_5$.

For purposes of illustration let us consider the case of direct allowed transitions for which $\alpha_n = A\,[\hbar\omega - E_g]^{\frac{1}{2}}$

$A$ = constant

$\hbar\omega$ = energy of the incident photon

$E_g$ = energy gap

$\alpha_2$ and $\alpha_3$ consist of a series of sharp peaks at photon energies such that

$$\hbar\omega_2 = E_2 + m\hbar\Omega$$

$$\hbar\omega_3 = E_3 + m\hbar\Omega$$

$$m = 0, 1, 2 \ldots$$

where $E_2$ is the energy of the $I_2$ or $I_5$ emission or absorption line

$E_3$ is the energy of the $I_3$ absorption line

$\hbar\Omega$ is the ($k = 0$) LO phonon energy.

The variation of the absorption coefficients with photon energy are shown qualitatively in Figure 4.5.

Let us also neglect, for now, all rethermalization of electrons and excitons. This assumption is quite justified in view of the fact that the exciton emission did not change in

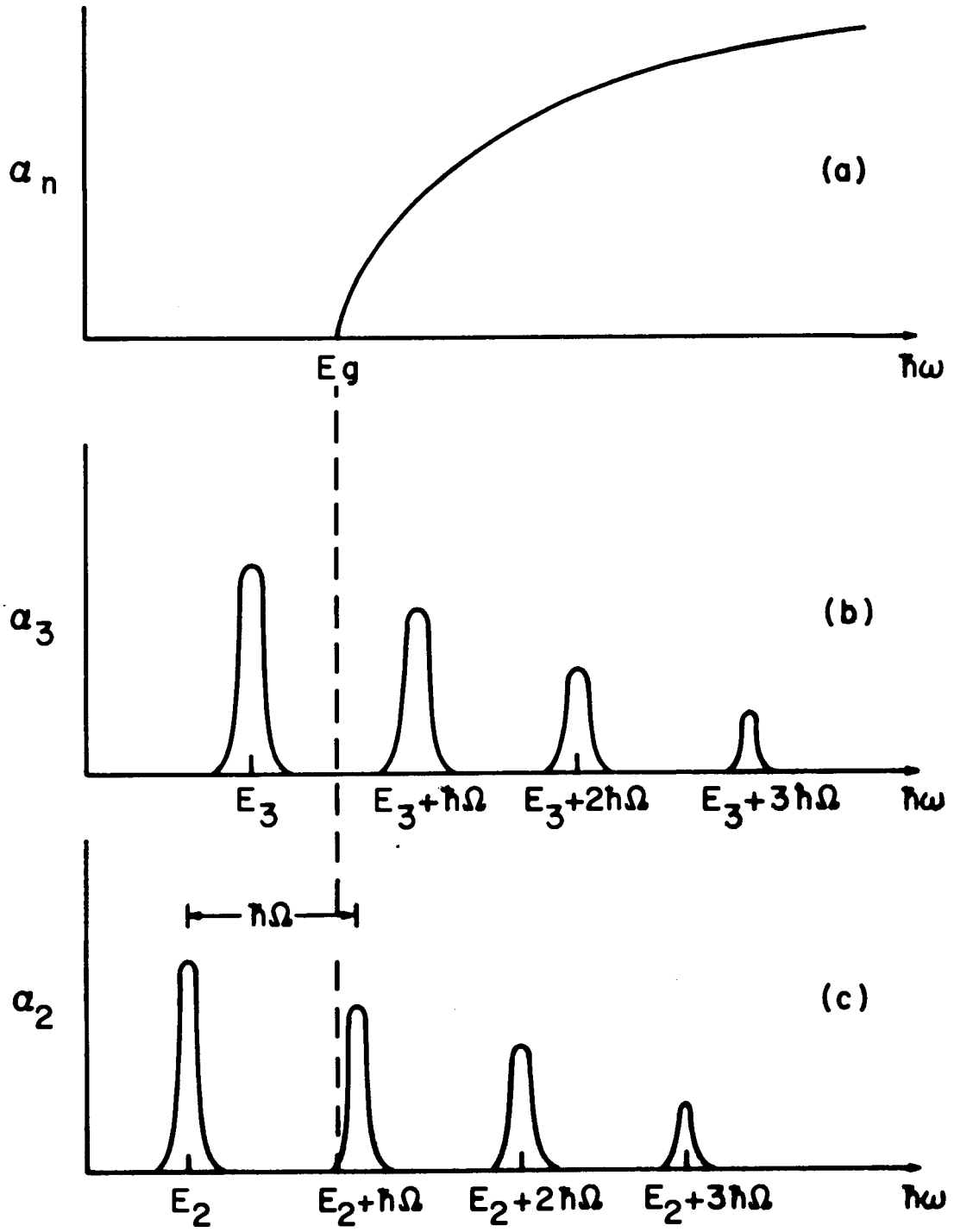


Figure 4.5 Qualitative variation of absorption coefficient with photon energy. (a) direct interband absorption (b) absorption due to formation of excitons on ionized donors (c) absorption due to formation of excitons on neutral donors.

intensity as the specimen temperature was lowered to 1.6°K from 4.2°K.

If $N_D$ = total donor density

$N_{Dn}$ = density of donors neutralized by one electron

$N_{De}$ = density of ionized donors with one exciton

$N_{Den}$ = density of neutral donors with one exciton

$N = N_D - N_{Dn} - N_{De} - N_{Den}$ density of bare ionized donors

$G$ = rate of formation of free electrons

$G_2$ = rate of formation of excitons bound to neutral donors $\propto N_{Dn}$ or

$G_2 = \beta_2 N_{Dn}$ $(\beta_2 \propto \alpha_2)$

$G_3$ = rate of formation of excitons bound to ionized donors $\propto N$ or

$G_3 = \beta_3 N$ $(\beta_3 \propto \alpha_3)$

$S_{Dn}$ = capture cross-section for electrons by ionized donors

$S_{De}$ = capture cross-section for electrons by ionized donors to which an exciton is bound.

$\tau_1$ = lifetime of electrons on neutral donors

$\tau_2$ = radiative lifetime of excitons on neutral donors

$\tau$ = lifetime of electrons for non-radiative processes.

The transitions which occur are shown schematically in Figure 4.6, and the associated rate equations are

$$\frac{dn}{dt} = G - \frac{n}{\tau} - nNS_{Dn}v - nN_{De}S_{De}v \qquad (4.4.1)$$

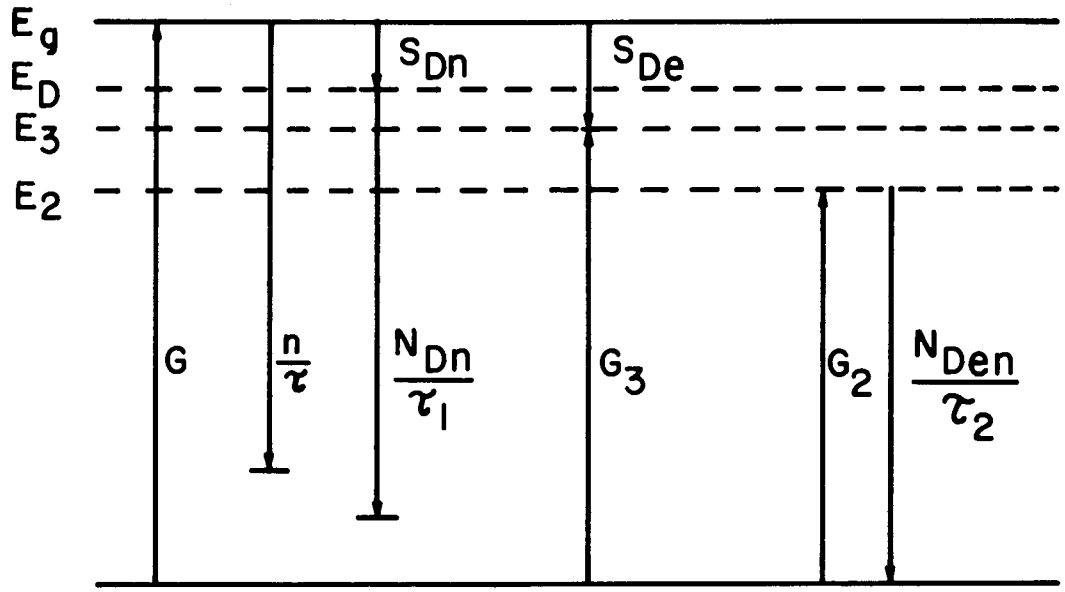


Figure 4.6 Energy band diagram showing transitions involved in exciton emission model.

$$\frac{dN_{Dn}}{dt} = nNS_{Dn}v - \frac{N_{Dn}}{\tau_1} - G_2 + \frac{N_{Den}}{\tau_2} \qquad (4.4.2)$$

$$\frac{dN_{De}}{dt} = G_3 - n\, N_{De}\, S_{De}\, v \qquad (4.4.3)$$

$$\frac{dN_{Den}}{dt} = G_2 + nN_{De}\, S_{De}v - \frac{N_{Den}}{\tau_2} \qquad (4.4.4)$$

where radiative recombination at $I_3$ in Equation (4.4.3) is neglected, as none is observed experimentally.

The quantity of interest is $N_{Den}/\tau_2$ in steady state as the exciton emission intensity is proportional to this quantity. The above equations can be solved for the steady state case giving N, $N_{Dn}$, $N_{De}$ and $N_{Den}$ in terms of n and the material parameters. n is determined from a cubic equation with the material parameters and the incident light intensity as constants. We find:

$$N_D = \frac{(G - n/\tau)}{\beta_3 + nS_{Dn}v}\left\{1 + \tau_1(\beta_3 + nS_{Dn}v) + \frac{\beta_3}{nS_{De}} + \beta_2\tau_1\tau_2(\beta_3+nS_{Dn}v)+\beta_3\tau_2\right\} \qquad (4.4.5)$$

from which n is determined, and

$$\frac{N_{Den}}{\tau_2} = \beta_2\tau_1 \ (G - n/\tau) + \frac{\beta_3 \ (G - n/\tau)}{\beta_3 + nS_{Dn}v} \qquad (4.4.6)$$

Consider two cases:

(a) $\beta_3 = 0$ and the energy of the incident light is at a peak in $\beta_2$

$$\frac{N_{Den}}{\tau_2} = \beta_2\tau_1 \ (G - n/\tau) \qquad (4.4.7)$$

(b) $\beta_2 = 0$ and the energy of the incident light is at a peak in $\beta_3$

$$\frac{N_{Den}}{\tau_2} = \frac{\beta_3 \ (G - n/\tau)}{\beta_3 + nS_{Dn}v} \qquad (4.4.8)$$

n is not the same in both (a) and (b) except in the limit of low light intensity when it is a solution of

$$\frac{n\tau}{\tau_T} = (G\tau - n)\left(1 + \frac{n\tau_1}{N_D\tau_T}\right) \qquad (4.4.9)$$

where $\tau_T = \frac{1}{S_{Dn} \ N_D \ v}$ = capture time for electron by ionized donors (if $N \approx N_D$, i.e. low light levels).

The ratio of the intensities of the peaks in the two series is then

$$\frac{I_2}{I_3} = \frac{N_{Den}\ (\beta_3 = 0)}{N_{Den}\ (\beta_2 = 0)}$$

$$= \frac{\beta_2}{\beta_3}\ \tau_1\ n\ S_{Dn}\ v \qquad (4.4.10)$$

$$= \frac{\beta_2}{\beta_3}\ \frac{\tau_1}{\tau_T}\ \frac{n}{N_D}$$

and $n/N_D$ is determined by

$$\frac{n}{N_D}\ \frac{\tau}{\tau_T} = \left(\frac{G\tau - n}{N_D}\right)\left(1 + \frac{n\tau_1}{N_D\tau_T}\right) \qquad (4.4.11)$$

Equation (4.4.10) is physically quite transparent. First, the ratio $I_2/I_3$ should obviously depend on $\beta_2/\beta_3$. Secondly, the shorter $\tau_1$, i.e. the faster the electrons on the donors leave the donors, the fewer neutral donors will be present on which the complex responsible for $I_2$ can be directly formed, conversely short $\tau_1$ increases the density of ionized donors on which $I_3$ can be formed, and therefore short $\tau_1$ enhances $I_3$. Thirdly, the larger $n/\tau_T$ which is proportional to the rate at which electrons are trapped on ionized donors, the larger the

density of neutral donors and the larger the $I_2$ and the smaller the $I_3$ contribution. Finally, the higher the density of ionized donors, which in our approximation of low light levels is taken as the total donor density, the larger the intensity of the $I_3$ peaks.

Since $\tau_1$, $\tau_T$, $\tau$ and $N_D$ are not known it is difficult to say what the relative heights of the peaks in the $I_2$ and $I_3$ series are.

If we include rethermalization of the excitons bound to neutral and ionized donors and characterize this rethermalization by rethermalization times $\tau_2'$ and $\tau_3'$ for excitons bound to neutral and ionized donors respectively we find that

$$\frac{I_2}{I_3} = \frac{\beta_2}{\beta_3}\frac{\tau_1}{\tau_T}\frac{n}{N_D} + \frac{\beta_2}{\beta_3}\frac{S_{Dn}}{S_{De}}\frac{\tau_1}{\tau_3'} \qquad (4.4.12)$$

and n is a solution of the same equation as in the absence of rethermalization (Equation 4.4.11). The second term above is due to rethermalization of the excitons bound to ionized donors and increases as the rethermalization time decreases.

Both $I_2$ and $I_3$ are affected equally by the rethermalization of excitons bound to neutral donors. The density of excitons on neutral donors is:

(a) $\beta_3 = 0$

$$N_{Den} = \beta_2 \tau_1 \frac{(G - n/\tau)}{(\frac{1}{\tau_2} + \frac{1}{\tau_2'})} \tag{4.4.13}$$

(b) $\beta_2 = 0$

$$N_{Den} = \frac{\beta_2 \, S_{De} \, (G - n/\tau)}{S_{Dn}(n \, S_{De} \, v + \frac{1}{\tau_3'})(\frac{1}{\tau_2} + \frac{1}{\tau_2'})} \tag{4.4.14}$$

and we see both terms are diminished in the same way as the rethermalization time $\tau_2'$ decreases.

The excitation spectrum of the $I_2$ exciton (4868.3A) in sample A has been studied as a function of temperature and as a function of the illumination intensity during cool down from room temperature to 4.2°K.

If this sample is kept in the dark at room temperature and cooled in the dark, it appears as if all donors are ionized, as the excitation spectrum, shown in Figure 4.7a, exhibits the same doublet structure as sample 2. As the helium boils off and the sample temperature rises, the spectrum changes to that shown in Figure 4.7b. The series of peaks based on $I_3$ is now absent and the total intensity of the peaks based on $I_2$ is diminished by a factor of about 5 (note the relative intensity scales in Figure 4.7a and b. This is consistent with the onset of rethermaliza-

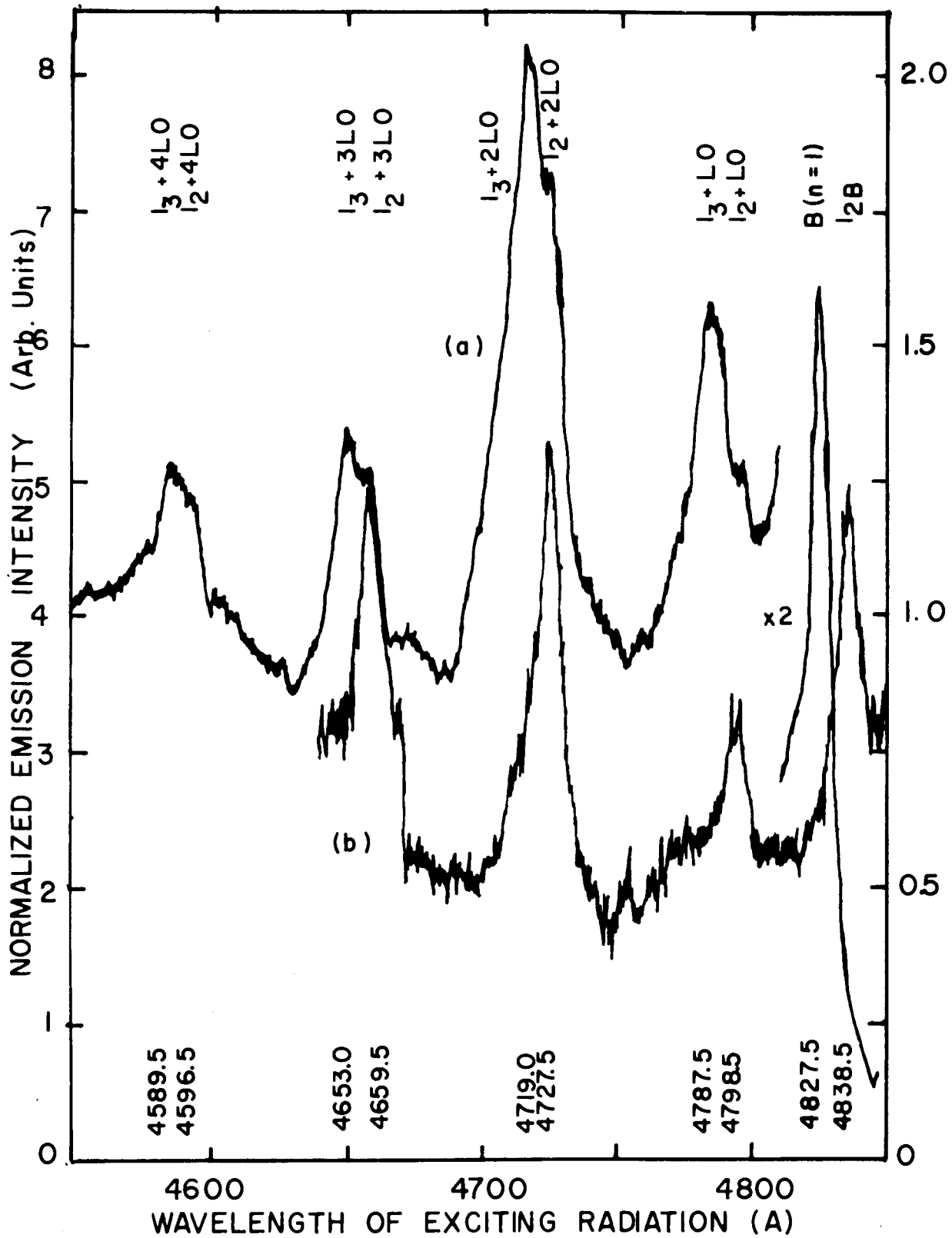


Figure 4.7 Excitation spectrum of the 4868.3A $I_2$ emission line in crystal A. Sample cooled in the dark. (a) Spectrum at 4.2°K, intensity scale on left (b) Spectrum at temperature above 4.2°K, intensity scale on right.

tion of excitons bound to neutral and ionized donors.

The binding energy of excitons bound to neutral donors is the energy difference between the free A exciton and the energy of the emitted light. The binding energy of the excitons bound to ionized donors is less than this by the spacing of the peaks in the two series. From the spacing of $4.6 \pm 1.1$ mev, the binding energies of the two excitons are

| | Binding Energy |
|---|---|
| $I_2$ | 7.2 mev |
| $I_3$ | 2.6 mev |

Thus the exciton is very weakly bound to the ionized donor and it will not take too large an increase in temperature above 4.2°K (kT ~ 0.4 mev) for rethermalization to be important.

Note also in Figures 4.7a and b that as the temperature rose from 4°K the peak corresponding to the formation of free B excitons gradually shifted in energy to $I_{2B}$ corresponding to the formation of B excitons directly on a neutral donor.

If sample A is cooled under illumination by above-band-gap radiation then the doublet structure is absent and a peak is

present corresponding to $I_{2B}$, as shown in Figure 4.8. Also the $I_1$ emission is absent. In one experiment the crystal was allowed to warm up slightly (the helium boiled off) and then cooled down again. On warming the peak at $I_{2B}$ shifted gradually to the free B exciton and upon cooling remained there. After a period of several hours the doublet structure gradually appeared and the peak corresponding to the formation of free B excitons became very strong, (see Figure 4.9 ). Also the $I_1$ emission grew and became very intense.

It would appear that the donors which were neutralized by the external light during cooling are meta-stable in the sense that the neutralizing electron remains on the donor for a long time. After a while the electron is released and the ionized donor density increases allowing the $I_3$ series to appear.

The observation in sample A that the $I_{2B}$ peak is present when the peaks corresponding to $I_3 + n\hbar\Omega$ are absent and that the free B exciton peak is present when the $I_3 + n\hbar\Omega$ peaks are present is intuitively plausible. When the $I_3 + n\hbar\Omega$ peaks are present a large density of ionized donors exists which must be neutralized before the complex $I_{2B}$ can be created. Equivalently, the density of neutral donors on which to form $I_{2B}$ will be small and the peak corresponding to $I_{2B}$ will be small. The free B exciton on the other hand is created irrespective of the neutral donor density and will diffuse through the crystal until it is captured by an impurity site where it will recombine. When the neutral donor density is large i.e. when the $I_3 + n\hbar\Omega$ peaks are

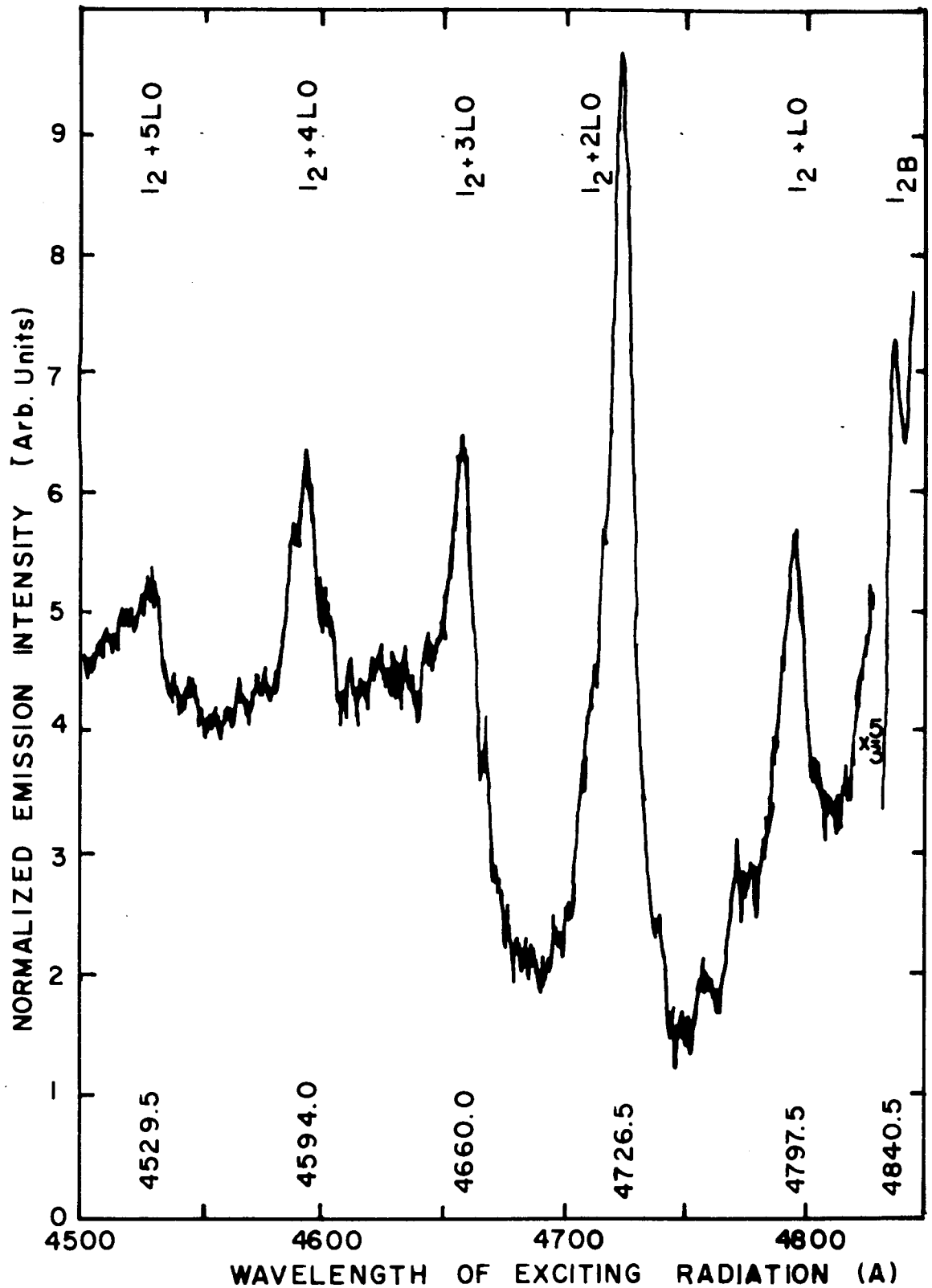


Figure 4.8 Excitation spectrum of the 4868.3A $I_2$ emission line in crystal A at 4.2°K. Sample cooled under u.v. illumination.

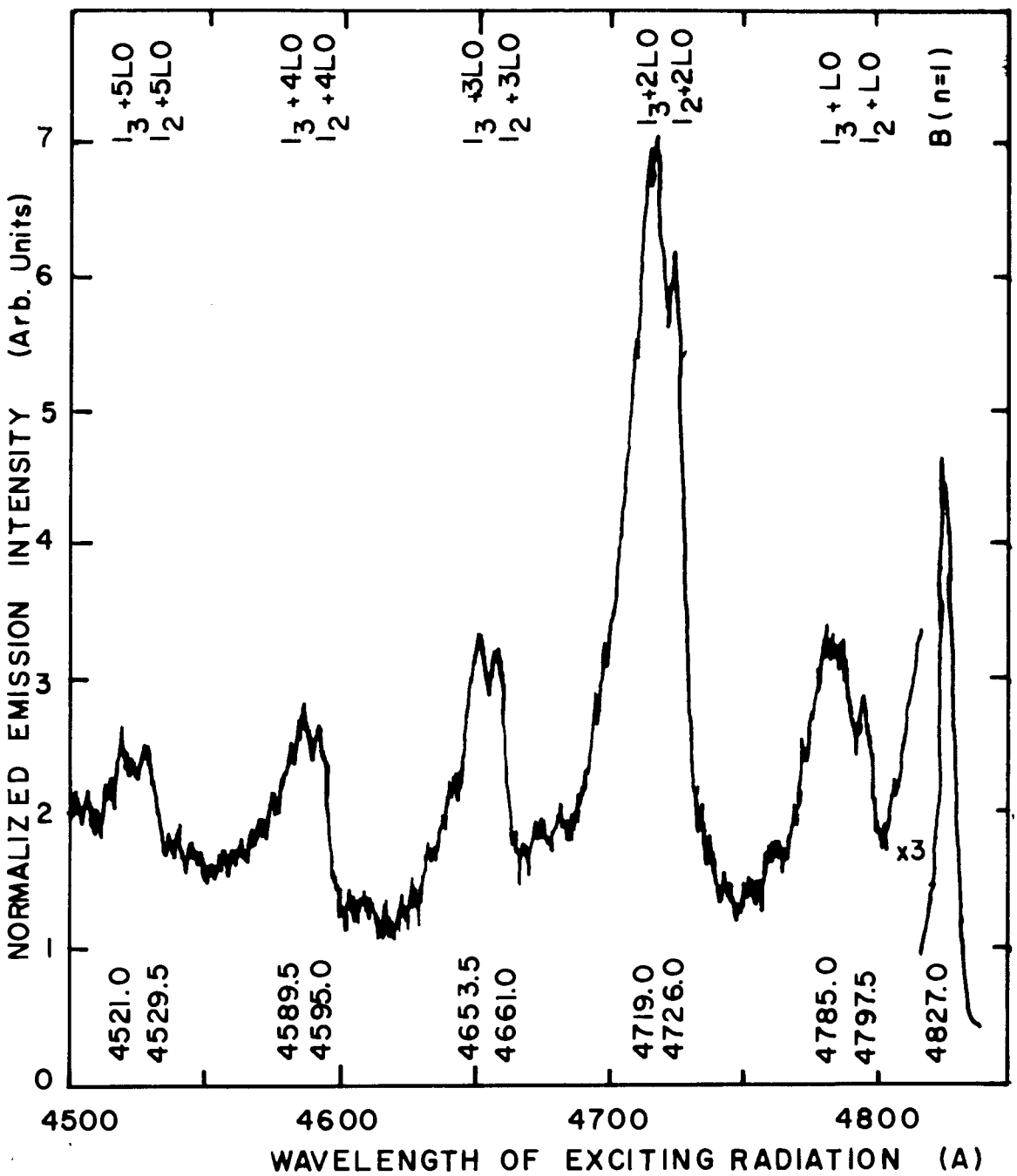


Figure 4.9 Excitation spectrum of the 4868.3A $I_2$ emission line in crystal A at 4.2°K. See text for experimental conditions.

absent, the peak $I_{2B}$ should be enhanced over the case when the $I_3 + n\hbar\Omega$ peaks are present, which is indeed the case (Figures 4.8 and 4.9). When the $I_3 + n\hbar\Omega$ peaks are absent one would expect peaks at both $I_{2B}$ and B to occur, however only the $I_{2B}$ peak is present in sample A. The reason for the absence of the free B exciton peak in this instance is not understood, although it could arise from differences in the capture cross-section for such an exciton by neutral and ionized donors. Alternately, it could be present but less intense than the $I_{2B}$ exciton and therefore not resolved, the relative intensity of the $I_{2B}$ and free B exciton peaks depending on the relative and also absolute density of neutral and ionized donors.

Why the $I_1$ emission is absent at first is not at all clear, but we may at least speculate that the absence of the $I_1$ emission and the series of peaks in the $I_2$ emission based on $I_3$ must somehow be related.

## 4.4 Conclusions

From the optical excitation spectrum of the $I_1$ emission line in CdS we find that the complex responsible for this emission is created by the direct formation of bound excitons on an impurity or other localized site and by the formation of free excitons which are subsequently trapped or bound to the localized site.

From the optical excitation spectra of the $I_5$ and $I_2$ emission lines we find that the complexes responsible for these emission lines are also created by the formation of free excitons which are subsequently bound to a localized site, but more importantly they are created by direct phonon assisted formation of an exciton bound to an ionized or neutral donor.

The presence of this phonon structure in both the $I_2$ and $I_5$ excitation spectra is indicative of the physical similarity of the two impurity-exciton complexes, although it is the presence of the doublets in the excitation spectra and the coincidence of the separation of the peaks with the $I_2$ - $I_3$ separation that provides the strongest evidence that both $I_2$ and $I_5$ are excitons bound to neutral donors. The presence of the additional peak at 4838.5A in the excitation spectrum of $I_5$ in crystal 2 which has been labelled $I_{5B}$ and identified, by comparison with $I_{2B}$, as the direct formation of a B exciton on the impurity site, merely adds further support to the above identification of $I_5$.

One further feature of note in the $I_5$ and $I_2$ excitation spectra is the fact that the $I_5$ + LO and $I_2$ + LO peaks are weaker than the corresponding two-phonon lines. On the basis of perturbation theory one would expect the one-phonon line to be the most intense and the other higher order lines to diminish very rapidly in intensity. The creation of a bound exciton with the simultaneous emission of one phonon is a second order process, and if we assume perturbation theory to be applicable then the intensity of the one-phonon peak will involve a summation over a set of inter-

mediate states separated in energy from the ground state by $I_5$ + LO. If the proper states over which the summation is to be made are one electron states then these will be located at $I_5$ + LO above the A valence band edge. By coincidence $I_5$ + LO is very close to the band gap energy so that the intermediate states will be those near the conduction band edge where the density of states is very small, thus causing the one phonon line to be abnormally weak. The argument that it is these states over which the summation is taken is supported by the near absence of a peak at $I_5$ + LO when the incident light is polarized E$\|$c as for this polarization the valence band states for the A valence band are only very weakly active. In view of the extraordinarily strong phonon coupling it is somewhat doubtful whether perturbation theory is applicable. Perhaps a more realistic approach would be to regard the phonon coupling as a resonance phenomenon.

Recently a brief report on the excitation spectrum of an $I_2$ emission line at 4867.14A appeared[56] in which strong phonon coupling was also observed, only in the report peaks in the $I_2$ emission occur when the energy of the incident photon is equal to A + nLO, where A is the free A exciton energy. In this case the free A exciton is formed with phonon cooperation and is subsequently trapped on the neutral donor where emission at $I_2$ takes place. Why the phonon peaks should be based on the free exciton rather than the bound exciton is not known. The same authors[14,15]

have previously reported oscillations in the photoconductivity of CdS crystals grown in the same way as those used above, in which minima in the photoconductivity were observed whenever the energy of the incident photons was equal to A + nLO. In crystals such as ours where strong phonon structure in the $I_2$ and $I_5$ excitation spectra is seen based on the bound exciton we should also see similar structure in the photoconductivity; this is evident from Equation (4.4.5), where the free electron density is shown to be a function of both $\beta_2$ and $\beta_3$. Of our crystals, crystal A would be the most likely candidate as here the $I_2$ emission is the strongest, i.e. $\beta_2$ and $\beta_3$ are largest.

As a final comment, it is indeed curious that LO phonon structure is seen in the emission spectrum of $I_1$, while phonon structure is seen in the excitation spectrum of $I_2$ and $I_5$.

# 5. ELECTRON BEAM EXCITED SPECTRA

## 5.1 Introduction

This chapter describes the apparatus and experimental techniques used to obtain electron beam excited emission spectra of luminescent semiconductors. Spectra obtained from evaporated thin films of CdS are described and interpreted in terms of the recombination of free electrons with bound holes and bound electrons with bound holes. By varying the penetration depth of the high voltage electrons it is shown how surface effects may be separated from bulk effects.

## 5.2 Apparatus

The apparatus used for electron beam excitation is shown schematically in Figure 5.1. The electron gun design was developed at Lawrence Radiation Laboratories[57] for low voltage (< 30Kv) electron beam welding. The power supply, vacuum system and helium dewar have been designed by the author.

### 5.2.1 The Electron Gun

A full scale cross-section of the gun is shown in Figure 5.2. The focussing lens which is connected electrically to the cathode is so designed as to shape the electric field between the anode and cathode in such a way as to bring the electrons to a reason-

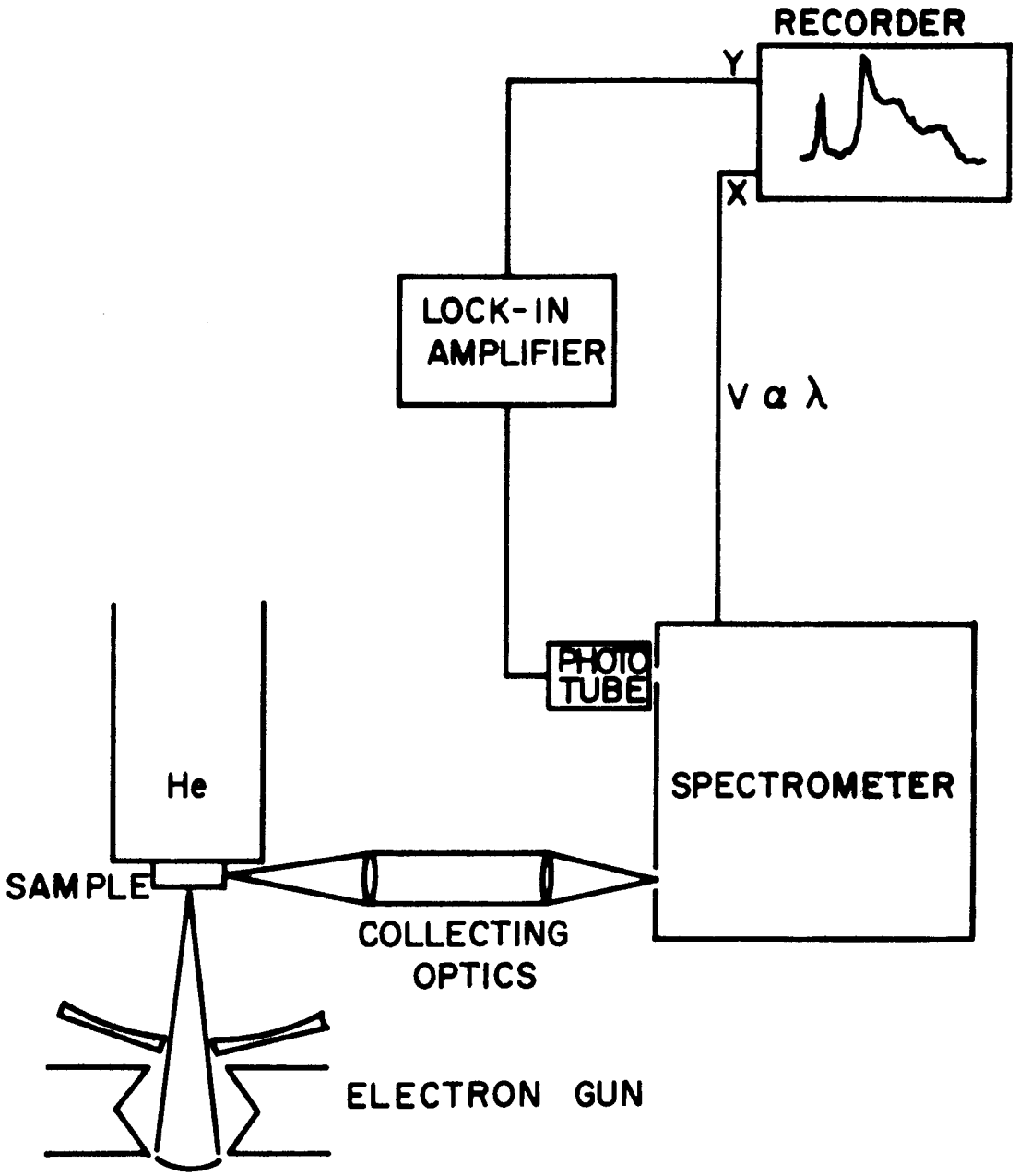


Figure 5.1 Schematic of apparatus used to obtain electron beam excited spectra of luminescent materials.

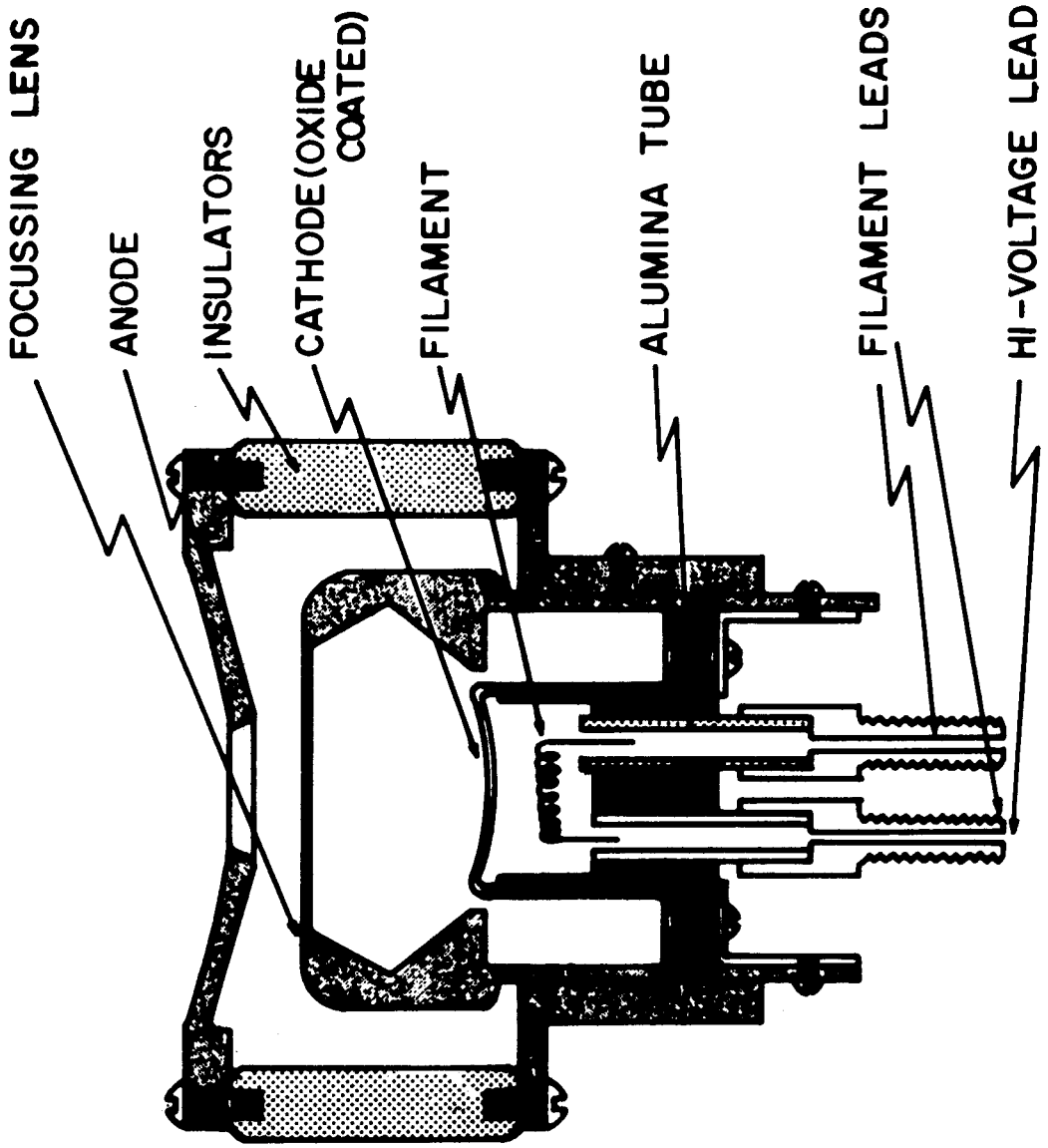


Figure 5.2 Full scale cross-section of electron gun[5]. The gun has cylindrical symmetry.

ably well defined focal point about three inches from the anode. The focal length and cross-sectional area of the focal region may be altered by moving the cathode further into or out of the focussing lens. Changing the separation between anode and lens also alters the focal length of the gun but not to the same extent as the cathode position.

This focussing property is demonstrated in Figure 5.3. Here are shown the lines of constant potential obtained using an electric field plotter and a two-dimensional analog of the electron gun, which has cylindrical symmetry. When the cathode is close to the anode the lines of constant potential are much less curved than when the cathode is far from the anode. This is particularly true for those lines near the cathode. Thus for small anode-cathode separations the electrons are focussed further from the anode.

An inherent disadvantage of a high power gun with a large cathode such as this one is the relatively large beam cross-section, 1-2 mm, and the large amount of radiation from the cathode which heats the sample. Some improvement can be obtained, at a sacrifice of beam current, by restricting the hole in the anode or by placing an aperture a few inches from the anode. Without these apertures, and with a properly prepared oxide cathode, the gun is capable of delivering 250 ma at 25 Kv in pulses whose length depends on the external circuitry. In our experiments a pulse duration of 1.6$\mu$s was used.

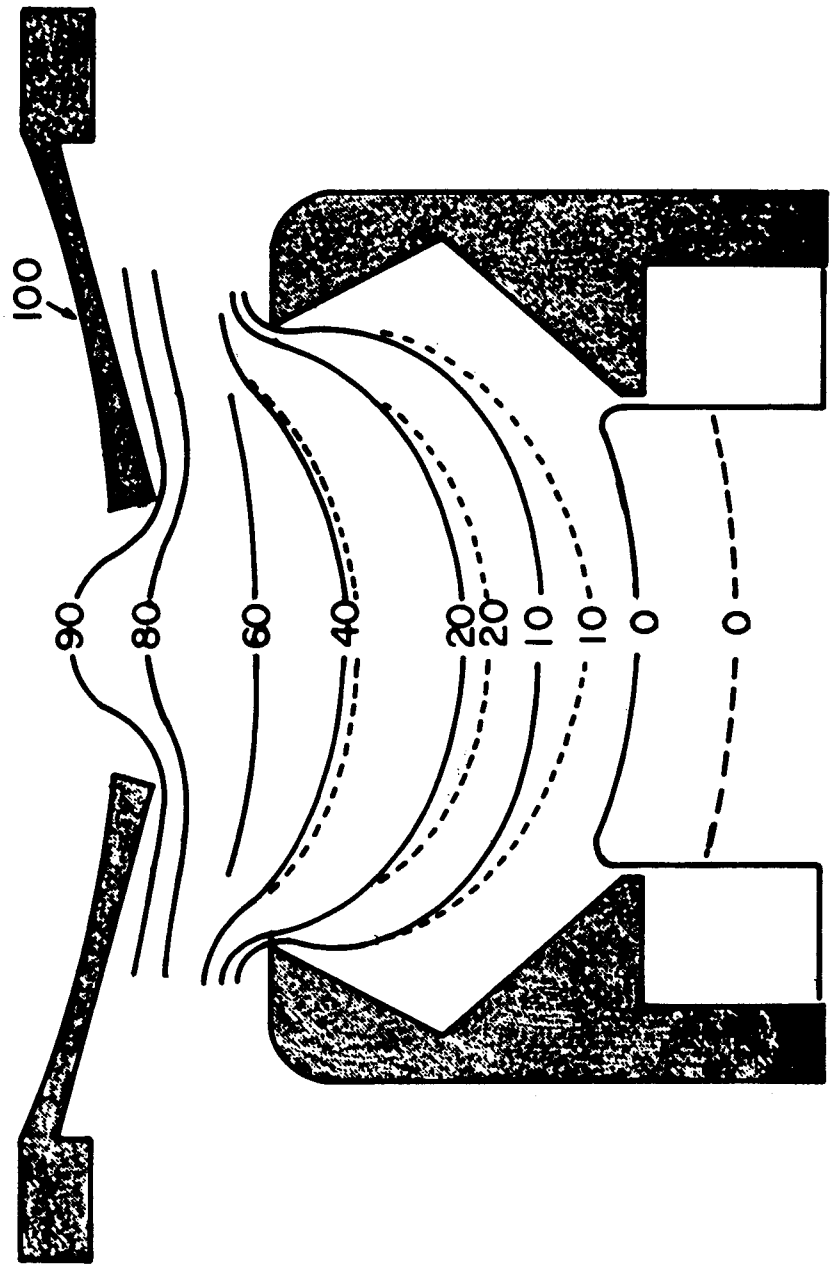


Figure 5.3 Lines of constant potential in the electron gun between anode and cathode.
---- cathode far from anode.
—— cathode close to anode.

The cathode is heated radiantly by a filament located immediately below the cathode. The magnetic field produced by the large filament currents required, approximately 100 amps., is sufficiently large that defocussing effects are important. For this reason half wave rectified current is used; the filament current and gun voltage being on in alternate half cycles.

### 5.2.2 Electron Gun Power Supply

A schematic diagram of the electrical circuitry is shown in Figure 5.4. The pulse forming network is really a long section of RG-8A/U cable which is charged to a high positive voltage V, the same voltage as the thyratron. When a trigger pulse is applied to the thryatron, the thyratron will for practical purposes be a short circuit thereby connecting a load resistance of 50 ohms, the characteristic impedance of the cable, across the cable. This will give rise to a pulse of height V/2 and duration twice the transit time of the cable across the input of the pulse transformer. This pulse is inverted and stepped up in the pulse transformer and applied to the cathode of the electron gun.

With this gun the anode and sample are held at ground potential while the cathode lens and filament are pulsed negatively. The filament current is supplied by a filament transformer whose insulation between primary and secondary windings must be capable of withstanding the high voltage pulse applied to the gun.

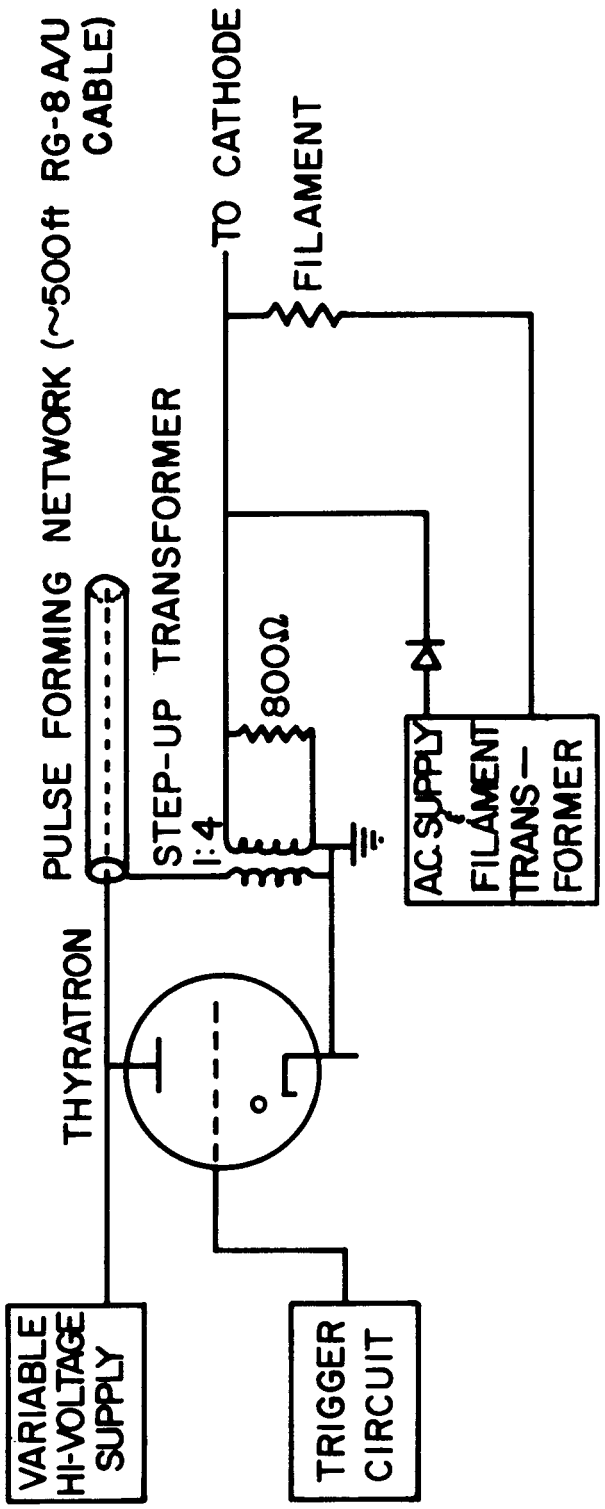


Figure 5.4 Schematic of electron gun power supply.

### 5.2.3 Vacuum System and Gun Steering Assembly

The electron gun is mounted by three-point supports in a vacuum system which can be pumped out to pressures less than $10^{-6}$ torr with a 2" NRC oil diffusion pump. The supports, which are mounted on the circumference of the anode, rest on one conical point and two wedges. The wedges can be moved normal to the axis of gun raising or lowering one side of the gun and thereby moving the electron beam across the sample which is located above the gun on the end of the helium finger of a dewar.

The filament leads are oil cooled copper tubes which pass through a 1" thick lucite plate. Vacuum seals are made by O-rings around the tubes which are pressed up against the lucite plate by brass flanges.

## 5.3 Sample Preparation

The samples used in this study of electron beam excited luminescence were thin CdS films 5,000-10,000A thick which had been evaporated onto a glass substrate over a layer of evaporated aluminum to avoid space charge effects. The films were evaporated under such conditions[58] as to produce an agglomeration of small hexagonal crystallites 300-500Å across with the crystal c-axis oriented preferentially normal to the substrate. The evaporation conditions are given in Table 5.1. The films had a room temperature electron concentration of about $10^{16}$ $cm^{-3}$. No subsequent

| Material | Substrate Temperature | Vacuum System Pressure | Deposition Rate |
|---|---|---|---|
| CdS | 100° C | $10^{-6}$ torr. | 300 A/min. |
| $SiO_x$ | 200° C | $10^{-4}$ torr. $O_2$ | |
| $CaF_2$ | 22° C | $4 \cdot 10^{-6}$ torr. | |

Table 5.1 Thin Film Deposition Conditions

heat treatments were used in attempts to increase the grain size in the films.

As one of the objects of this study was to use the electron beam as a tool in the investigation of surface effects, the surface potential of the films was altered by evaporating $CaF_2$ or $SiO_x$ onto the CdS films.[24] It has been shown that evaporation of $CaF_2$ produces a depletion layer on the CdS surface while $SiO_x$ produces an enhancement layer. The $SiO_x$ coatings were glass-like in their appearance which, combined with the relatively high oxygen pressure during deposition, suggests that the films were closer in composition to $SiO_2$ than to SiO. Energy band structures of CdS films with $CaF_2$ and $SiO_x$ coating are shown in Figure 5.5 and a cross-section of the layered films is shown in Figure 5.6.

Several samples were evaporated onto the same substrate without breaking the vacuum. Usually a 4 x 3 array of $\frac{1}{2}$ inch diameter circular samples was evaporated. Each of the three rows of four samples had a different surface treatment, usually one had $CaF_2$ on top of the CdS, another row $SiO_x$ and the third row was left bare. The samples in each row were generally of different thicknesses.

To obtain the electron beam excited emission spectra of the films prepared in this way the substrate was scratched with a diamond scribe and broken and the sample to be investigated was mounted with silver paste on a bevelled copper block which screwed onto the end of the helium finger of a dewar.

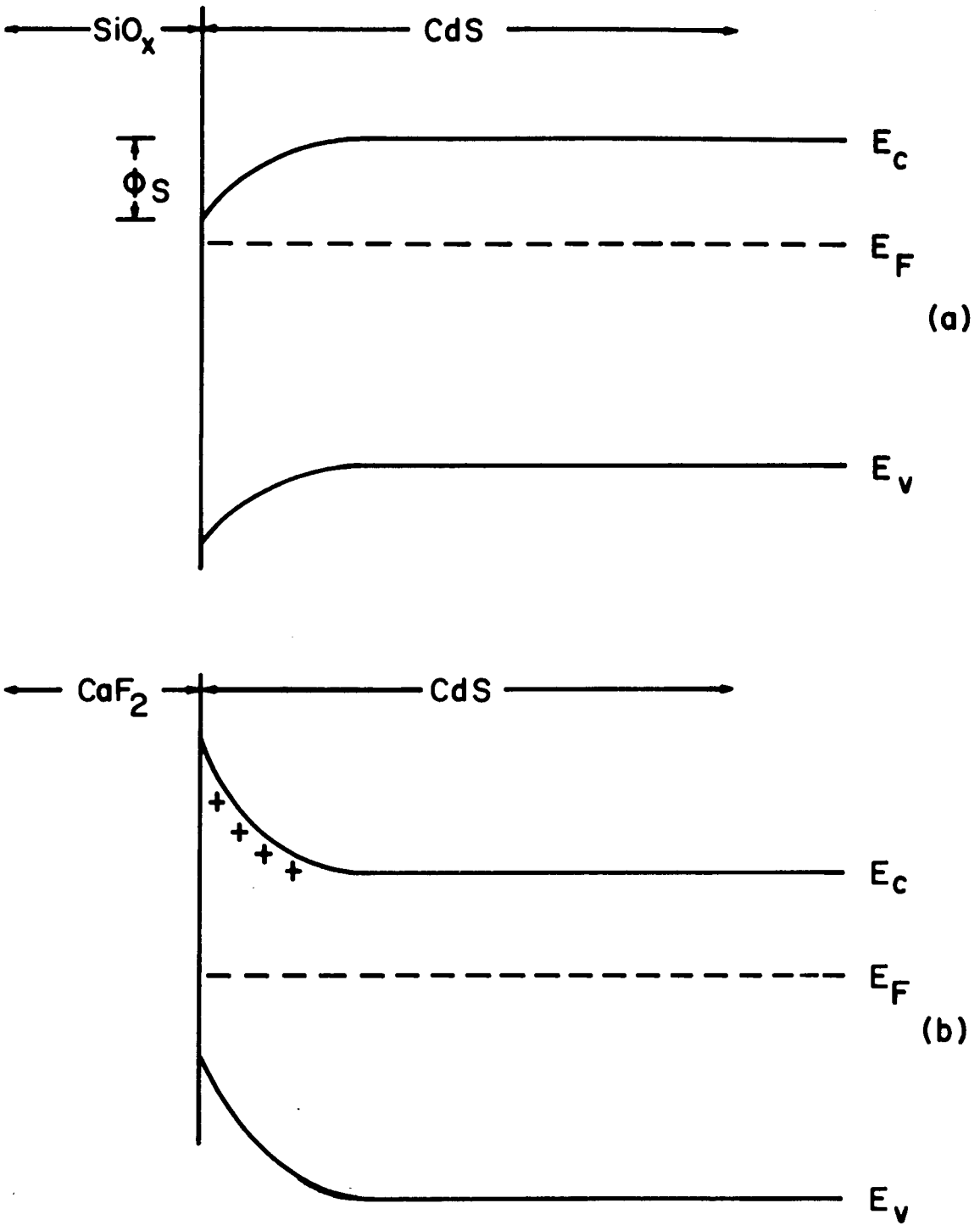


Figure 5.5 Energy band diagrams of CdS covered with (a) $SiO_x$ and (b) $CaF_2$.

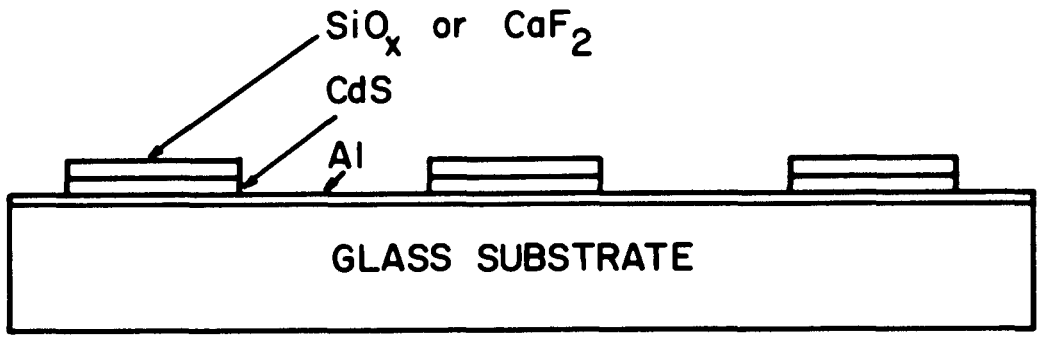


Figure 5.6 Cross-section of evaporated CdS films.

Thermal contact with the coolant was not very good and when liquid nitrogen, and in particular when liquid helium, was used as coolant the sample temperature in the absence of electron beam excitation was probably a few tens of degrees Kelvin above the bath temperature. This temperature was likely raised further by radiant heating from the hot cathode of the electron gun located some 10-15 cm below the sample.

## 5.4 Spectra of CdS Films

Typical emission spectra of thin CdS films, with no coating and coated with $SiO_x$ and $CaF_2$ taken at liquid helium and liquid nitrogen temperatures are shown in Figures 5.7 and 5.8. The similarity of these spectra with those of the green edge luminescence in single crystals of CdS, shown in Figures 2.1 and 2.2, is apparent except for the peak at short wavelengths.

The low energy emission shows a series of peaks, equally spaced in energy with a mean spacing of $40 \pm 3$ mev. The spacing is, within experimental error, equal to the ($k = 0$) LO phonon energy of single crystal CdS. In our films, while the relative intensity of the high and low energy peaks depends, at fixed temperature, on the surface treatment, the high energy peak diminishes in intensity relative to the low energy series as the temperature is lowered. This is the same temperature dependence the free-bound and bound-bound emission lines in single crystal CdS exhibit.[30] Also, in the films, the high energy peak is

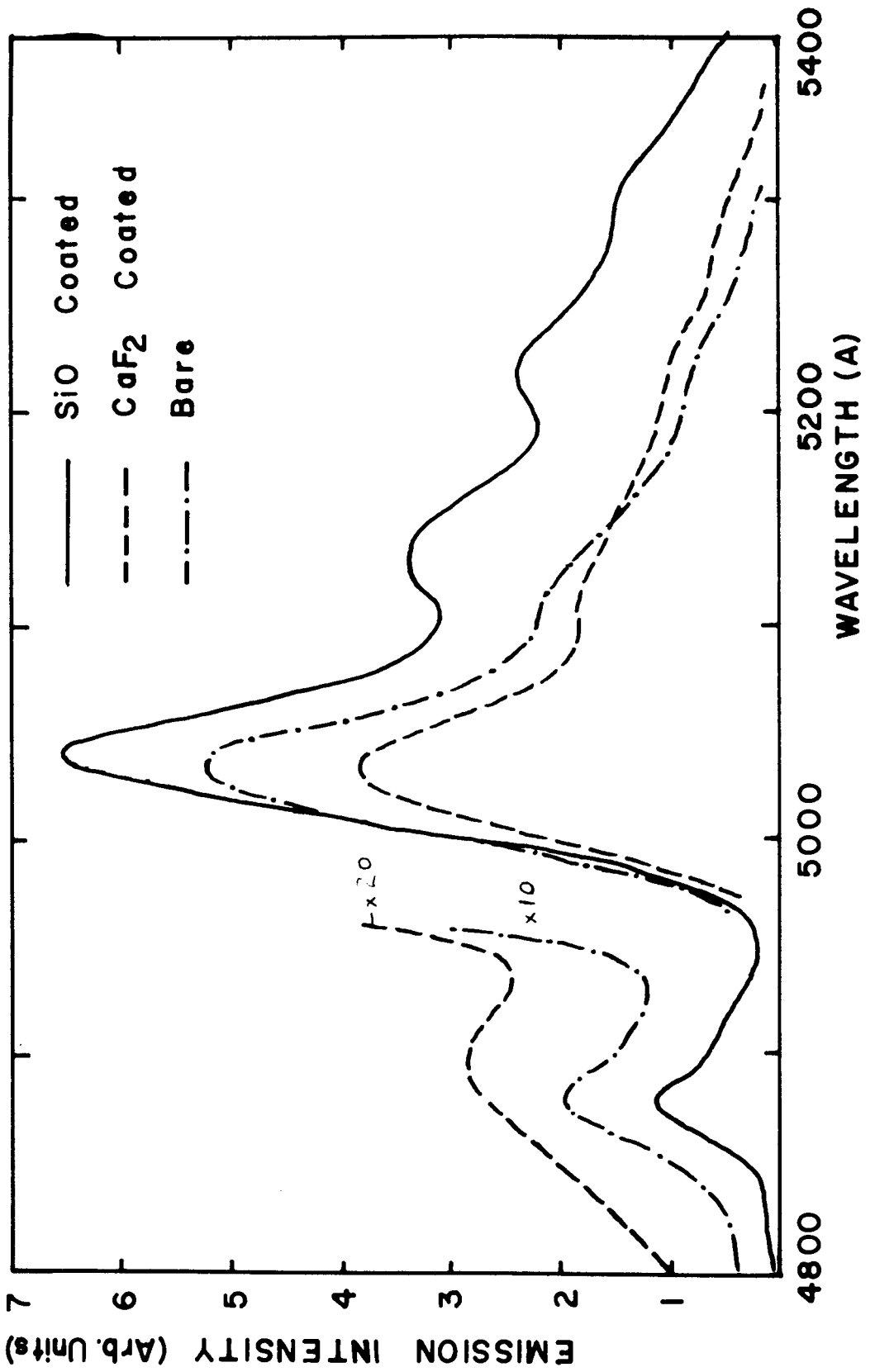


Figure 5.7 Emission spectrum of CdS films at liquid helium temperature. Beam conditions: $SiO_x$:9kv, 20 ma., $CaF_2$:9kv, 12 ma, bare: 10kv, 20 ma (intensity scale should be increased by a factor of 5 over coated films).

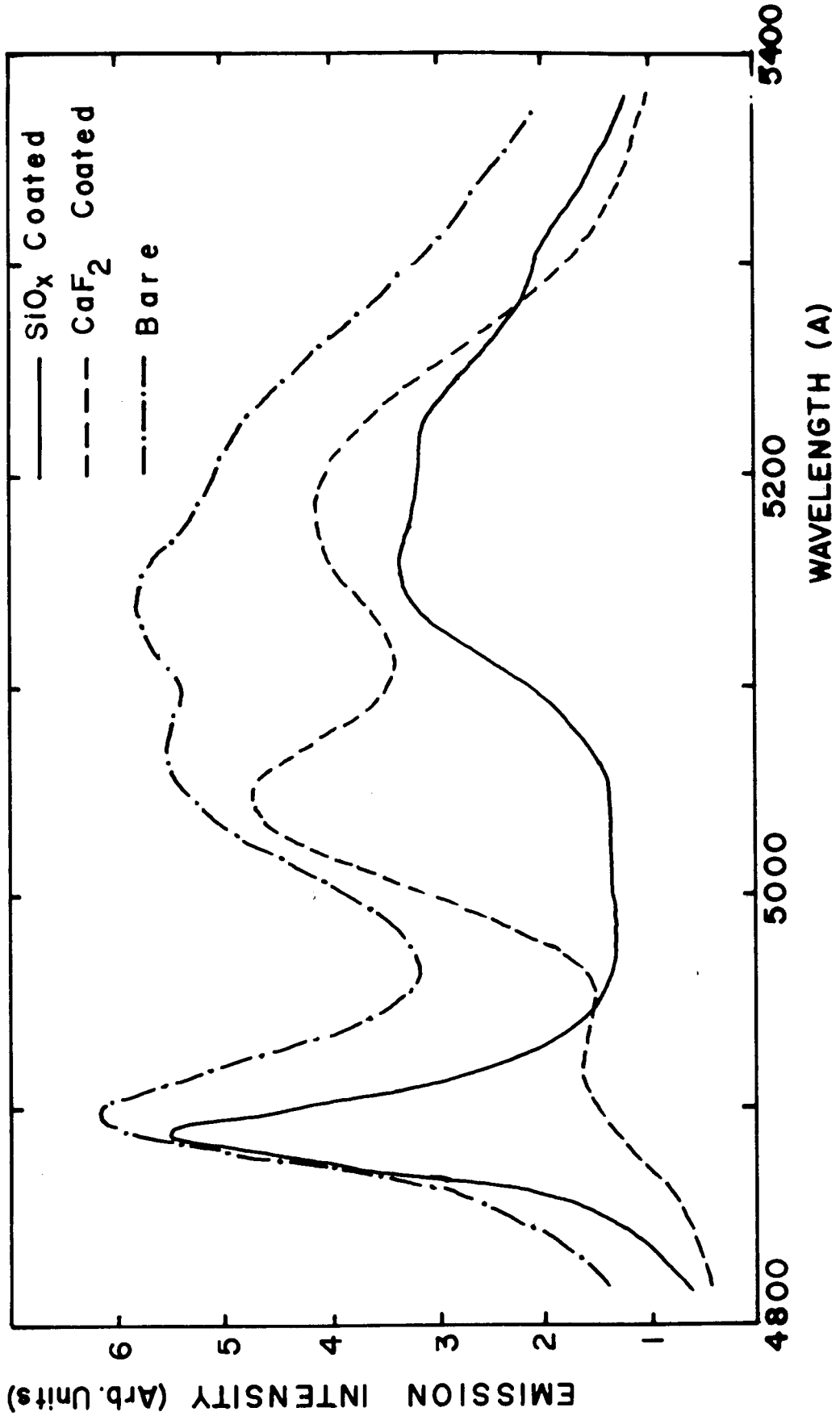


Figure 5.8 Emission spectrum of CdS films at liquid nitrogen temperature. Beam conditions: $SiO_x$:9kv, 40 ma, $CaF_2$:12kv, 30 ma, Bare: 10kv, 41 ma.

less intense in $CaF_2$ coated samples where the surface is depleted of electrons than in the $SiO_x$ coated samples where the surface electron concentration is enhanced. Furthermore, in the $SiO_x$ coated samples the intensity of the high energy peak diminishes relative to the low energy series as the beam voltage or electron penetration depth is increased (Figure 5.9). In this case we are generating electrons and holes further from the enhanced surface concentration of electrons.

All this evidence points quite conclusively to the high energy peak being due to the recombination of free electrons with bound holes. The low energy series, by virtue of its similarity with the low energy series in single crystal CdS we identify as the recombination of bound electrons with bound holes, and the simultaneous emission of n LO phonons (n = 0, 1, 2).

Since the free-bound and bound-bound emission both occur at energies different from the corresponding transitions in single crystals the donor and acceptor ionization energies must be different in the films from those in single crystals.

There is one feature of the free-bound transition in these films that is not present in the free-bound emission in single crystals, and that is the variation in the energy, or wavelength, of the free-bound line with beam voltage in $SiO_x$ covered films and in some bare films. This is most noticeable at helium temperatures. This variation is shown in Figure 5.10 and is a consequence of the downward bending of the energy bands at the CdS surface.

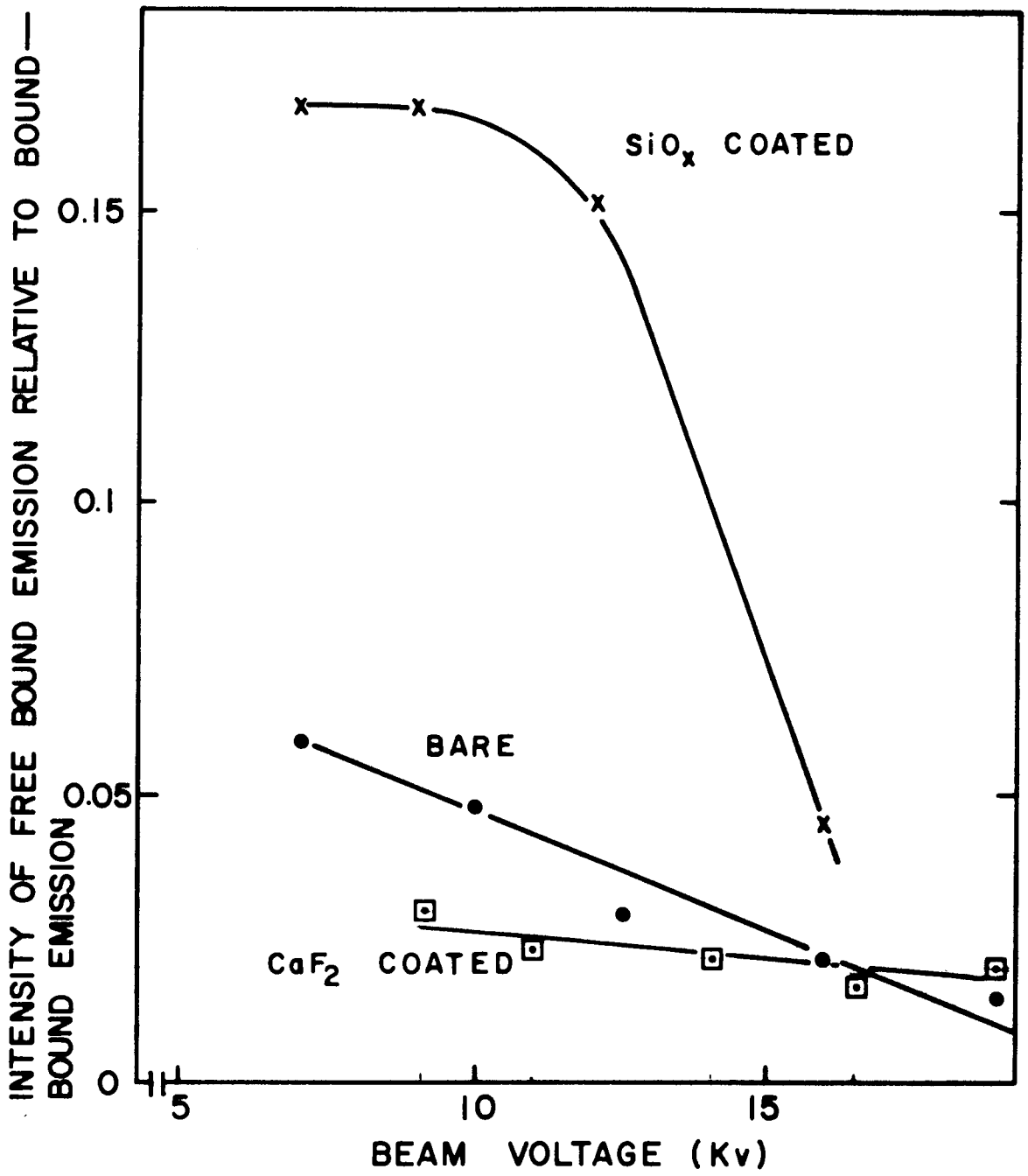


Figure 5.9 Intensity of free-bound emission relative to bound-bound emission at liquid helium temperature as a function of beam voltage at constant beam current.

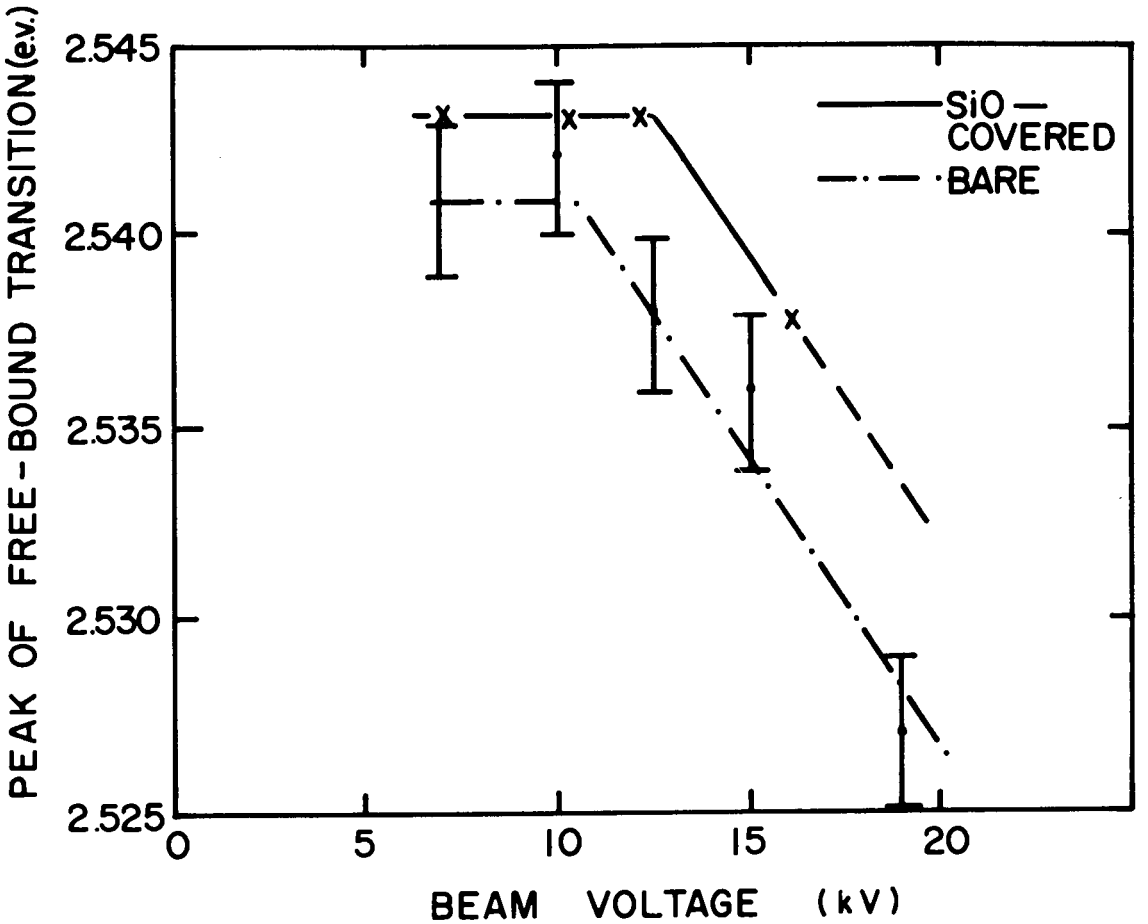


Figure 5.10 Energy of free-bound emission peak in CdS films at liquid helium temperature as a function of beam voltage.

In the absence of surface treatments or with flat energy bands throughout the luminescing region of the semiconductor the radiative recombination rate of an electron of kinetic energy $E_k$ with a bound hole is

$$R = N_A \, n(E_k) \, v \, S(E_k) \qquad (5.4.1)$$

where $N_A$ = density of neutral acceptors

$n(E_k)$ = density of free electrons with kinetic energy $E_k$ and velocity v.

$S(E_k)$ = radiative capture cross-section for an electron by a neutral acceptor.

Colbow[13] has shown that in the approximation of an energy independent capture cross-section and using a Boltzmann distribution for the free electrons, the maximum transition rate occurs for $E_k = kT$. Thus the peak in the f-b emission will occur at an energy $E_{f-b}$ such that

$$E_{f-b} = E_g - E_A + kT \qquad (5.4.2)$$

from which the acceptor binding energy may be determined.

When the bands are bent down the electrons near the surface see a potential well and become bound or confined to a region near the surface. Haering and O'Hanlon[24] have shown that in a CdS film evaporated under the same conditions as ours that a 2000A thick layer of $SiO_x$ can enhance the conductance per square

of the film at room temperature by an amount corresponding to the addition of about 1000A to the thickness of the film. Since the density of carriers at the surface will be larger than in the bulk (the Fermi energy is now closer to the band edge or even into the conduction band) the enhancement layer will likely be much smaller than 1000A and it will be necessary to treat the "free" electrons in the enhancement layer quantum mechanically. Duke[59] has solved this problem and finds that in the direction normal to the surface a series of bound states occur. This is shown qualitatively in Figure 5.11.

If reference is made to the enlarged band diagram in Figure 5.11 of the films near the surface we see that holes generated and then bound to acceptors near the surface are likely to have a larger matrix element for a transition involving electrons bound near the surface than electrons further away from the surface. These electron-hole pairs will recombine emitting light at energy

$$E_{f-b} = E_g + E_i - E_A - (\varphi_s - \varphi_A) + kT \qquad (5.4.3)$$

where $\varphi_A$ is the potential at the acceptor site and $E_i$ is the energy of the ith bound state measured from the conduction band edge at the CdS-$SiO_x$ interface. As long as the acceptor is located a distance z from the surface which is less than the distance $z_i$, the classical turning point for an electron of energy $E_i$ in the potential well, then the emission will occur at an energy

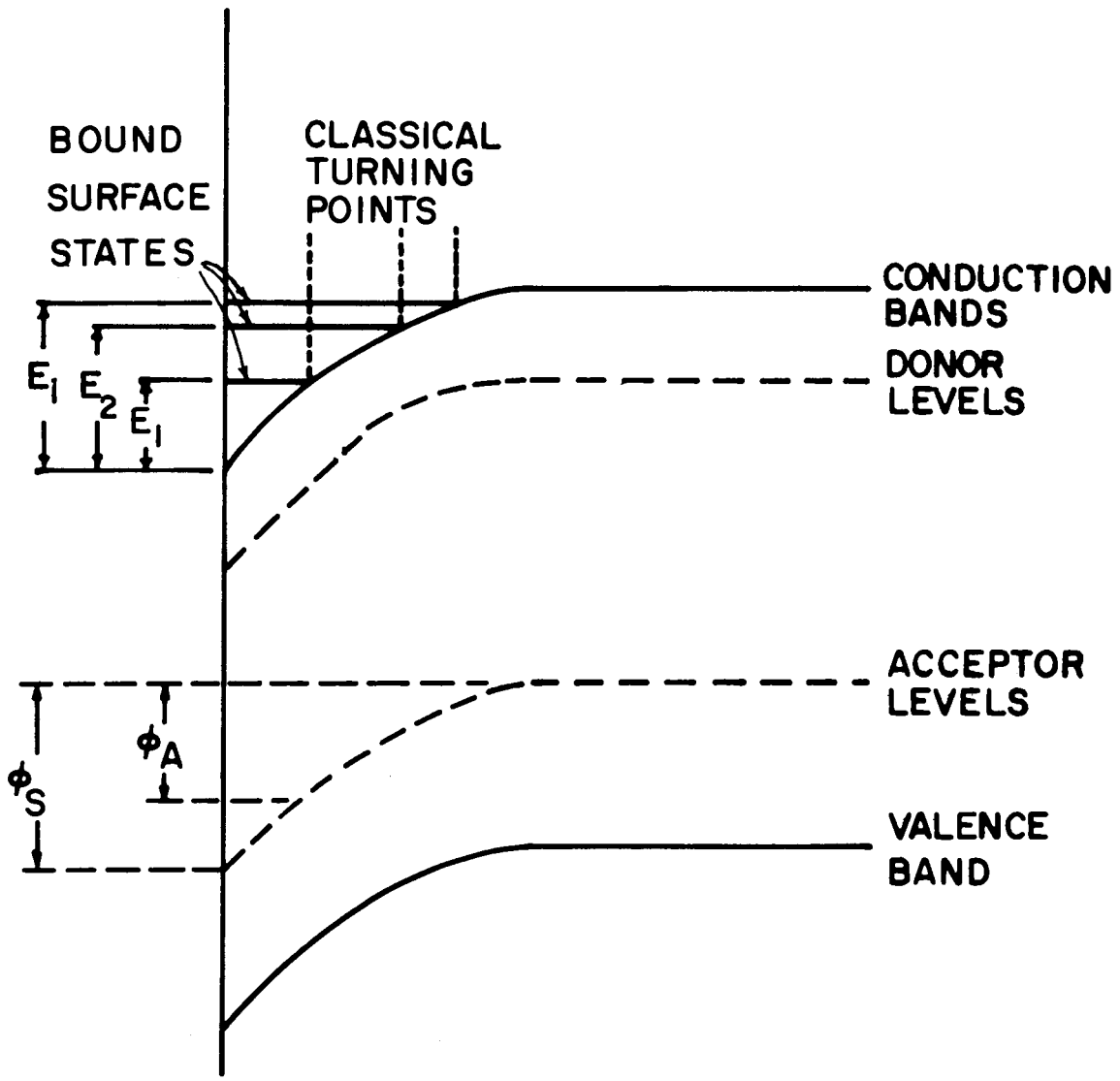


Figure 5.11 Energy band diagram showing surface states.

greater than the f-b peak in the bulk material. Our experimental curves of the f-b peak position vs. beam voltage suggest that at low beam voltages the electron penetration is less than the classical turning points for many of the bound state electrons but as the beam energy increases most of the electrons and holes are generated deeper inside the film where the bands are flat and we observe an emission peak which is characteristic of the bulk material.

Since the peak position is constant up to beam voltages of 10kv it would appear as if the range of the potential well was of the order of 1500A, the depth to which 10kv electrons excite fairly efficiently (see Figure 3.7). Alternately, the density of electrons in the potential well may well exceed the density of electrons generated by the high voltage primary electrons and since as shown the luminescent intensity at an energy E depends on the electron density, the emission resulting from the recombination of an electron in the surface region will dominate until the total number of electrons generated outside the surface region becomes comparable to the number in the surface region. This simple argument is complicated by the spatial dependence of the holes bound to acceptors, which is likely to be similar to the differential energy loss of the primary electrons, but in the absence of detailed knowledge of this spatial dependence and the form of the matrix element for radiative recombination, the estimate of 1500A for the range of the potential well must certainly be regarded as being an upper bound.

The Fermi energy at the surface is of the order of 2 or 3 times $\Delta E_{max}$ above the conduction band edge where $\Delta E_{max}$ is the total shift in energy of the f-b emission with beam voltage, or equivalently the total shift in the f-b emission from low voltage electrons incident in a $SiO_x$ covered film to a $CaF_2$ coated film where the potential well does not exist. From Figure 5.10, $\Delta E_{max} \approx 17$ mev and $E_F$ is 30 - 45 mev above the conduction band edge at the $SiO_x$-CdS interface.

To calculate the acceptor binding energy we see that it is necessary to use data on the $SiO_x$ covered films taken with large beam voltages or films coated with $CaF_2$. Using $E_{f-b} = 2.527$ ev, kT ~ 1 mev and $E_g = 2.582$ ev. $E_A \simeq 55$ mev which is much less than in single crystal CdS[13] where $E_A = 169.6$ mev.

From Figures 5.7 and 5.8 it can be seen that as the temperature of the specimen is lowered the strength of the b-b phonon replica emission is decreased and, in the case of the $SiO_x$ covered films, the phonon replica emission becomes quite well resolved. The phonon replicas in the $CaF_2$ covered films are not at all well resolved, and in an effort to see if the built in electric field at the surface produced sufficient line broadening to reduce the resolution, the line shape of the b-b emission in the presence of a uniform electric field was calculated.

Thomas[1] et al have shown that in the case where the impurity envelope wave functions have a simple hydrogenic form, and one of the impurities is much more weakly bound than the

other, the matrix element for radiative recombination will be proportional to $\psi(r) = C \exp(-r/r_B)$ where $\psi(r)$ is the envelope wavefunction of the more weakly bound particle, $r_B = [2m^*E_b/\hbar^2]^{-\frac{1}{2}}$, $E_b$ = binding energy of the weakly bound particle, and r is the inter-impurity separation.

The transition probability is then

$$W(r) = W_{max.} \exp(-2r/r_B) \qquad (5.4.4)$$

For impurity pairs of reasonably large separation the energy of emission, in the absence of an electric field, will be

$$E_{b-b}(r) = E_g - (E_A + E_D) + \frac{e^2}{\kappa r} \qquad (5.4.5)$$

For simplicity let us take the zero of energy as $E_g - (E_A + E_D)$. The number of donors between r and r + dr is $4\pi\, nr^2 dr$. A distance range dr corresponds to an energy range

$$dE = \frac{e^2}{\kappa r^2}\, dr \qquad (5.4.6)$$

Therefore the recombination intensity per unit energy at energy E is

$$I(E)dE = W(r)4\pi nr^2 \frac{dr}{dE} dE$$

$$= 4\pi W_{max.} n(\frac{e^2}{\kappa})^3 \frac{e^{-(2e^2/\kappa r_B E)}}{E^4} dE \qquad (5.4.7)$$

To include the effect of a uniform electric field F applied in the z-direction we must let

$$E = \frac{e^2}{\kappa r} + e\ Fr\ Cos\ \theta \qquad (5.4.8)$$

where r Cos $\theta$ is the z-component of the interimpurity separation. Consider now those donors located a distance r from an acceptor. Those donors which are located in an annular volume $2\pi r^2$ Sin$\theta$d$\theta$dr have the same energy E and the transition rate from this volume, assuming the impurity wavefunctions have not been distorted by the field so that the overlap is unchanged, is

$$2\pi nr^2 W_{max.}\ e^{-r/a}\ Sin\theta d\theta dr \qquad (5.4.9)$$

where $a = r_B/2$. But $Sin\theta d\theta = \frac{-dE}{er}$ and the above transition rate becomes

$$\frac{2\pi nW_{max.}\ e^{-r/a}\ rdr\ dE}{eF} \qquad (5.4.10)$$

Now, over a surface of constant r

$$\frac{e^2}{\kappa r} - eFr \leq E \leq \frac{e^2}{\kappa r} + eFr \qquad (5.4.11)$$

and to calculate the line shape we need to integrate over all possible r at constant E, subject to the above inequality. This yields, for $\frac{4e^3F}{\kappa E^2} > 1$ and $\frac{4e^3F}{\kappa E^2} < 1$ respectively

$$I(E)dE = \frac{2\pi n W_{max.} a^2}{eF} \left\{1 + \frac{E}{2eFa}\left(-1 + \sqrt{1 + \frac{4e^3F}{\kappa E^2}}\right)\right\} X$$
$$\exp\left\{-\frac{E}{2eFa}\left(-1 + \sqrt{1 + \frac{4e^3F}{\kappa E^2}}\right)\right\} \qquad (5.4.12)$$

$$I(E)dE = \frac{2\pi n W_{max.} a^2}{eF} \left\{\left[1 + \frac{E}{2eFa}\left(-1 + \sqrt{1 + \frac{4e^3F}{\kappa E^2}}\right)\right] \exp\left[-\frac{E}{2eFa}\left(-1 + \sqrt{1 + \frac{4e^3F}{\kappa E^2}}\right)\right]\right.$$
$$- \left[1 + \frac{E}{2eFa}\left(1 - \sqrt{1 - \frac{4e^3F}{\kappa E^2}}\right)\right] \exp\left[\frac{-E}{2eFa}\left(1 - \sqrt{1 - \frac{4e^3F}{\kappa E^2}}\right)\right] \qquad (5.4.13)$$
$$\left. + \left[1 + \frac{E}{2eFa}\left(1 + \sqrt{1 - \frac{4e^3F}{\kappa E^2}}\right)\right] \exp\left[-\frac{E}{2eFa}\left(-1 + \sqrt{1 - \frac{4e^3F}{\kappa E^2}}\right)\right]\right\} dE$$

These equations have been computer calculated using the

dimensionless variables $\epsilon = E/E_c$ and $\gamma = 2E_F/E_c$ where $E_c = e^2/\kappa r_B$ and $E_F = eFr_B$. The results of this calculation are shown in Figure 5.12 for several values of $\gamma$, or equivalently the electric field.

The experimental conditions under which our data is taken are not quite such as to allow a detailed comparison of our theory with experiment. It is well known from time resolved spectra on flash excited single crystals of CdS that the fastest decaying bound-bound transitions are those of highest energy, involving bound electrons and holes of small separation. This is reasonable as it is the closely spaced electrons and holes that have the largest overlap of their wavefunctions. It has also been determined, see Figure 5.13, that the light emission from our films follows the excitation fairly closely, although there appears to be some afterglow, and it is reasonable to say that repopulation of impurities takes place on a large scale. This also implies that fast decaying transitions will be enhanced and our experimental curves are likely to have their high energy side emphasized. Since our theory does not take the dynamics of this repopulation into account our theoretical and experimental line-shapes will not agree. Nevertheless, the effect of an electric field, should there be an effect, should be qualitatively similar to that in Figure 5.12, where the electric field shifts the emission line toward higher energies. Colbow[60] has shown that a shift toward higher energies with increasing electric field is

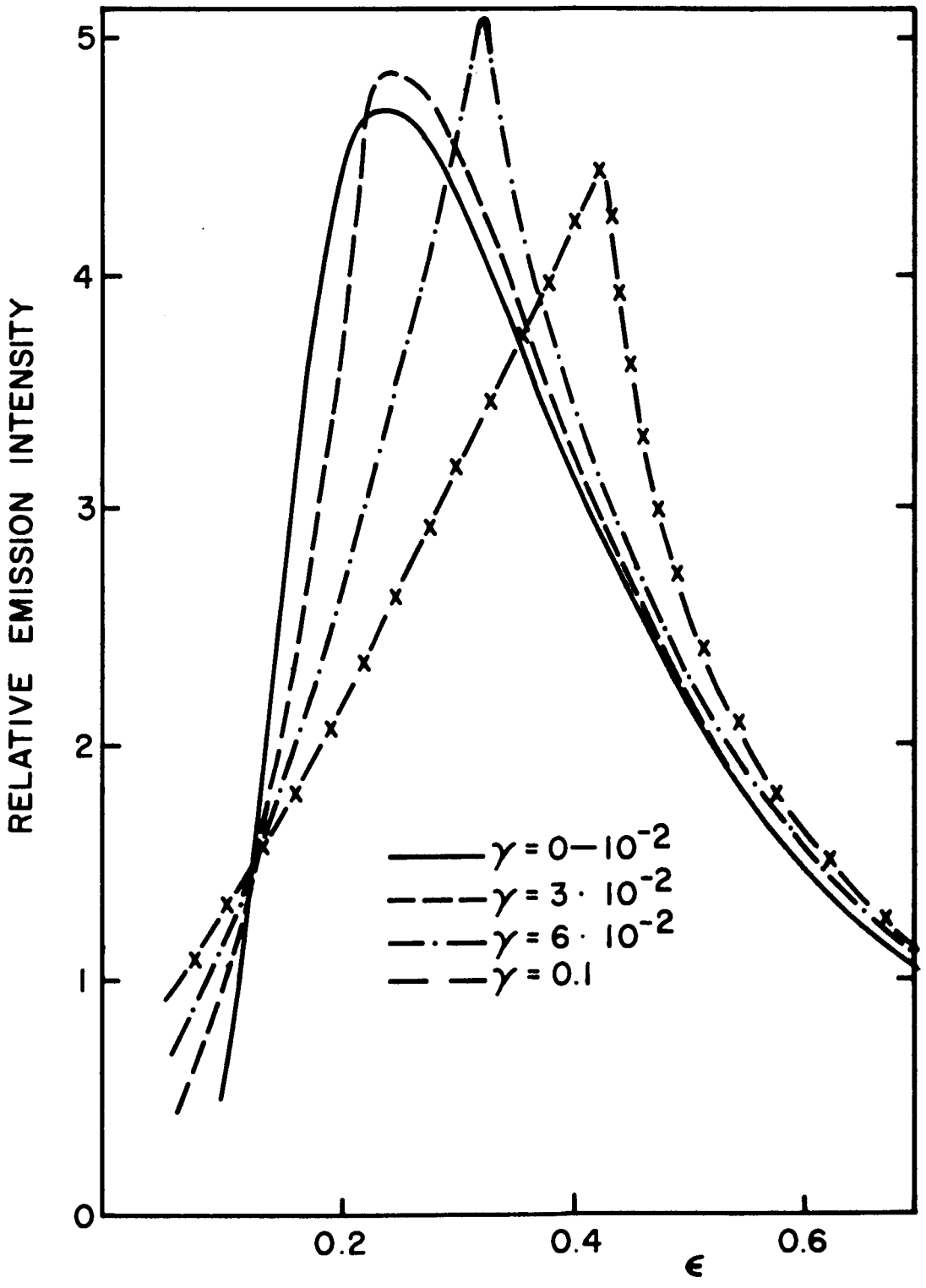


Figure 5.12 Calculated line shape of the bound-bound emission with different values of the electric field parameter $\gamma$.

(a)

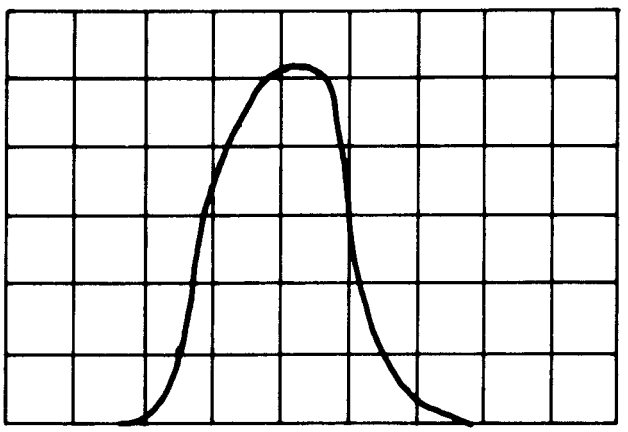

(b)

Figure 5.13 Oscilloscope traces of (a) voltage applied to electron gun, and (b) light output from evaporated films of CdS. Horizontal scale 1$\mu$s/div.

also to be expected if only the change in overlap of the electron and hole wavefunctions is considered. A full analysis of the problem would have to include this effect as well.

Experimentally, the line shape on the high energy side of the zero phonon peak is the same whether the film is coated with $SiO_x$ or with $CaF_2$, and the peak position is also unchanged. Thus there must be some other mechanism operative in broadening the bound-bound emission peaks in those films coated with $CaF_2$.

Similar experiments were tried with single crystals of high resistivity CdS which were coated with 2000A of $CaF_2$ or $SiO_x$ as soon as possible after having been cleaved. The spectra obtained at a beam voltage of 10kv and beam current of 1 ma are shown in Figures 5.14 and 5.15. As is evident the coatings have only a minor effect on the spectra, so that the effect seen in the films must be due to the nature of the evaporated CdS or possibly the higher conductivity of the films.

Only a crude estimate of the donor binding energy can be made from our data. In single crystals the zero phonon bound-bound peak occurs at an energy approximately 15 mev above $E_g - (E_A + E_D)$. If we assume the same shift in our films then from the energy at the peak, 2.459 ev, the known band gap for single crystal CdS at 4°K,[3] 2.582 ev, and the previously calculated acceptor energy we find a donor binding energy of 93 mev, to which an uncertainty of at least 5-10 mev must be attached.

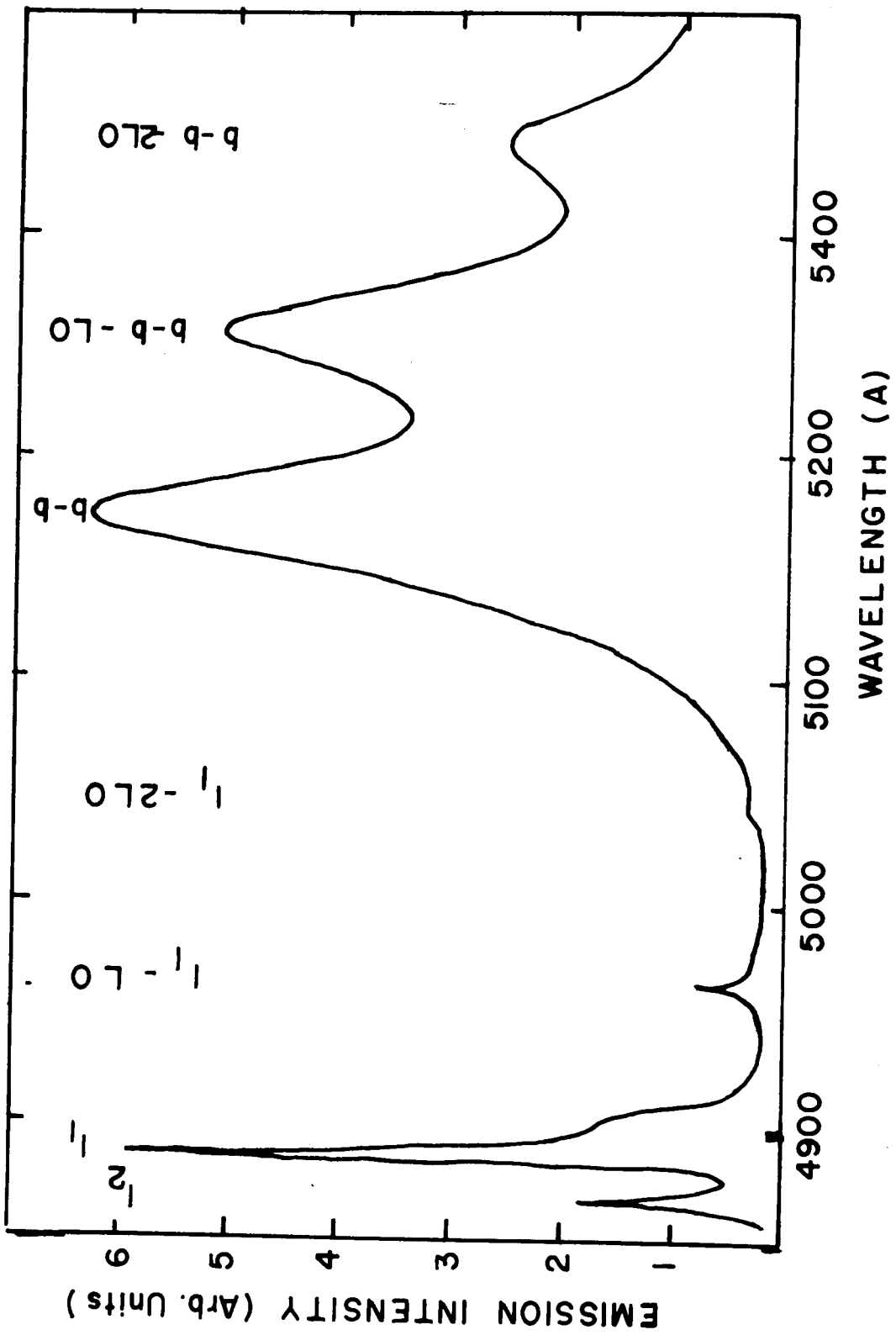


Figure 5.14 Emission spectrum of $CaF_2$ coated CdS single crystal at liquid helium temperature. Beam voltage 10kv.

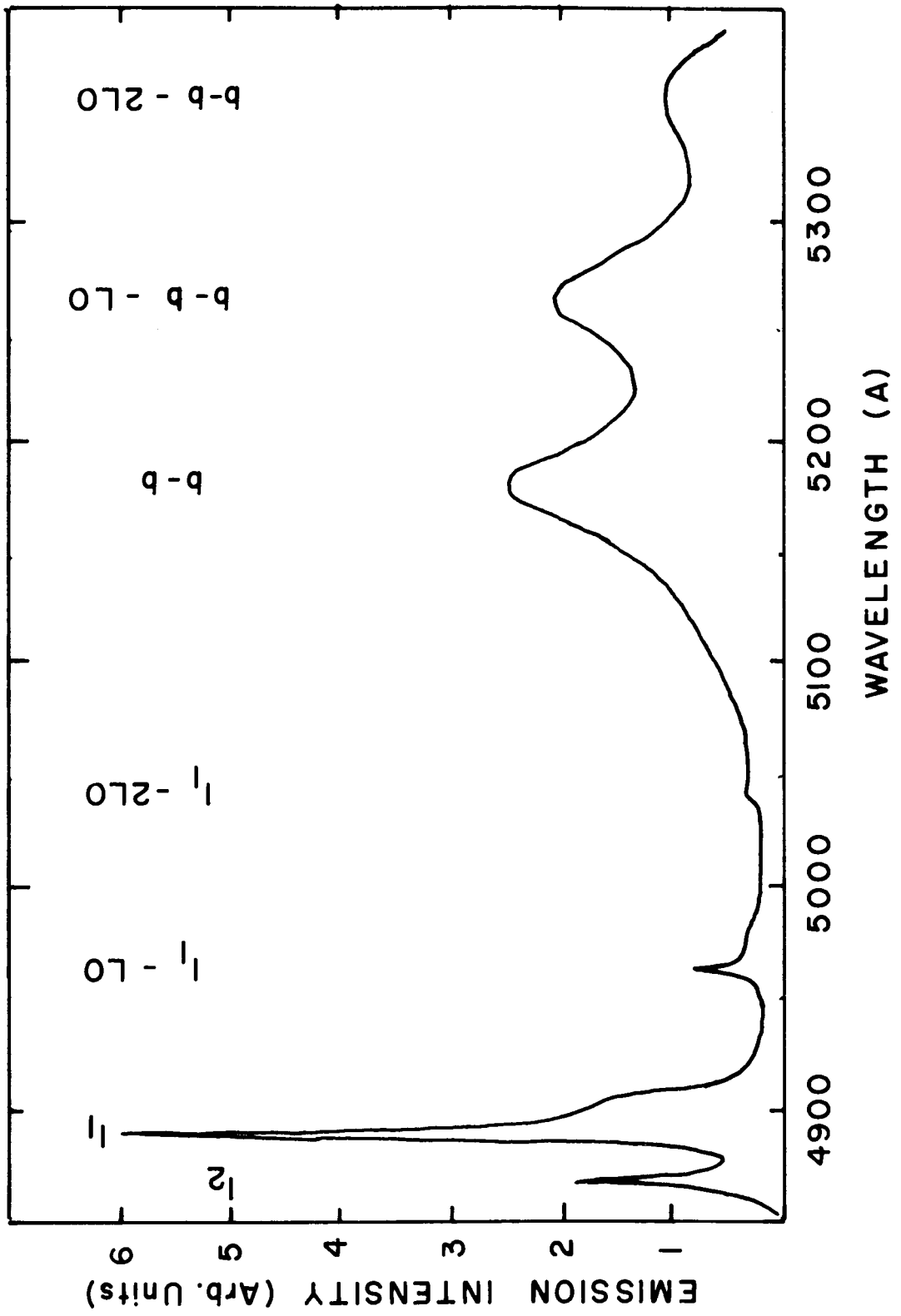


Figure 5.15 Emission spectrum of $SiO_x$ coated CdS single crystal at liquid helium temperature. Beam voltage 10kv.

## 5.5 Conclusions

In this chapter we have described some spectra obtained from vacuum evaporated thin films of CdS. The spectral lines have been shown to result from the recombination of electrons bound to donors with holes bound to acceptors, and from the recombination of "free" electrons with bound holes. The effect of positive and negative surface potentials on the free-to-bound luminescence has been demonstrated using the penetration depth of high voltage electrons to separate bulk effects from surface effects.

The effect of surface treatment on the bound-to-bound emission is still not fully understood and further work into the effect of the nature of both the evaporated CdS and the coating on the emission would be desirable.

# 6. SUMMARY AND CONCLUSION

This thesis has been concerned with some luminescent properties of single crystals and evaporated thin films of CdS, as determined by optical and electron beam excitation.

A comparison of optical and electron beam excitation mechanisms has been made and the circumstances under which each technique is of advantage determined. It has been shown that electron beam excitation is advantageous when high excitation intensity is required, such as in semiconductor lasers or when a particular luminescence process is inefficient, or when it is desired to distinguish surface from bulk effects which can be readily done by varying the penetration depth, or the energy, of the incident electrons and thereby creating electron-hole pairs at variable distances from the surface of the material. Optical excitation is of particular value when it is desired to create momentumless excitations, such as free electrons and holes or intrinsic and bound excitons, and in studying the excitation spectra of luminescent complexes. Each of these techniques has been used to advantage in studying luminescence from single crystals and evaporated thin films of CdS.

The optical excitation spectra of two bound exciton emission lines seen in single crystals of CdS have been obtained. It has been shown that the complex responsible for the $I_1$ emission line at 4888.5A, resulting from the recombination of an exciton

bound to a neutral acceptor, is created by the direct formation of bound excitons, the hole of the exciton originating from any of the three valence bands of CdS. The $I_1$ complex is also created by the formation of any of the three intrinsic excitons and subsequent capture of these excitons by the neutral acceptor.

The complex responsible for the $I_2$ and $I_5$ emission lines in the wavelength interval 4867-4869.5A are also created by the formation of intrinsic excitons and subsequent capture of these by the neutral impurity site, but more importantly peaks in the emission are observed whenever the energy of an incident photon is equal to the energy of the bound exciton plus an integral number of (k = 0) LO phonons indicating that the complex is formed directly with the simultaneous emission of a number of LO phonons. In some crystals which are nearly perfectly compensated the exciton-impurity complex is formed with phonon emission either on an ionized impurity which subsequently captures an electron to neutralize the site or an electron is captured first followed by creation of an exciton on the now neutral site. Both these processes lead to the formation of the same neutral impurity-exciton complex, on which the exciton recombines emitting light at the wavelength corresponding to $I_2$ or $I_5$. The presence of the peaks corresponding to the formation of the exciton on both neutral and ionized impurities has allowed one to identify the $I_5$ complex as an

exciton bound to a neutral donor. The identity of this line has been somewhat in doubt.

Electron beam excitation has been used to obtain luminescence spectra of evaporated thin films of CdS. The spectra have been identified as resulting from the recombination of bound electrons with bound holes and free electrons with bound holes. If the sample is coated with a 2000A thick layer of $SiO_x$, causing the energy bands of the CdS to be bent downward at the $SiO_x$ interface, the energy of the free to bound transition depends on beam voltage. At low beam voltages the energy of the emission is higher than at high beam voltages. This has been shown to be a consequence of the higher energy, as measured from the conduction band edge, of the "free" electrons near the $SiO_x$-CdS interface.

# Appendix

## OXIDE CATHODE PREPARATION

The cathodes are made of 0.010" thick nickel. Discs 1 3/8" in diameter are cut and then pressed into the required button shape using a die designed for this purpose. After the buttons have been thoroughly cleaned ultrasonically in successive baths of methyl alcohol and acetone, the following procedure is then followed:

I. Preliminary treatment of cathode buttons:

(a) Bake at 1000°C for 15 minutes in vacuum furnace

(b) Cool to 300°C

i. at or below 300°C use dry nitrogen to let furnace up to atmospheric pressure and remove buttons from furnace

(c) Spray buttons with 320 mesh powdered nickel

1. apply about 0.005" thickness using a paint spray gun or atomizer with amyl acetate as the vehicle and substituting dry nitrogen for compressed air. Alternately, pour a slurry of nickel powder and amyl acetate over the button, moving the slurry around until a uniform coating of nickel has been obtained, and then let the amyl acetate evaporate.

II. Sintering and oxide coating procedure

(a) Place buttons in furnace, heat to 900°C, bake for 5 minutes,

(b) Cool to 150°C

i. at 150°C let up to dry nitrogen

(c) Spray button with oxide coating

i. keep coat fairly light. About the right thickness has been obtained when the surface, after the amyl acetate has evaporated, has just turned white from the light grey colour it has when the nickel powder has been sintered.

ii. if oxide preparation needs thinning use amyl acetate.

iii. if extra buttons are coated with the preparation, store in an inert atmosphere (dry nitrogen will do for a period of several months) or activate the cathodes in a vacuum furnace (see below) and then store in an inert atmosphere.

III. Activation procedure

(a) Install button in gun

(b) Heat as rapidly as possible to 1000°C

i. important - keep pressure below $5 \times 10^{-5}$ torr. In heating to 1000°C considerable outgassing will be experienced, so that patience at this

stage is a virtue if good cathodes are desired. If too heavy a coating of the oxide preparation has been applied, or if the mixture was still wet when the cathode was installed, it is likely that 1000°C will never be reached. Also, cathodes with a heavy coating will show poor emission efficiency.

ii. hold at temperature for 2 minutes.

iii. drop to 850°C, which should be at or near the operating temperature.

iv. after shut down, let gun cool for 30 minutes before letting up to atmospheric pressure, again with dry nitrogen. This provides for longer cathode life.

v. it is good practice to go back to the activation temperature of 1000°C for 2 minutes after the gun has been at atmospheric pressure.

# REFERENCES


1. D. G. Thomas, J. J. Hopfield and W. M. Augustyniak, Phys. Rev. 140, A202 (1965).

2. J. J. Hopfield, J. Phys. Chem. Solids 10, 110 (1959).

3. D. G. Thomas and J. J. Hopfield, Phys. Rev. 116, 573 (1959).

4. D. G. Thomas, J. J. Hopfield and M. Power, Phys. Rev. 119, 570 (1960)..

5. J. J. Hopfield, J. Phys. Chem. Solids 15, 97 (1960).

6. J. J. Hopfield and D. G. Thomas, Phys. Rev. 122, 35 (1961).

7. D. G. Thomas and J. J. Hopfield, Phys. Rev. Lett. 7, 316 (1961).

8. D. G. Thomas and J. J. Hopfield, Phys. Rev. 128, 2135 (1962).

9. D. C. Reynolds, C. W. Litton and T. C. Collins, Phys. Stat. Sol. 9, 645 (1965)..

10. D. C. Reynolds, C. W. Litton and T. C. Collins, Phys. Stat. Sol. 12, 3 (1965).

11. F. L. Pedrotti and D. C. Reynolds, Phys. Rev. 127, 1584 (1962)..

12. D. G. Thomas, J. J. Hopfield and K. Colbow, Proceedings of the Symposium on Radiative Recombination in Semiconductors (Dunod Cie., Paris, 1964) p. 67.

13. K. Colbow, Phys. Rev. 141, 742 (1966).

14. Y. S. Park and D. W. Langer, Phys. Rev. Lett. 13, 392 (1964).

15. D. W. Langer, Y. S. Park and R. N. Euwema, Phys. Rev. 152, 788 (1966).

16. R. R. Haering and I. P. Batra, Can. J. Phys. 46, 829 (1968).

17. H. F. Ivey, Electroluminescence and Related Effects (Academic Press, New York, 1963).

18. F. F. Morehead, in Physics and Chemistry of II-VI Compounds, edited by M. Aven and J. S. Prener (John Wiley and Sons, Inc., New York, 1967) p. 613.

19. K. V. Shalimova, V. N. Khirin and O. I. Korolev, Soviet Physics Journal 1, 61 (1965).

20. K. V. Shalimova, V. N. Khirin and O. I. Korolev, Optics and Spectrosc. 20, 256 (1966).

21. K. V. Shalimova, V. N. Khirin and O. I. Korolev, Optics and Spectrosc. 20, 587 (1966).

22. J. F. Hall, J. Opt. Soc. Am. 46, 1013 (1956).

23. J. Conradi and R. R. Haering, Phys. Rev. Lett. 20, 1344 (1968).

24. R. R. Haering and J. F. O'Hanlon, Proc. I.E.E.E. (corrs.) 55, 692 (1967).

25. F. A. Kröger, Physica 7, 1 (1940).

26. C. C. Klick, J. Opt. Soc. Am. 41, 816 (1951).

27. L. R. Furlong, Phys. Rev. 95, 1086 (1954).

28. M. Bancie-Grillot, E. F. Gross, E. Grillot and B. S. Razbirin, Optics and Spectrosc. 9, 287 (1960).

29. L. S. Pedrotti and D. C. Reynolds, Phys. Rev. 119, 1897 (1960).

30. L. S. Pedrotti and D. C. Reynolds, Phys. Rev. 120, 1664 (1960).

31. D. C. Reynolds and C. W. Litton, Phys. Rev. 132, 1023 (1963).

32. D. A. Cusano in Physics and Chemistry of II-VI Compounds edited by M. Aven and J. S. Prener (John Wiley and Sons, Inc., New York, 1967) p. 709.

33. R. H. Bube, Photoconductivity in Solids (John Wiley and Sons, Inc., New York, 1960).

34. P. K. Weimer in Physics of Thin Films Vol. 2, Edited by G. Haas and R. E. Thun (Academic Press, New York, 1964) p. 147.

35. H. F. Ivey, Electroluminescence and Related Effects (Academic Press, New York, 1963).

36. W. Kohn, Solid State Physics 5, 258 (1953).

37. A. Vecht in Physics of Thin Films, vol. 3, edited by G. Haas and R. E. Thun (Academic Press, New York, 1966) p. 165.

38. F. Stern, Solid State Physics 15, 299 (1963).

39. L. Schiff, Quantum Mechanics (McGraw-Hill Book Company, New York, 1955), Chapter 10.

40. H. S. W. Massey, Advances in Electronics 4, 1 (1952).

41. U. Fano, Ann. Rev. Nucl. Science 13, 1 (1963).

42. c.f. D. Pines, Elementary Excitation in Solids (W. A. Benjamin, Inc., New York, 1964).

43. D. Pines, Rev. Mod. Phys. 28, 184 (1956).

44. L. V. Spencer, Phys. Rev. 98, 1597 (1955).

45. R. O. Lane and D. J. Zaffarano, Phys. Rev. 94, 960 (1954).

46. H. Kanter and E. J. Sternglass, Phys. Rev. 126, 620 (1962).

47. W. Ehrenberg and D. E. N. King, Proc. Phys. Soc. 81, 751 (1963).

48. C. J. Bakker and C. Segre, Phys. Rev. 81, 489 (1951).

49. J. R. Young, Phys. Rev. 103, 292 (1956).

50. L. V. Spencer, NBS Monograph 1, September 10, 1959.

51. C. A. Klein in Physics of Quantum Electronics, edited by P.L. Kelley, B. Lax and P. E. Tannenwald, (McGraw-Hill Book Company, New York, 1966) p. 424.

52. W. W. Anderson, Appl. Optics 4, 626 (1965).

53. D. G. Thomas, R. Dingle and J. D. Cuthbert in II-VI Semiconducting Compounds, 1967 International Conference, ed. by D.G. Thomas (W.A. Benjamin, Inc., N.Y. 1967) p. 863.

54. H. J. Stocker, C. R. Stannard Jr., H. Kaplan and H. Levinstein, Phys. Rev. Lett. 12, 163 (1964).

55. J. G. McCallum, Private Communication, 1968.

56. Y. S. Park and J. R. Schneider, Phys. Rev. Lett. 21, 798 (1968).

57. K. Aalund and R. Hill, Electronics 37, 32 (1964).

58. J. F. O'Hanlon, Ph.D. Thesis, Simon Fraser University (unpublished) 1967.

59. C. B. Duke, Phys. Rev. 159, 632 (1967).

60. K. Colbow, Phys. Rev. 139, A274 (1965).

61. R. E. Halsted and M. Aven, Phys. Rev. Lett. 14, 64 (1965).